Adsorption of tannic acid to surfaces

by

Hannah Wiebe

A thesis submitted to McGill University
in partial fulfillment of the requirements of the degree of

Master of Science

Department of Chemistry
McGill University
Montreal, Quebec, Canada

December 2022

Abstract

Tannic acid (TA), a compound derived from trees, is part of the class of astringent polyphenolic compounds known as tannins. Tannins have historically been used in leather tanning and textile dying processes, and nowadays, TA is used in chemical processes such as corrosion inhibition and metal nanoparticle synthesis. Polyphenols are known to play roles in many biological processes within the plants from which they are derived, and this has inspired their use in new materials to impart properties such as antioxidant or antimicrobial capabilities. Recently, studies have revealed the potential use of TA as a naturally derived drug against the SARS-CoV-2 virus due to its ability to bind to relevant viral proteins with high affinity. In this work, the adsorption of TA to different materials is studied to demonstrate the potential applications of TA-derived coatings. Studies on the adsorption of TA to gold surfaces provide a fundamental understanding of the adsorption mechanisms of TA. Adsorption kinetics and mono- and multilayer formation mechanisms are studied with a focus on behaviour in physiological-like conditions. TA coatings formed on gold may be promising for biomedical applications such as in medical implants. Studies on the adsorption of TA to cellulosic kraft pulp fibers open the door to one possible application of TA as a coating material in cellulose-based papers and textiles. The adsorption kinetics are studied in addition to the effects of different post-adsorption treatments on TA uptake. Prototype paper samples made from the TA-functionalized fibers are developed and characterized. The ability of TA to bind to and precipitate proteins, including proteins involved in SARS-CoV-2 infectivity makes it an interesting compound for use in cellulosic paper-based filtration materials such antiviral face masks.

Résumé

L'acide tannique (AT), un composé dérivé des arbres, fait partie de la classe des composés polyphénoliques astringents connus sous le nom de tanins. Historiquement, les tanins ont été utilisés dans les processus de tannage du cuir et de teinture des textiles. Aujourd'hui, l'AT est utilisé dans des processus chimiques tels que l'inhibition de la corrosion et la synthèse des nanoparticules métalliques. Les polyphénols sont connus pour leur rôle dans de nombreux processus biologiques au sein des plantes dont ils sont issus, ce qui a inspiré leur utilisation dans de nouveaux matériaux pour leur conférer des propriétés telles que des capacités antioxydantes ou antimicrobiennes. Récemment, des études ont révélé l'utilisation potentielle de l'AT en tant que médicament d'origine naturelle contre le virus SRAS-CoV-2, en raison de sa capacité à se lier aux protéines virales pertinentes avec une grande affinité. Dans ce travail, l'adsorption de l'AT sur différents matériaux est étudiée afin de démontrer les applications potentielles telles que des revêtements fonctionnalisés par l'AT. Les études sur l'adsorption de l'AT sur des surfaces en or fournissent une compréhension fondamentale des mécanismes d'adsorption de l'AT. La cinétique d'adsorption et les mécanismes de formation de monocouche et de multicouches sont étudiés en mettant l'accent sur le comportement dans des conditions de type physiologique. Les revêtements de l'AT formés sur une surface d'or peuvent être prometteurs pour des applications biomédicales telles que les implants médicaux. Des études sur l'adsorption de l'AT sur des fibres cellulosiques de pâte kraft ouvrent la voie à une application possible de l'AT comme matériau de revêtement dans les papiers et les textiles à base de cellulose. La cinétique d'adsorption est étudiée ainsi que les effets de différents traitements post-adsorption sur l'adsorption de l'AT. Des prototypes de papiers fabriqués à partir de fibres fonctionnalisées à l'AT sont développés et caractérisés. La capacité de l'AT à se lier aux protéines et à les précipiter, y compris les protéines impliquées dans l'infectiosité du SRAS-CoV-2 en fait une molécule intéressante pour une utilisation dans les matériaux de filtration à base de papier cellulosique tel que les masques antiviraux.

Acknowledgements

First and foremost, I would like to thank my supervisor, Professor Theo van de Ven, for his guidance, encouragement, and willingness to teach. Prof. van de Ven taught me a lot about chemistry, but more importantly, he also taught me to question and investigate every detail. I learned that there is always an explanation to be found even if it isn't obvious at first, a lesson I will always keep with me. I am immensely grateful for his support.

I would also like to thank Professor Roger Gaudreault for his supervision, collaboration, and help in guiding so much of my work. His dedication to research inspired and deepened my appreciation for the field.

I'm thankful for the current and former members of the van de Ven group whose support, camaraderie, and encouragement were so important to my time in the lab—Sierra, Yiwei, Amin, Martin, Roya, Jane, Ghazaleh, and Marzieh, it was a pleasure to work with all of you. Special thanks to Hadi for his ingenuity and enthusiasm for research, and to Mandana for welcoming me to the group and teaching me so much in my first few weeks.

I would like to thank Professor Nathalie Tufenkji and the members of her research group for welcoming me into their lab to use their equipment, especially for accommodating me in the lab schedule in a time of many restrictions.

Finally, I want to thank my family and friends for helping me believe in my own abilities. To my parents, I'm so grateful for your unwavering support and encouragement, I hope I make you proud. To my friends, thank you for being there when I needed to go hang out in a park and turn off my brain. Lastly, thank you to my wonderful partner Aidon (and our sweet cat Wendy) for being there to support me at the end of every long day, I love you. Thank you all for inspiring and encouraging me at every step of the way.

Table of Contents

List of Figures

Chapter 1

Chapter 2

Chapter 3

List of Tables

List of Abbreviations

ACE2	Angiotensin-converting enzyme 2
AuNP	Gold nanoparticle
DI	Deionized (water)
DOPA	3,4-dihydroxy-L-phenylalanine
FTIR	Fourier transform infrared (spectroscopy)
KP	Kraft pulp
LD_{50}	Median lethal dose ("lethal dose, 50%")
PBS	Phosphate buffered saline
QCMD	Quartz crystal microbalance with dissipation monitoring
RBD	(Spike protein) receptor binding domain
SARS-CoV-2	Severe acute respiratory syndrome coronavirus 2
SPR	Surface plasmon resonance
TA	Tannic acid
TMPRSS2	Transmembrane protease serine 2
3CLpro	3-chymotrypsin like protease

Contribution of Authors

This thesis contains two manuscripts.

Chapter 2 consists of a manuscript titled "Adsorption of tannic acid onto gold surfaces," which has been submitted for publication. The supporting information for this manuscript is included in Appendix 1. Hannah Wiebe designed and conducted the experiments, analyzed the data, and wrote the manuscript. The research was conducted under the supervision of Dr. Theo van de Ven and Dr. Roger Gaudreault, who gave guidance and advice and edited the manuscript. Phuong Trang Nguyen conducted surface plasmon resonance (SPR) measurements under the supervision of Dr. Steve Bourgault at UQAM, and wrote the sections describing the methodology and analysis of the SPR data.

Chapter 3 consists of a manuscript titled "Adsorption of tannic acid onto kraft pulp fibers," which has been prepared for submission. Hannah Wiebe and Dr. Mohammadhadi Moradian designed and conducted the experiments. Hannah Wiebe analyzed the data and wrote the manuscript. Dr. Mohammadhadi Moradian and Dr. Theo van de Ven gave supervision and advice and edited the manuscript.

Appendix 2 consists of excerpts from "Molecular Interactions of Tannic Acid with Proteins Associated with SARS-CoV-2 Infectivity" by Mohamed Haddad & Roger Gaudreault et al. For this work, Hannah Wiebe conducted the experiments on protein-tannic acid interactions using a quartz crystal microbalance with dissipation monitoring (QCMD). Dr. Roger Gaudreault and Dr. Theo van de Ven gave supervision and advice. The included sections from the text include QCMD results and discussion, a description of the experiments, and relevant theory for analysis of the data, written by Hannah Wiebe and edited by Dr. Roger Gaudreault and Dr. Theo van de Ven.

Chapter 1: Introduction

In the design of new materials and chemical processes, researchers often turn to nature to inspire solutions. Biomimetic processes are developed to emulate natural systems, and biorenewable feedstocks offer sustainable sources for new materials. The concept of green chemistry arose in efforts to develop more environmentally-friendly chemical processes that prevent pollution and other negative impacts on health and the environment. *The Twelve Principles of Green Chemistry*, published in 1998 by Paul Anastas and John C. Warner, established several ways for researchers to develop sustainable processes, including the use of renewable materials and the design of non-toxic, degradable products.[1] Natural materials and processes can provide elegant and green solutions to many research questions we aim to address. A fundamental understanding of the underlying mechanisms of these processes is key to the use of natural materials in the research and development of advanced materials and sustainable technologies; for instance, the study of adsorption is relevant to the formation of bioinspired coatings and films.

The objective of this work is to study the adsorption of the green polyphenol tannic acid (TA) to different surfaces, and develop an understanding of the ways in which the chemical properties of TA affect its ability to form coatings on these surfaces.

Tannic acid, a useful plant polyphenol

TA is a plant polyphenol, the structure of which, as seen in Figure 1A, consists of a central glucose ring with 10 galloyl (3,4,5-hydroxyphenyl) groups—this structure is thus also known as decagalloyl glucose. TA is part of the class of tannins, a group of astringent polyphenols found in plant tissues such as the bark, leaves, or roots.[2] Although tannins are found in a wide variety of plants, commercial TA is extracted from the gall nuts of oak and sumac trees, particularly the species *Rhus semialata* and *Quercus infectoria*.[3] The primary biological function of tannins in plants is their ability to bind and precipitate proteins.[4] Protein precipitation is thought to play a role in plant defense mechanisms—for example, the astringent sensation caused by tannin complexation with proteins found in saliva can be repellent to herbivores.[4] Ironically, tannins are also responsible for the astringent or "dry" mouthfeel of beverages such as red wine and tea,[3, 4] often considered by humans to be a desirable property.

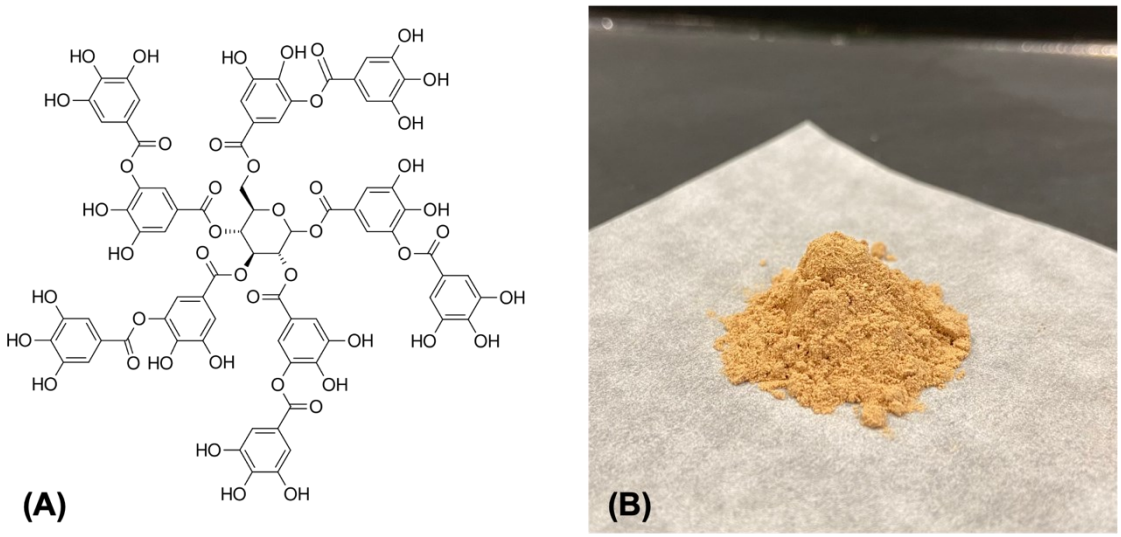

Figure 1: (A) Structure of tannic acid (TA) and (B) TA in its solid form.

TA is commonly supplied in solid form as a light brown powder (Figure 1B), and is water-soluble. It has a relatively low toxicity with a median lethal dose (LD_{50}) orally of 2,260 mg/kg in rats.[5] This is a similarly low toxicity to that of other related gallotannins, polyphenols which contain galloyl groups. For example, corilagin (a plant polyphenol with promising pharmacological effects[6]) and epigallocatechin gallate (the most abundant polyphenol in tea) have oral LD_{50} values of 3500–5000 mg/kg in mice[5] and 186.8–1868 mg/kg in rats,[7] respectively. Gallic acid, the hydrolysis product of hydrolysable gallotannins such as TA, has an oral LD_{50} of 5000 mg/kg in rats.[5]

Chemistry of TA

Many of the unique properties and molecular interactions of TA with other species arise from its structure, with 25 phenolic hydroxyl groups located on the external galloyl moieties (Figure 1A). Some of the key chemical interactions of TA include the formation of complexes with proteins, the breakdown of TA by hydrolysis, and the redox chemistry of TA.

Protein binding

As mentioned above, one of the key properties of tannins is their ability to bind and precipitate proteins. Tannin-protein interactions are based on hydrogen bonds between phenolic hydroxyl groups and the amide and carboxyl groups of amino acids.[3, 8] Since both tannins and proteins possess multiple hydrogen-bonding sites, large insoluble complexes can form between them, leading to protein precipitation.[8] Large polyphenols like TA, with its numerous galloyl

groups, have higher protein-binding affinities than smaller tannins due to the number of bonding sites.[3]

Metal ion complexation

In addition to protein binding, the ability of TA to chelate metal ions is one of its most well-known properties. The predominant theory for the mechanism of TA metal chelation involves the formation of complexes between phenols and metal ions. The galloyl moieties of TA, with two or three neighbouring hydroxyl groups, serve as binding sites for metal ions.[9] Taking iron chelation as an example, Fe^{2+} binds to two adjacent hydroxyl groups, causing deprotonation. The complex then oxidizes in the presence of O_2, forming a Fe^{3+}-polyphenol complex.[3, 9]

Hydrolysis

TA is known as a hydrolysable gallotannin; hydrolysable tannins are those that can be broken down via hydrolysis of carboxylic ester linkages into their constituent products, sugars and phenolic carboxylic acids (D-glucose and gallic acid, in the case of TA).[10] In contrast, compounds known as condensed tannins are polyphenols linked by C–C bonds that cannot be broken down in this way.[4, 10] This distinction is significant in how these two classes of tannins are metabolized in the gastrointestinal tract. The bioavailability of most hydrolysable tannins is low due to their large size and interactions with proteins in the gut.[11] Unlike condensed tannins, hydrolysable tannins can be broken down into the basic units gallic acid and ellagic acid, which can be absorbed.[11] However, both condensed and hydrolysable tannins can ultimately be metabolized by gut microbiome,[11] and although their metabolism takes different pathways, the resulting bioavailable polyphenol metabolites can be beneficial to many physiological processes (e.g., anti-inflammatory, anticarcinogenic, neurological and cognitive) and to the gut microbiome itself.[11, 12]

Redox chemistry

TA is a well-known antioxidant; the many hydroxyl groups of TA make it a good candidate for redox reactions. In particular, the reducing ability of TA has been used in the synthesis and stabilization of metal nanoparticles.[13] The hydroxyl groups of TA can participate in redox reactions as shown in Figure 2. The phenolic hydroxyl groups of TA deprotonate above their pKa (almost all –OH groups have been shown to be dissociated at pH 7).[14] Upon loss of a proton, the –OH groups can be oxidized to form C=O bonds; this resulting structure is sometimes referred to as the quinone form.[13] In physiological-like conditions (e.g., phosphate buffered saline (PBS) buffer, with a pH of 7.4), although some oxidation can occur, complete oxidation of TA is not likely—

rather, a mix of protonated, deprotonated, and oxidized forms of TA may be present.[15] When the donated electrons are used to reduce metal ions (from metal salts), the formation of metal nanoparticles stabilized by TA can occur.[13] Consideration of the likelihood of TA oxidation in different conditions is important because it can have an impact on its interactions with different species. For example, in one study, TA partially oxidized in physiological conditions (PBS at 37ºC) was shown to still interact with amino acids and chelate iron, but had diminished antioxidant capability and anti-cancer activity.[16]

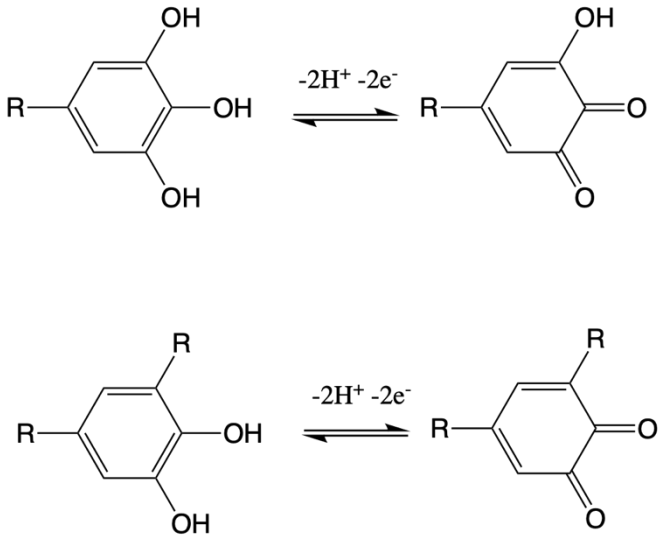

Figure 2: Redox scheme of galloyl groups of TA. Adapted from Chariyarangsitham et al.[15]

The redox mechanism of TA is similar to the redox chemistry of catechol groups, which transform into quinones under oxidizing conditions.[17] Both the oxidized and unoxidized forms of catechol are highly reactive—the former has a strong affinity to metal, metal oxide, and polymer surfaces, and the latter is reactive with thiol, amine, and other quinone groups.[17, 18] The chemistry of the catechol and its oxidized quinone form is the subject of much recent work. For example, 3,4-dihydroxy-L-phenylalanine (DOPA), an amino acid found in the specialized adhesive proteins of marine mussels, contains a catechol functional group.[19] Research on DOPA has led to the development of bioinspired adhesive materials that interact strongly with a wide variety of surfaces.[17, 20] In addition, films formed via in-situ oxidative self-polymerization of dopamine were shown to deposit on inorganic and organic surfaces and could participate in several secondary surface reactions.[21] This work on DOPA and dopamine catechol chemistry has inspired research on the film-forming abilities and surface interactions of similar natural phenols and polyphenols.

For example, films of epigallocatechin gallate, epicatechin gallate, epigallocatechin, and TA were shown to deposit spontaneously via adsorption from solution to several different substrates.[22] These films were formed in mildly alkaline conditions in the presence of dissolved oxygen; oxidation was suspected to play a role in the initial surface deposition and self-polymerization of these films, similarly to polydopamine formation.[22] Because of its functionality and many possible interactions, TA is an interesting naturally-derived candidate for surface modification.

Historical and modern applications of TA

TA has seen widespread use historically owing to its useful chemical properties, namely its ability to bind proteins and form complexes with metal ions.[3] Tannins were traditionally used in the tanning of animal skins due to their ability to stabilize and crosslink collagen protein fibers,[3, 8] and the ability of TA to chelate iron and other metals led it to be used in historical dyeing processes and in writing ink until the 20th century.[3] Nowadays, tannins such as TA are used in many other industries. Tannin-based corrosion inhibitors, which prevent surface corrosion of industrial equipment by forming a protective layer, are rising in popularity because of their renewability.[23] TA is also used as a reducing and stabilizing agent in metal nanoparticle synthesis as the phenolic groups in its structure can undergo redox reactions to reduce metal ions from salts, forming stable metal nanoparticles.[13]

TA as an antiviral, antibacterial, anti-COVID material

Recently, the use of TA as an antimicrobial material has gained attention in the literature. A recent review by Kaczmarek summarized studies on the antiviral (Influenza A virus, Papilloma viruses, noroviruses, Herpes simplex virus type 1 and 2, human immunodeficiency virus (HIV)) and antibacterial (*Staphylococcus aureus*, *Escherichia coli*, *Streptococcus pyogenes*, *Enterococcus faecalis*, *Pseudomonas aeruginosa*, *Yersinia enterocolitica*, *Listeria innocua*) properties of TA and highlighted its use in biomaterials.[24] The antiviral capacity of TA is thought to arise from its ability to bind to viral receptor proteins.[24] The antibacterial properties of TA may be attributed to complexation with essential bacterial enzymes, substrates, nutrients, and/or metal ions, interactions with bacterial cell membrane proteins, and interference with microbial metabolism.[2, 3, 24]

TA has also been studied in the context of the recent COVID-19 pandemic caused by severe acute respiratory syndrome coronavirus 2 (SARS-CoV-2), declared a pandemic by the World Health Organization in March 2020.[25] Recently, some of the authors of the manuscripts in this

thesis (H.W., R.G., T.v.d.V) were involved in a study on the interactions of TA with proteins involved in the infectivity of SARS-CoV-2. In this work, TA was found to inhibit the interaction between the viral spike protein receptor binding domain (RBD) and the human receptor protein, angiotensin-converting enzyme 2 (ACE2).[26] TA was also found to bind and inhibit the enzymatic activity of transmembrane protease serine 2 (TMPRSS2) and 3-chymotrypsin like protease (3CLpro), key proteins involved in cell entry and replication of the virus, respectively.[26] This work suggests that TA may be a promising antiviral drug candidate in the context of the COVID-19 pandemic. Appendix 2 contains excerpts from this work that are relevant to the other manuscripts in this thesis.

TA in functional coatings and materials

Much of the recent literature regarding TA has focused on its use as a coating or as an additive in materials. For instance, TA coatings formed by spontaneous surface deposition demonstrated antibacterial properties and a significant antioxidant effect yet showed virtually no observable toxicity to mammalian cells.[22] In addition, when incorporated into biopolymer-based materials such as collagen hydrogels, chitosan films, or cellulosic films and textiles, TA has been found to enhance properties of these materials such as antioxidant ability, antimicrobial activity, or inhibition of biofilm formation.[24, 27, 28]

With the recent focus on functional TA-based coatings, an understanding of the mechanisms of coating formation on various surfaces or materials is crucial. In many cases, these coatings are formed by adsorption, the mass-transfer process by which a species (adsorbate) adheres to a surface (adsorbent). Adsorption is often discussed in the context of removing a species from a gas or liquid; e.g., adsorption is often a means of contaminant removal in wastewater treatment. However, it is also a common process in material fabrication—adsorption of a desired species from solution can be used to form films or coatings on a substrate. Adsorption processes are studied to determine the parameters of these processes, e.g., the ideal concentration range of the coating solution, required contact times and kinetics, and final thicknesses of layers formed on different substrates.

Adsorption of TA onto gold surfaces

In this work, the adsorption of TA to different surfaces is investigated by experimental methods at different scales to study the effect of the physical and chemical properties of TA on its coating forming properties. In Chapter 2, "Adsorption of tannic acid onto gold surfaces," a quartz

crystal microbalance with dissipation monitoring (QCMD) and surface plasmon resonance (SPR) are used to precisely monitor TA layer formation on bare gold surfaces.

Quartz crystal microbalance with dissipation monitoring

The QCMD is an instrument which measures the resonance frequency of an oscillating quartz crystal; as mass is deposited or removed at the surface of the crystal sensor, the resonance frequency changes. Under certain assumptions, a negative frequency shift measured by the system can be correlated to an amount of mass depositing on the surface using a linear relation known as the Sauerbrey equation,[29] given by Equation 1.

$$\Delta m = -\frac{C}{n}\Delta f \quad (1)$$

Here C is the sensitivity constant (17.7 ng cm^{-2} Hz^{-1} for a quartz crystal with oscillation frequency of 5 MHz), n is the resonance overtone (1, 3, 5, 7, or 9), and Δf is the change in the measured resonance frequency at overtone n.[30] The QCMD also measures the dissipation factor (ΔD), a measurement of energy losses due to dissipation. Dissipation can be thought of as a representation of the rigidity of an adsorbed mass; a higher dissipation factor corresponds to a less rigid film. One condition for the application of the Sauerbrey equation is that the ratio $-\Delta D/\Delta f$ should be no more than 10^{-7}, i.e., the film is considered rigid.[31]

QCMD sensors are available in a wide variety of substrate coatings on the crystal allowing for the measurement of species interactions with many surfaces. Gold was chosen as a simple, relatively inexpensive, inert substrate to understand TA layer formation mechanisms with nanoscale mass resolution. QCMD also allows for surface adsorption/desorption processes to be monitored in real-time, facilitating kinetics analysis.

Adsorption of TA onto kraft pulp fibers

Chapter 3, "Adsorption of tannic acid onto kraft pulp fibers," focuses on TA adsorption on the surface of kraft pulp (KP), a material most commonly used to manufacture paper products.

Cellulose and the structure of wood

KP is a material derived from wood from trees, consisting primarily of fibers of cellulose. Cellulose is the most abundant biorenewable resource on Earth, found not only in plants but also in bacteria, algae, and other biomass.[32] Cellulose is a biopolymer whose structure, shown in Figure 3, consists of repeating D-glucose units linked by a β-1,4-glycosidic bond. The structure possesses

three hydroxyl functional groups per glucose unit, which can participate in a variety of chemical reactions and lend cellulose its characteristic hydrophilicity.

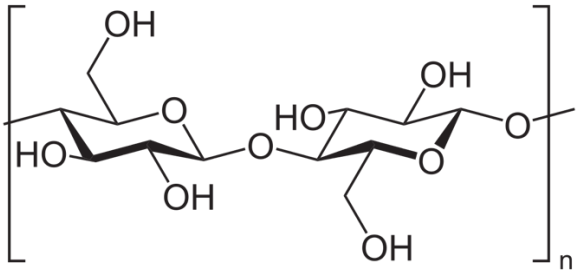

Figure 3: Structure of a repeat unit of cellulose.

Cellulose is found in plant cell walls, especially in the stalks, stems, trunks, and other woody plant tissues, where it maintains the structure of these tissues.[33] In wood, the oriented linear molecules of cellulose are found alongside the branched polymers lignin and hemicellulose to form the components of the wood cell wall.[32, 33] Lignins are structural polyphenolic molecules, and hemicelluloses are polysaccharides that possess some carboxylic acid groups and lend a negative charge to wood fibers.[34] The hierarchical structure of wood cells, illustrated in Figure 4, begins with cellulose molecules. Chains of cellulose, also known as elementary fibrils with a diameter of 2–4 nm, are organized into bundles known as microfibrils 10–25 nm in diameter.[32] Microfibrils are a supramolecular structure consisting of alternating regions of ordered and disordered, or crystalline and amorphous regions. Microfibrils combine into larger fibrils, which then combine with hemicellulose in the cell wall to form fibers.[33]

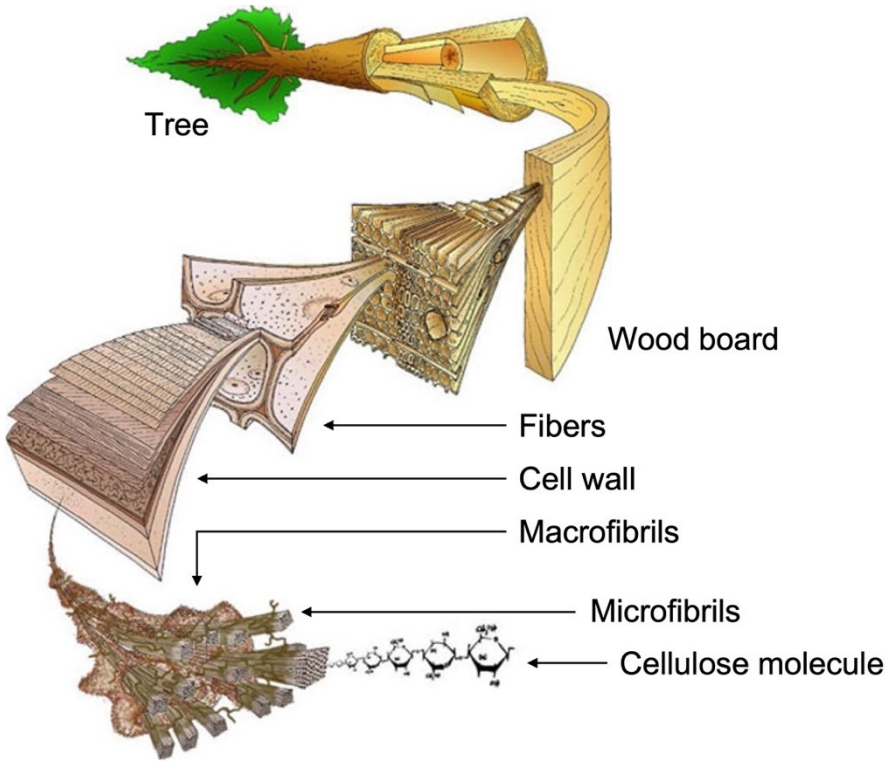

Figure 4: Illustration of the hierarchically organized structure of wood. Artwork adapted from J.J. Harrington, University of Canterbury, 2002.[35] Individual cellulose molecules are organized into the larger structures that make up fibers and ultimately the structure of wood.

The wood cell, as shown in Figure 5, has several components with differing compositions. The middle lamella (ML), found between adjacent cells, is high in lignin and contributes to the structure and organization of wood cells. The primary wall (P) consists mainly of randomly oriented cellulose microfibrils. The secondary wall (S), higher in cellulose and low in lignin, is composed of three layers in which microfibrils are organized in different orientations with respect to the axis of the cell. At the center is the lumen, a void space at the core of the cell. Figure 5 also shows a bordered pit, which facilitates intercellular transport of water and biomolecules.[36]

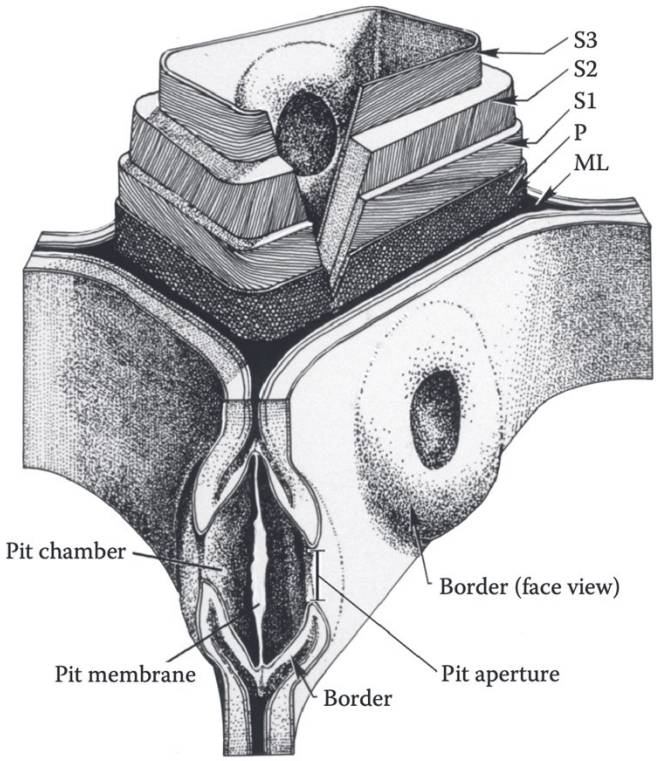

Figure 5: Structure of a wood cell wall, adapted from *Handbook of Wood Chemistry and Wood Composites* by R.M. Rowell.[36] The layers of the plant cell can be seen, beginning with the middle lamella (ML) between adjacent cells, followed by the primary wall (P), and the secondary wall (S), divided into three layers (S1, S2, S3). The hollow lumen and a pit on the cell wall are also shown.

Kraft pulping process

The cellulosic material of interest in Chapter 3 is bleached softwood kraft pulp, a material prepared from wood by the kraft pulping process. In this process, wood chips are reacted with a mixture of sodium hydroxide (NaOH) and sodium sulfide (Na_2S) known as kraft liquor. The wood chips are cooked at 165–175 ºC, then washed to yield KP while the spent liquor can undergo a recovery and conversion process.[37, 38] The aim of wood chemical pulping is to break down and remove most hemicelluloses and lignin, leaving the highly cellulosic secondary wall of the wood cell.[37, 39] The mechanism of delignification involves two processes for the introduction of hydrophilic functional groups, thereby increasing the solubility of lignin: the cleavage of linkages between phenylpropane units, which introduces hydroxyl groups, and the process of sulfonation, which generates sulfonic acid groups.[38] Bleached KP contains about 85% cellulose and 15% hemicellulose, and is very low in lignin.[36]

Uses of cellulose

Some of the earliest human uses of cellulose include the burning of wood as a source of heat and power, the construction of buildings from wood logs and planks, the use of pulp to make paper, and the manufacture of textiles from cotton fiber. Nowadays, chemical modification to alter the structure and/or chemical composition of cellulose fibers has opened the door to the development of an even wider variety of cellulosic materials, such as micro- and nanocrystalline cellulose, films, and hydrogels.

TA and cellulose have been used in combination in the past and in more recent research. Historically, TA has been used as a mordant in textile dyeing. Mordants such as TA improve the uptake, wash-fastness, and colour depth of textile dyes, e.g., by forming complexes with metal salts or natural dyes.[40-42] More recently, several studies reviewed in Chapter 3 have employed TA as an antimicrobial additive in many biopolymer-based materials including cellulosic fibers. However, to our knowledge, TA adsorption to KP fibers without chemical modification has not been investigated.

Green chemistry for the development of new materials

In the development of new materials and especially consumer products, green chemistry is increasingly relevant given changing social attitudes about environmental sustainability, pollution, and renewability. The image of a product as "renewable" is a selling point as consumers are becoming more driven by sustainability.[43] Both TA and cellulose, being naturally-derived biorenewable materials, are excellent candidates for the development of alternatives to petroleum-derived products. For example, in Chapter 3 we discuss the potential applications of TA-modified cellulose-based filters in face masks. This work seeks to further our understanding of the underlying physical and chemical processes involved in the formation of TA-functionalized materials, so that these functional materials can later lead to sustainable advancements in industry.

Chapter 2: Adsorption of tannic acid onto gold surfaces

Hannah Wiebe [1,2], Phuong Trang Nguyen [3], Steve Bourgault [3], Theo G.M. van de Ven [1,2], Roger Gaudreault [2,3,4,*]

[1] Department of Chemistry, McGill University, 3420 University Street, Montreal, QC H3A 2A7, Canada
[2] Quebec Centre for Advanced Materials (QCAM), 3420 University Street, Montreal, QC H3A 2A7, Canada
[3] Department of Chemistry, Succursale Centre-Ville, Université du Québec à Montréal, Montréal, QC, Canada
[4] Department of Physics, Succursale Centre-Ville, Université de Montréal, Case Postale 6128, Montreal, QC H3C 3J7, Canada
* Correspondence: roger.gaudreault@umontreal.ca

Abstract

Thin film coatings are widely applicable in materials for consumer products, electronics, optical coatings, and even biomedical applications. Wet coating can be an effective method to obtain thin films of functional materials, and this technique has recently been studied in depth for the formation of bioinspired polyphenolic films. Naturally-occurring polyphenols such as tannic acid (TA) have garnered interest due to their roles in biological processes and their applicability as antioxidants, antibacterial agents, and corrosion inhibitors. Understanding the adsorption of polyphenols to surfaces is a core aspect in the fabrication processes of thin films of these materials. In this work, the adsorption of TA to gold surfaces is measured using a quartz crystal microbalance with dissipation monitoring (QCMD) and surface plasmon resonance (SPR) for a wide range of TA concentrations. The adsorption kinetics and layer formation mechanisms are investigated, finding that in physiological-like conditions TA readily adsorbs on gold and is able to form multilayer coatings within minutes.

Keywords: tannic acid, polyphenols, thin films, deposition, QCMD, SPR, green chemistry

Introduction

Coatings are used to functionalize surfaces in nearly every industry, conferring desired properties and enhancing the performance of surfaces for targeted applications. Wet coating, a process by which molecules from aqueous solutions are coated on surfaces, is a technique which

depends on the affinities and interactions between the molecules and the surfaces. Thus, an understanding of adsorption kinetics and interactions between precursor molecules and surfaces is critical to the use of those molecules in industrial coating processes and specific applications.

The use of natural compounds for bio-inspired coatings has been an area of interesting research in recent years; for instance, research on polydopamine (pDA) films formed by in-situ oxidative polymerization of dopamine, inspired by catechol-rich compounds found in mussel adhesive proteins, has motivated the study of other versatile coatings from naturally-occurring polyphenols.[1-3] Polyphenols are abundant in plants where they are involved in processes such as plant pigmentation, defense against UV radiation, radical scavenging, and complexation with metal ions.[2] Many polyphenols found in foods are known for their health benefits, e.g., counteracting radicals associated with medical conditions such as cardiovascular disease and cancer,[4] as well as being potential inhibitors to mitigate neurodegenerative diseases.[5, 6] Tannic acid (TA), the focus of this study, is a hydrolysable tannin with a molecular structure consisting of a central glucose ring with 10 galloyl moieties. Tannins are a class of plant-derived polyphenols known for their astringency and ability to bind and precipitate proteins.[1]

The use of TA as a low-cost and very low toxicity (LD_{50}: 2260 mg/kg b. weight (oral rat)[6]) precursor for surface coating opens the door to a wide variety of potential applications in both industrial and medical fields. For example, Gaudreault et al. showed TA as an effective corrosion inhibitor for aluminum oxide (Al_2O_3) surfaces between a pH of 9 to 11.[7] Also, silica and polystyrene surfaces coated with TA have been found to exhibit antioxidant and antibacterial properties, respectively.[2] TA was also recently studied as a candidate to prevent SARS-CoV-2 infectivity due to its ability to bind with high affinity to relevant proteins and inhibit the activity of certain proteases, namely the cellular TMPRSS2 and the viral $3CL^{pro}$ (M^{pro}).[8, 9]

Despite the demonstrated potential of TA to form multifunctional coatings, adsorption of TA in physiological conditions has not been studied for a wide range of concentrations. Ball and Meyer studied the deposition of TA from solution (0.1–50 mg/mL (60 µM–30 mM)) onto gold-coated quartz crystal microbalance (QCM) sensors at a pH of 5.0, at which TA oxidation is minimal.[3] At 20 mg/mL TA, they showed that the QCM negative frequency shift reaches a plateau as TA forms a monolayer within minutes. However, their experimental conditions (very high TA concentration and low pH) are far from human physiological conditions. In contrast, studies of TA adsorption at higher pH found different adsorption behaviours, i.e., prolonged TA deposition and

greater layer thickness. For instance, Sileika et al. reported that coatings spontaneously deposited onto gold surfaces from TA solutions (2 mg/mL (1.2 mM)) in buffered saline, with a pH of 7.8.[2] The authors observed a film thickness of approximately 65 nm after 8 h of incubation in TA solution, and they suspected that oxidation reactions induced the formation of TA coatings.[2] In addition, Geißler et al. studied the formation of TA films on titanium surfaces using QCM with dissipation monitoring (QCMD), at a concentration of 1 mg/mL (0.6 mM) and a pH of 7.8, and observed continuous deposition of TA from solution up to 5 h.[10] Thus, pH and buffer likely play an important role in the adsorption behaviour of TA. Notably, Barrett et al. mentioned that a minor pH change from pH 7.8 to 8 largely decreased the coating-forming ability of TA on a titanium dioxide (TiO_2) substrate, although these different pH levels were also associated with different buffer systems, to which the discrepancy may be attributed.[1] Weber et al. suggested that silicic acid (Si_{aq}) plays a role in the continuous buildup of TA coatings by enabling polymerization via cross-linking or coordination chemistry.[11] Using similar experimental conditions as Geißler et al., the authors[11] reported fast (5 min) formation of a TA monolayer on titanium surfaces at pH 7.8, whereas in the presence of orthosilicic acid TA deposited continuously for 8 h. Their results suggest that TA-Si complexation plays a role in TA multilayer adsorption rather than oxidative polymerization.[11]

In this work, the adsorption of TA to gold surfaces under physiological-like conditions is studied for a wide range of TA concentrations, using QCMD and surface plasmon resonance (SPR). The effects of the experimental conditions on the aggregation and oxidation of TA and the resulting impact on TA adsorption are discussed, supported by UV-Vis spectrophotometry and Fourier Transform Infrared Spectroscopy (FTIR). The adsorption kinetics are investigated, and a theoretical model is proposed to explain the adsorption behaviour and the mechanisms of monolayer and multilayer formation.

Experimental

Materials

TA and phosphate buffered saline (PBS) powder for preparing 0.01 M solutions (pH 7.4, NaCl 138 mM, KCl 2.7 mM) were acquired from Sigma-Aldrich. Sodium hydroxide (NaOH, 2 M) was acquired from Merck. Deionized (DI) water was used in all experiments.

Preparation of TA Solutions

A 1 mM TA stock solution was prepared by dissolving 85 mg of TA in 50 mL of PBS solution. NaOH (2 M) was added dropwise to adjust the pH of the solution to 7.4. The TA stock solution was filtered through a 0.45 μm syringe filter and diluted with filtered PBS to the desired concentrations (1 μM–500 μM). Solutions were used within 5 h of preparation.

QCMD Experiments

Adsorption experiments were done using a QCMD (QSense Explorer, Biolin Scientific). Before each experiment, gold-coated quartz crystal sensors (QSX 301, Biolin Scientific) were cleaned by first pre-rinsing with DI water, then the sensors were submerged in 2% Hellmanex solution while in a sonication bath for 20 min. Next, the sensors were rinsed 10 times with water, rinsed once with ethanol, and rinsed 10 times again with water. Finally, they were dried under compressed air, and placed in a UV/Ozone cleaning chamber for 20 min to remove any remaining contaminants.

At the start of each adsorption experiment, a baseline resonance frequency was established using water. Then, a TA solution was introduced using a peristaltic pump (RegloAnalog, Ismatec) to maintain a flowrate of ~100 μL/min. All experiments were performed at room temperature (22ºC). The resonance frequency and dissipation shift of the crystal were measured continuously as the analyte flowed over the sensor. To determine the adsorption isotherm of tannic acid to the gold surface, solutions with a broad range of TA concentrations (1, 5, 10, 100, 500, and 1000 μM) were tested with this method. Experiments were repeated at least in duplicate for each TA concentration. To study desorption, at the end of some experiments, the analyte was switched from TA solution to PBS and flowed for 10 min.

The Sauerbrey equation[12] describes the relationship between the shift in the resonance frequency of an oscillating quartz crystal and the mass deposited on the surface,

$$\Delta m = -\frac{C}{n}\Delta f \tag{1}$$

where C is the sensitivity constant (17.7 ng/cm^2/Hz for a 5 MHz quartz crystal), n is the overtone number (1, 3, 5, …) and Δf is the shift in the resonance frequency at overtone n.[13] In our experiments, only the third overtone (n = 3) was used.

The Sauerbrey equation assumes a homogeneously distributed mass that does not slip on the sensor surface, and the equation is only valid for rigid molecular systems. The dissipation

factor (ΔD) quantifies dissipative energy losses, which are higher for less rigid adsorbed masses.[7] The mass deposited on the sensor can be considered rigid if the ratio of the dissipation shift to the frequency shift, $-\Delta D/\Delta f$, is smaller than 10^{-7}.[7, 13]

SPR Experiments

For SPR determination of TA adsorption on the gold surface, a P4SPR multi-channel SPR instrument (Affinité Instruments; Montréal, Canada) was used. A non-functionalized gold sensor chip was used. PBS was used as the running buffer for the three sensing channels and the reference channel. 1 mL of various concentrations of TA (1 μM–1 mM) was injected over the three measurement (sensing) channels for 30 min followed by a surface regeneration with two washes of 500 μL of 10mM NaOH. The average time between the preparation of each solution and the injection of each concentration of TA into the SPR was 5 min. All experiments were performed in duplicate. Responses are reported as the average responses of the change in plasmon resonance wavelength (nm) for the three measurement channels (with the response of the reference channel subtracted). Results are reported in arbitrary units; the adsorbed mass was not determined.

Stability of TA Solutions

Conductivity

The conductivity of TA solutions was measured to determine the critical aggregation concentration (CAC) of TA in DI water, as described by Al-Soufi et al.[14] First, a 5 mM TA solution was prepared in DI water. The conductivity of the solution was measured using the conductivity probe of a Metrohm 836 Titrando instrument. Water was added in increments to gradually dilute the solution to a final concentration of 250 μM while measuring the conductivity at each dilution. To measure the conductivity from 0 to 250 μM, aliquots of a 500 μM stock solution were added to 50 mL of water, also while measuring the conductivity at each addition. Straight lines were fit to the plot of conductivity vs. TA concentration at low and high concentrations of TA; the CAC was found from the TA concentration at the intersection of the lines.

UV-Vis Spectrophotometry

The pH- and time-dependent stability of TA solutions was also measured by UV-Vis spectrophotometry. 10 μM TA solutions were prepared in DI water (with an unadjusted pH of 4.5) and in PBS (with pH adjusted to 7.4). The absorbance spectra of the solutions from 200 to 500 nm were measured in a quartz cuvette using a Cary 300 TCA instrument, with measurements taken over a 24 h period.

Fourier Transform Infrared Spectroscopy

The effect of the buffer and pH on the functional groups of TA was studied by FTIR. TA powder, the precursor for all other experimental methods, was dried in a vacuum desiccator for 8 h to remove moisture. In addition, a 1 mM TA solution was prepared in PBS (pH 7.4). This solution was dried in the vacuum desiccator to evaporate water and to minimize exposure to air. The resulting solid and TA precursor powder were characterized using a Bruker Alpha II FTIR spectrometer with attenuated total reflectance (ATR) accessory. The spectra were obtained by combining 32 scans in the wavelength range of 4000 to 400 cm^{-1} with a resolution of 2 cm^{-1}.

Results and Discussion

Estimates of Monolayer Coverage

Here, we estimate the monolayer coverage of TA in terms of mass per unit area. First, we note the mass of one TA molecule (m_{TA}),

$$m_{TA} = \frac{M}{N_A} \tag{2}$$

where M is the molecular weight of TA (1701.2 g/mol), and N_A is Avogadro's number. We estimate the projected area of one TA molecule (A_{TA}) to be approximately 7.3 nm^2, corresponding to the area occupied by a TA molecule adsorbed flat on the surface (Figure S1). Dividing m_{TA} by A_{TA} yields a mass coverage per unit area:

$$\Gamma_{100\%} = \frac{m_{TA}}{A_{TA}} \tag{3}$$

We find that $\Gamma_{100\%}$ = 0.39 mg/m^2, but since a random deposition of spheres forming a monolayer corresponds to only 55% coverage of the available surface area,[15] the estimated monolayer mass of TA per unit area ($\Gamma_{55\%}$) is about 0.21 mg/m^2.

However, the QCMD method measures not only adsorbed particles, but also the bound water molecules within and in between those particles in an adsorbed layer. For example, based on a comparison of SPR and QCMD methods, Solin et al. showed the percentage of water in films detected by QCMD to be more than 50% of the total weight.[16] In another work, we theoretically estimated the water content of adsorbed flat configuration of TA to be approximately 65%.[8] Accounting for a water fraction of 65%, a monolayer of TA including intrinsic and bulk water molecules would correspond to an apparent or effective mass of approximately 0.61 mg/m^2. By comparing the differences in results obtained from QCMD and nanoplasmonic spectroscopy,

Weber et al. estimated a water fraction of ~32% in their TA coatings.[11] However, they studied TA adsorption on titanium surfaces and also worked at a much higher NaCl concentration (600 mM) than in our work.

QCMD Experiments

In the QCMD experiments, frequency and dissipation readings were collected as TA solutions of different concentrations were flowed over a clean gold QCMD sensor. Using this technique, we analyze the adsorption of TA to a gold surface for a wide range of TA concentrations under physiological-like conditions. A negative frequency shift was observed over time for each tested TA concentration, indicating that mass adsorbed to the gold surface. An example of frequency and dissipation readings over the course of one experiment is shown in Figure 1, for a single adsorption experiment with 100 µM TA solution.

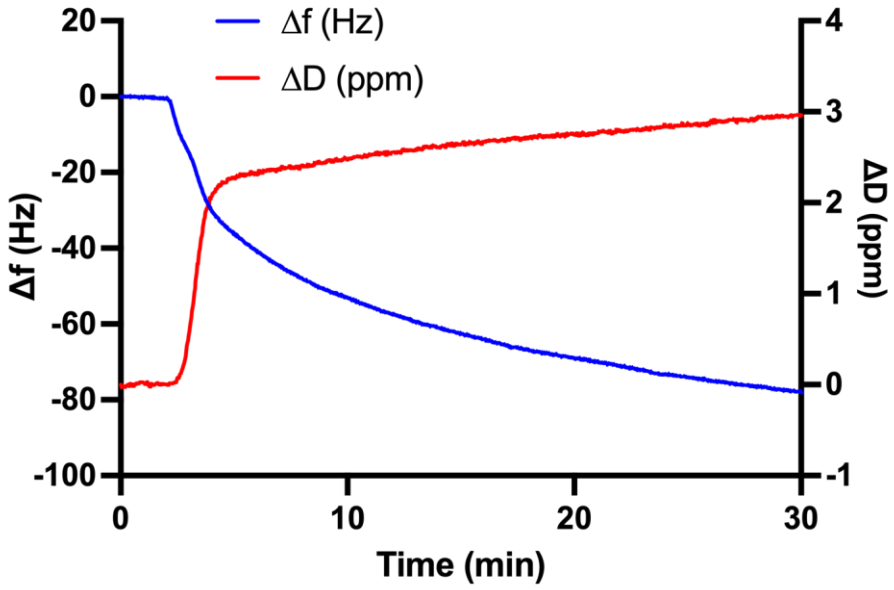

Figure 1: Frequency shift (Δf) and dissipation shift (ΔD) measured by a quartz crystal microbalance with dissipation monitoring (QCMD) during a single adsorption experiment with 100 µM tannic acid (TA) adsorbing on the gold sensor surface.

As shown in Table 1, the negative ratio of dissipation to frequency shifts ($-\Delta D/\Delta f$) was not larger than 10^{-7} throughout the timeframe of our experiments (30 min), so the system could be considered rigid, and the Sauerbrey equation was applied to convert the frequency shifts to values of apparent mass per unit area. The system did not reach equilibrium even when experiments were extended up to 2 h (Figure S2), in agreement with the observations of Geißler et al.,[10] who studied the kinetics of TA deposition on titanium surfaces using QCMD. The authors reported three

coating phases over a 24 hour period: (1) an initial rapid decrease in frequency over 2 h (compact and rigid, where $\Delta f \sim -15$ Hz within the first 30 s, likely the first layer of adsorbed TA), (2) a further decrease in frequency as the dissipation shift increased up to 5 h (softer layers), and finally, (3) a levelling of the frequency shift accompanied by an increase in dissipation (structural changes).[10] At longer times, the Sauerbrey assumption of a rigid molecular system becomes less reliable because of large increases in dissipation. Since we only carry out our experiments to 30 min, we escape a possible skew in our results due to softer layers and lower rigidity. Experiments extended for 2 h showed an increasing $-\Delta D/\Delta f$ ratio, indicating a decrease in rigidity approaching the empirical stiff-viscoelastic limit,[13] though it could still be considered a rigid system.

Table 1: Average ratio of dissipation shift (ΔD) to frequency shift (Δf) over time as measured by a quartz crystal microbalance with dissipation monitoring (QCMD) for various concentrations of tannic acid (TA) adsorbing to the gold sensor surface.

Time	$-\Delta D/\Delta f$					
	1 μM	*5 μM*	*10 μM*	*100 μM*	*500 μM*	*1 mM*
10 min	1.0×10^{-7}	8.0×10^{-8}	5.8×10^{-8}	5.3×10^{-8}	5.7×10^{-8}	5.9×10^{-8}
20 min	8.5×10^{-8}	8.1×10^{-8}	5.0×10^{-8}	4.7×10^{-8}	5.3×10^{-8}	5.3×10^{-8}
30 min	7.4×10^{-8}	8.3×10^{-8}	4.9×10^{-8}	4.8×10^{-8}	4.9×10^{-8}	4.7×10^{-8}
2 h	-	-	7.3×10^{-8}	-	9.6×10^{-8}	2.5×10^{-8}

Figure 2 shows the average apparent mass adsorbed to the gold QCMD sensor over a 30 minute period for each concentration of TA. A delay of approximately 90 s is observed from the start of the experiment to the time at which TA begins to adsorb; time t = 0 s occurs when the feed line is inserted in the TA solution and the pump is started, hence, there is a delay while the TA solution travels through the instrument tubing to reach the sensor chamber.

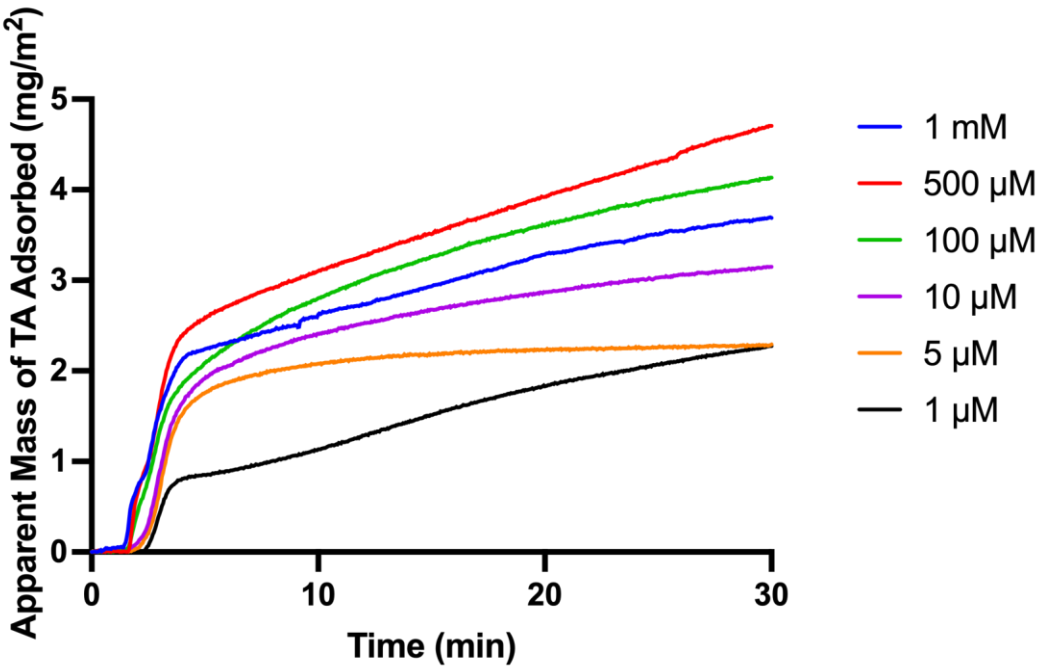

Figure 2: Kinetics of average apparent mass of TA adsorbed on the gold QCMD sensor surface for various concentrations of TA. The apparent mass is the Sauerbrey mass, which includes water molecules within (intrinsic) and between particles in the adsorbed layer.

At the end of some experiments, the analyte was switched to PBS to study desorption, and a slight amount of TA was removed; an average mass change of −3% (−0.2 ± 0.3 mg/m^2) was observed. The frequency shift stabilized within approximately 5 min of buffer flow, suggesting that most of the adsorbed TA is resistant to desorption when the TA solution is replaced with buffer of the same pH.

SPR Experiments

To support the findings by QCMD, SPR was also used to study the adsorption of TA to a gold surface in similar experimental conditions, i.e., a wide range of TA concentrations prepared in PBS with adsorption monitored for a 30 minute period. The SPR signal over this period is shown in Figure 3.

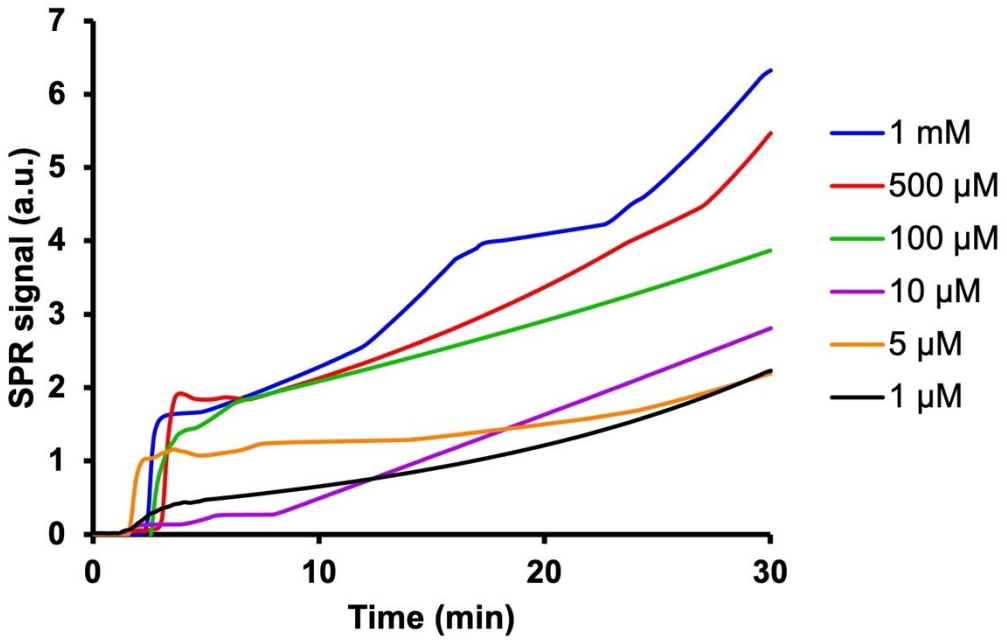

Figure 3: Average surface plasmon resonance (SPR) signal for various concentrations of TA adsorbing on a non-functionalized gold sensor.

As seen in Figure 3, the SPR signal, which correlates to the mass of TA adsorbed to the gold SPR sensor, increases over time and with increasing TA concentration. It is apparent that the general trend of TA adsorption to gold determined by SPR is similar to the QCMD results in Figure 2, with the exception of 1 mM TA—this concentration has the highest mass adsorbed after 30 min with SPR but not with QCMD. This discrepancy, addressed in more detail later in this text, may be due to the difference in time between solution preparation and measurement for the two methods.

Two Phases of Adsorption

Monolayer and multilayer hypothesis

In the QCMD and SPR data in Figure 2 and Figure 3, respectively, two phases of adsorption can be observed—fast initial adsorption, followed by a slower steady adsorption phase occurring within a few minutes of the start of adsorption. This transition suggests a shift in modes of adsorption, e.g., from monolayer to multilayer adsorption and/or molecular rearrangement of TA. The dissipation signal measured by QCMD also follows this trend, with a rapid increase in ΔD followed by a transition to a slower steady increase after a few minutes (Figure 1).

Interestingly, in Figure 2 we notice that the value of adsorbed mass at which adsorption transitions from fast to slow is distinctly different depending on the TA concentration. If this is indeed a transition from monolayer to multilayer coverage, then this transition value corresponds to the mass of the monolayer. We can better visualize this observation by plotting the adsorbed mass at the transition point, determined from the intersection of the first and second slopes of each curve in Figure 2, as a function of TA concentration. This plot of mass at the intersection of the slopes, which we refer to as the "monolayer mass," is shown in Figure 4 (squares). For comparison, the QCMD mass of TA adsorbed at t = 30 min is also plotted against TA concentration (circles). Both of these curves are akin to adsorption isotherms; however, these "isotherms" are only approximate as the system did not reach equilibrium at the end of the first phase nor by the end of the experiment. Despite this, Figure 4 suggests a high-affinity isotherm in which the initial slope of adsorbed mass vs. concentration is very steep, but plateaus at higher concentrations.

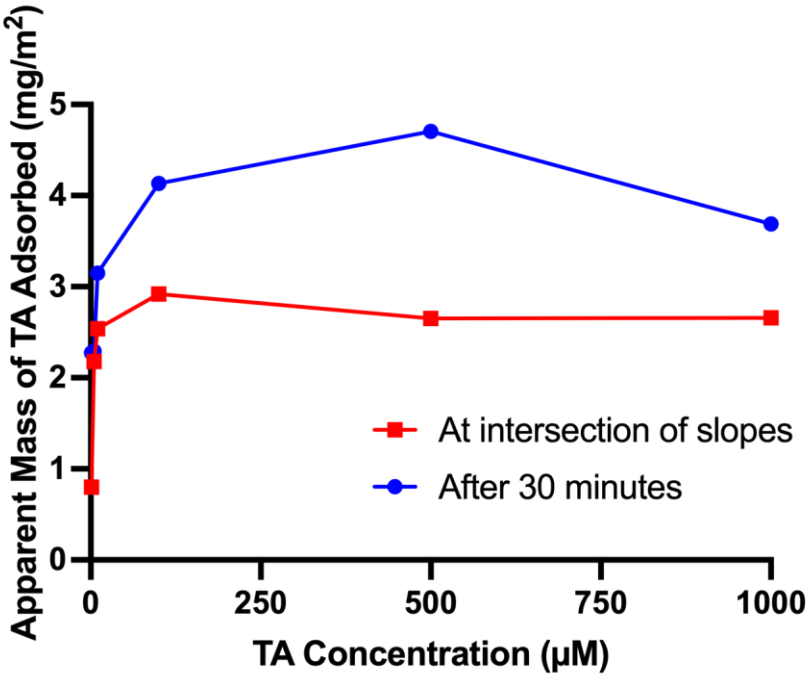

Figure 4: Adsorption "isotherm," apparent mass of TA adsorbed as a function of TA concentration, by two methods: at the intersection point between the first and second slopes of the QCMD adsorbed mass vs. time curves (Figure 2) (squares), and after 30 min of adsorption (circles).

Figure 4 shows that at the lowest TA concentration tested (1 μM), the intersection of the slopes (i.e., the monolayer) occurs at approximately 0.8 mg/m^2, close to our theoretical estimate of 0.61 mg/m^2 for TA molecules in a flat configuration. However, at concentrations above 5 μM,

the monolayer occurs around 2.2–2.9 mg/m^2, a much higher figure than our estimate. These different monolayer densities may be explained by the way TA molecules are arranged on the surface. Considering that TA is a roughly two-dimensional molecule, it is possible that it adsorbs with different configurations on the surface; also, the central β-D-glucose ring can be either in a chair or boat/skew-boat conformation (see Haddad & Gaudreault et al., Figure S17),[8] allowing flexibility in the molecular structure. At low TA concentrations, the kinetics of adsorption are slow, so TA molecules may have time to find a favourable flat configuration on the surface. Thus, the monolayer could occur at a lower mass per unit area. On the other hand, at high TA concentrations, the kinetics of adsorption may be much faster than reorientation, so TA molecules would adsorb edge-on in a denser configuration as they cannot reorient to lay flat. This proposed model is illustrated in Figure 5.

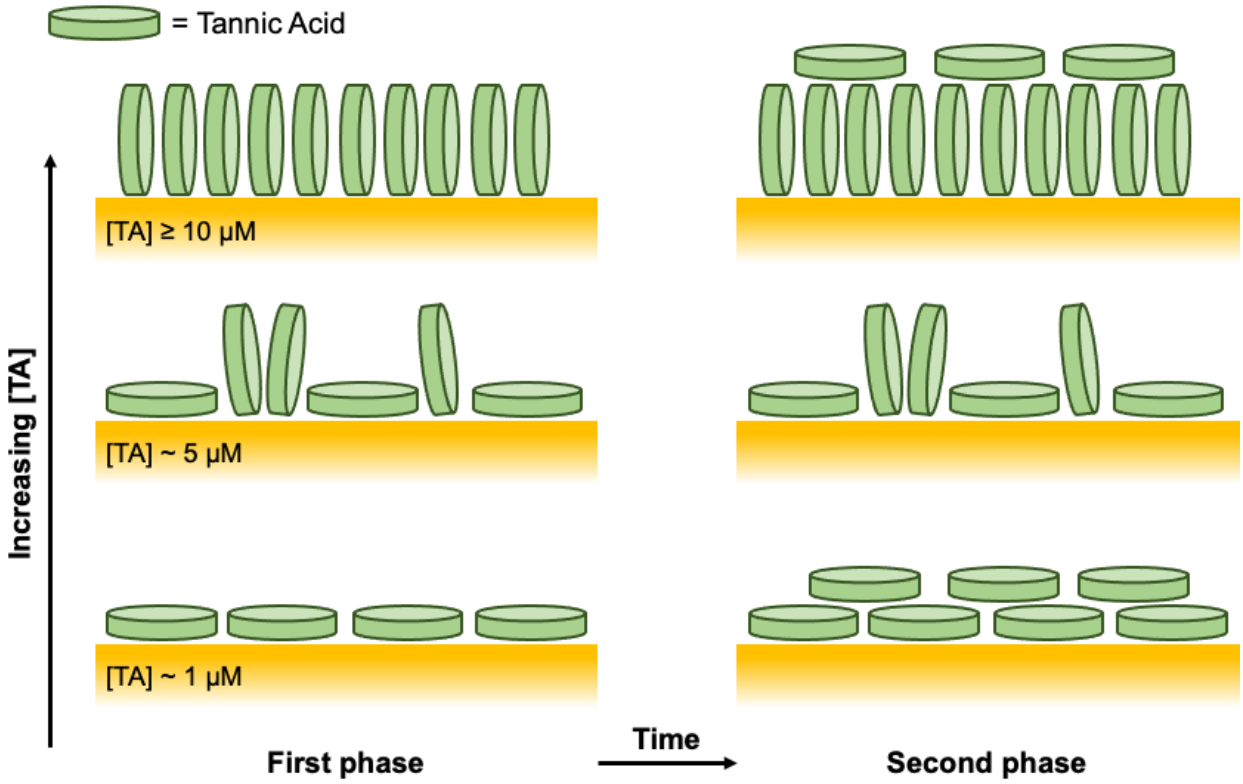

Figure 5: Illustration of the proposed scheme of adsorbed TA conformation dependent on concentration. The first phase corresponds to the first adsorption rate, in which a monolayer adsorbs. The second phase corresponds to the second adsorption rate, in which bi- and multilayers adsorb. At higher TA concentrations, molecules adsorb mainly edge-on in a denser configuration in the first phase, whereas at lower TA concentrations, molecules have time to rearrange and adopt a flat conformation on the surface. Between these regimes (e.g.,

approximately 5 μM), TA may adsorb in a mix of flat and edge-on orientations in the first phase; multilayer adsorption on this "rough" surface is difficult.

If the transition between flat and edge-on monolayer arrangement happens between 1 μM and 10 μM, then at 5 μM, a mixture of flatly adsorbed and edge-on adsorbed molecules (Figure 5) may be possible due to a competition in kinetics. This would lead to a relatively "rough" monolayer, making it difficult for TA molecules to adsorb on top, and reducing the adsorption rate in the second phase. Indeed, as can be seen in Figure 2, the slope of the curve in the second phase of adsorption is very low for 5 μM TA; bilayer adsorption is barely observable in the timeframe of our QCMD experiments. The SPR results in Figure 3 also show a distinct flattening of the 5 μM adsorption curve after the transition point, although eventually the signal increases again towards 30 min. This could be due to rearrangement of the rough monolayer to one on which a bilayer can begin to adsorb.

Furthermore, a shoulder is visible in the QCMD adsorbed mass vs. time curves (Figure 2) for some TA concentrations; coincidentally, this shoulder occurs between approximately 0.6 and 1.0 mg/m^2, i.e., near the mass of the monolayer in flat configuration. The shoulder may be due to a slight rearrangement of adsorbed TA, e.g., molecules adsorb first at a certain angle but quickly become more aligned and densely packed.

Adsorbed mass after 30 minutes

In addition to the plot of monolayer mass, the other curve in Figure 4 shows the QCMD mass adsorbed after 30 min plotted as a function of TA concentration (circles). Interestingly, Figure 4 shows that at 1 mM concentration, a smaller amount of TA is adsorbed after 30 min than for the lower concentrations of 500 and 100 μM TA. This is also apparent in Figure 2 where the curve of adsorbed mass at 1 mM TA falls below 500 and 100 μM. This could be attributed to extensive aggregation in the TA solution at high concentration. At 1 mM, a significant amount of TA may be in the form of large aggregates, which effectively depletes the amount of TA monomer in solution available to adsorb, and causes this concentration to deviate from the trend of increasing adsorbed mass at 30 min. The likelihood and conditions for TA aggregation are discussed in the following sections. However, this anomaly is not observed in the SPR results (Figure 3); the difference between the two methods may be attributed to the time delay between TA solution preparation and experimental measurement. SPR measurements were taken within 5 min of preparation of the TA solution, whereas with QCMD the TA solution was used within 30 min to

up to 5 h. The shorter time delay for SPR measurement may have prevented the formation of large aggregates in the highest-concentration TA solution, and therefore, the SPR signal after 30 minutes correlates with TA concentration.

Despite the slight effect of concentration, overall, it can be said that the amount of TA adsorbed after 30 min is effectively quite similar for TA concentrations of ~100 μM and higher. In other words, Figure 4 (circles) shows that increasing TA concentration above ~100 μM has a relatively small effect on the amount of TA adsorbed on a 30 minute timescale. This may be useful information for applications where a coating of TA may be desired at the lowest feasible concentration, e.g., in human physiological conditions. After 30 min, we find an apparent mass of TA adsorbed of approximately 3.7–4.7 mg/m^2 (average: 4.2 mg/m^2) at TA concentrations above 100 μM. This is near the reported 3.77 ± 0.21 mg/m^2 by Weber et al. (~300 μM TA, pH 7.8), which they observed as a stable coating after 5 min.[11] On the other hand, Geißler et al. observed a coverage of approximately 16 mg/m^2 after 30 min (~600 μM TA, pH 7.8, based on their reported Sauerbrey thickness of ~13 nm at 30 min),[10] and their coatings continued to build up as they did in our work. However, both of these studies were performed in bicine buffer with 600 mM NaCl,[10, 11] so the discrepancies between these studies and our work could be attributed to the differences in buffer and salt concentration.

Adsorption rate in first and second phases

In addition to the two "isotherms" in Figure 4, investigating the two distinct adsorption rates of TA may reveal insights about the formation of TA coatings. The two distinct slopes of each curve in Figure 2, corresponding to the "first" and "second" adsorption rates for two phases of adsorption, were approximated as straight lines. Figure 6 plots the adsorption rates determined from the steepest initial slope and second observable slope of each QCMD adsorbed mass vs. time curve as a function of TA concentration. The first adsorption rate tends to increase with TA concentration, while the second adsorption rate is quite low at all TA concentrations, i.e., less than 0.075 mg/m^2/min.

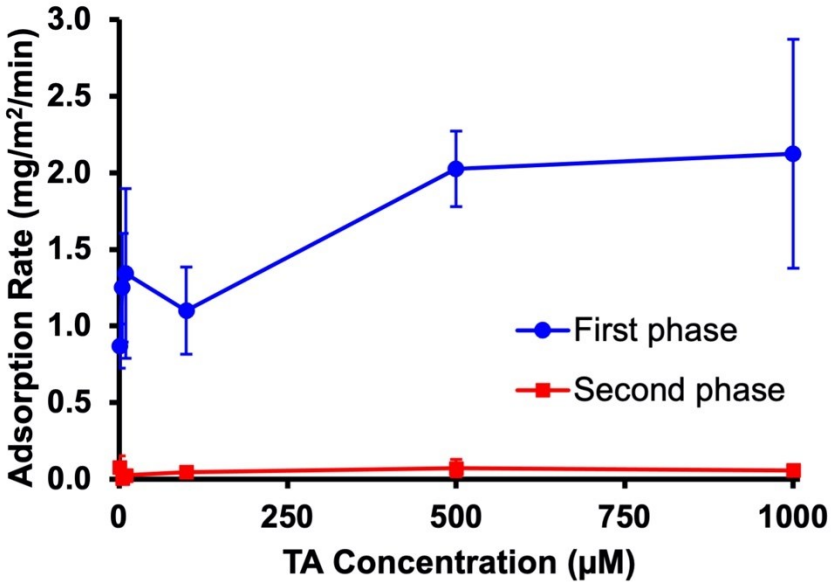

Figure 6: Rate of the first (circles) and second (squares) phases of TA adsorption as a function of concentration, determined by taking the slopes of the adsorbed mass vs. time curves (Figure 2) for the two distinct phases.

The first adsorption rate, in which a monolayer of TA forms on the gold surface, generally increases with TA concentration. However, this increase is quite small compared to the theory, which predicts that initial adsorption rate should scale proportionately with adsorbate concentration, i.e., a 1000-fold increase in the initial slope from 1 μM to 1 mM TA. This discrepancy may be attributed to aggregation in the TA solution limiting the amount of TA able to adsorb. As will be explained in the following section, it is likely that aggregation is present in our TA solutions due to the influence of buffer salts, the slightly alkaline pH, and the presence of dissolved oxygen-induced oxidation. If TA aggregates are unable to adsorb (or are easily desorbed by the shear forces exerted on them in the flow cell), the lowered effective concentration of TA monomers may result in the adsorption rate increasing slightly with concentration, but not to the full extent expected.

The second adsorption rate, as seen in Figure 6, is quite low and similar regardless of TA concentration. In this phase, TA is undergoing bi- and multilayer formation. TA adsorption on an existing TA layer may be a less favourable process than adsorption on gold, i.e., the adsorption efficiency of TA onto TA is less than the adsorption efficiency of TA onto gold. As a result of aggregation, the number of individual TA molecules able to adsorb on the first layer is approximately constant regardless of concentration, resulting in the absence of a discernible

concentration dependence. For a TA concentration of 5 μM, the adsorption efficiency is very low, which was attributed earlier to a mix of TA molecule orientations in the monolayer.

Aggregation and Stability of TA Solutions

The instability of TA in solution under certain conditions, likely leading to aggregation, may explain some observations in the experimental data. TA is known to self-associate and to aggregate at higher concentrations.[17] The minimum concentration that causes rapid self-association of a dispersion is referred to as the critical aggregation concentration (CAC). Reports of the CAC of TA vary; for instance, using laser light scattering, TA aggregates have been detected in solutions above a concentration of 1.8 mM (3 g/L), though the hydrodynamic diameter increased significantly outside the pH range of 3–7.5.[17] Our own conductivity measurements of TA in DI water suggest a CAC of approximately 0.7 mM (Figure S3) following a method for the determination of the critical micelle concentration (CMC) from conductivity data.[14]

However, various factors such as pH, salt concentration, and/or oxidation may induce TA self-association at lower concentrations. First, although the reported pKa of TA varies (e.g., from 6 to 8.5),[18] An and Dultz showed that the phenolic hydroxyl groups of TA are "almost completely dissociated" at pH 7.[19] Deprotonated TA solutions at pH 7.4 (0.3 mM (0.5 mg/mL), 100 mM NaCl) were found to undergo structural rearrangements when stored overnight, even in the absence of light and air, indicating an effect of higher pH on TA stability.[20] Second, salt-induced aggregation may occur more easily at a pH at which TA is less stable, thus high salt concentrations could further decrease the CAC. Geißler et al., working at a higher pH and salt concentration than in our work (0.6 mM (1 mg/mL) TA solutions, pH 7.8, 600 mM NaCl), observed a discontinuation in TA deposition after ∼5 h of solution flow, correlating with the precipitation of large aggregates and a change in colour in the coating solution.[10] The authors suggested that sufficiently large TA precipitates could not continue attaching to the existing coating.[10] Finally, oxidation of polyphenols is well established to occur in alkaline conditions in the presence of dissolved oxygen.[2, 10, 11, 20-22] Oxidation of phenolic hydroxyl groups can lead to greater intermolecular interactions and/or bonding[11] and is suspected to play a role in the buildup of polyphenol coatings.[2, 10, 11] Considering the effects of pH, salt, and oxidation, the CAC of tannic acid in our experimental conditions (pH 7.4, PBS with 138 mM NaCl) is likely to occur at a lower concentration than in DI water (~0.7 mM). Unsurprisingly, we observed visually that TA solutions are not stable in PBS at pH 7.4; e.g., higher concentration TA stock solutions formed precipitates and changed colour from

a transparent light brown to greenish and murky when stored longer than one day at room temperature.

Furthermore, in the surfactant concentration model described by Al-Soufi and Novo, the CMC may not occur at a sharp point, but rather the transition from surfactant molecules to micelles occurs in a transition region.[23] Within this region, the concentrations of both micelles and monomers increase with total concentration. This CMC model may be extended to the CAC for non-surfactant solutions.[23] The transition region of single TA molecules to aggregates is also quite broad (Figure S3). As concentration increases, TA may begin to form aggregates alongside a diminished increase in TA monomer concentration. This would explain the effects we observe on the initial adsorption rate—the presence of aggregates unable to adsorb could decrease the "effective" TA concentration, causing a smaller-than-expected increase in adsorption rate with concentration. Thus, similar to micelle solutions, where the concentration of individual surfactant molecules depends weakly on concentration above the CMC, the concentration of individual TA molecules depends weakly on concentration above the CAC.

UV-Vis Spectrophotometry

To confirm these suspected structural changes in TA molecules which may contribute to aggregation, TA solutions were studied by UV-Vis spectrophotometry over a 24 hour period. The spectra of TA solutions prepared in DI water (pH 4.5) and PBS (pH 7.4) are shown in Figure 7.

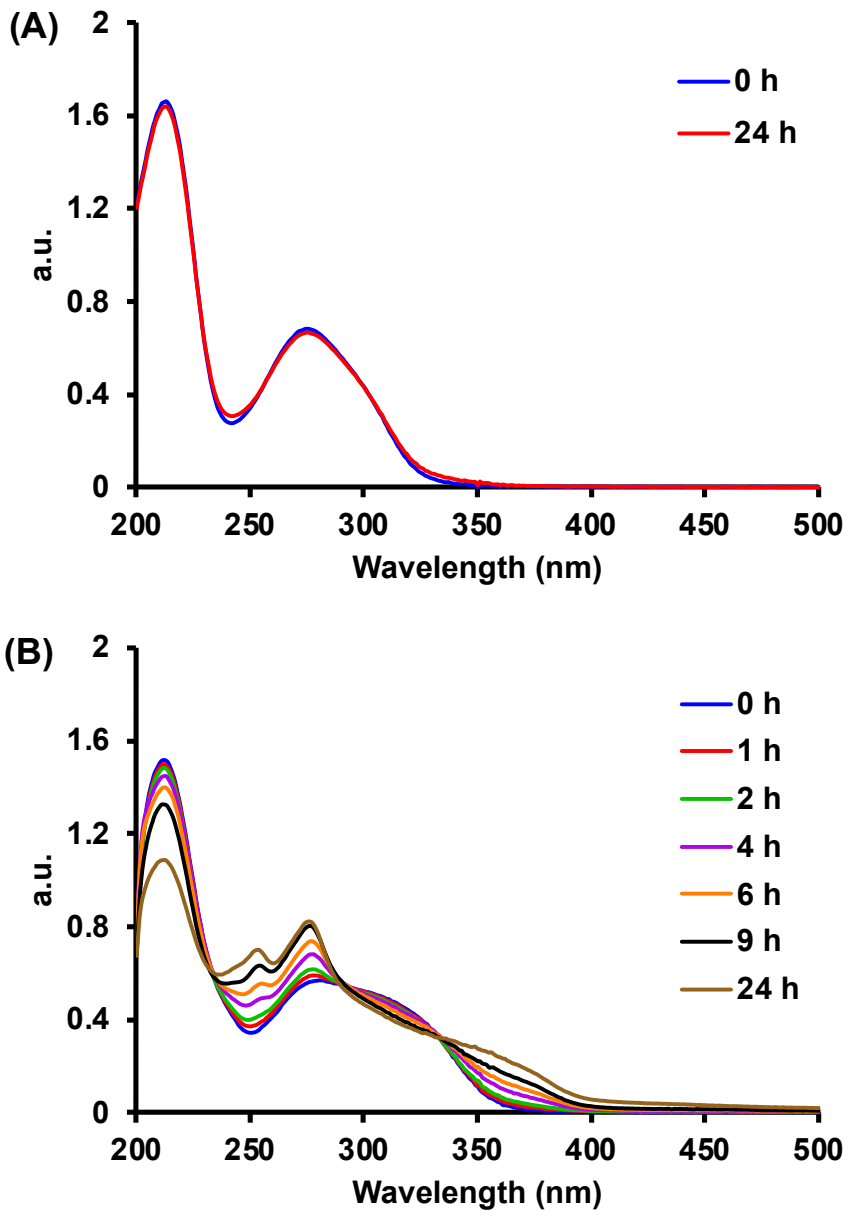

Figure 7: UV-Vis spectra of a 10 µM TA solution at various time intervals after solution preparation, (A) in deionized (DI) water, pH 4.5, and (B) in phosphate buffered saline (PBS), pH 7.4

At pH 4.5 the TA solution appears stable, with essentially no changes in the UV-Vis spectrum 24 h after solution preparation (Figure 7A). Absorbance peaks are present at 212 and 275 nm, the latter corresponding to non-ionized phenolic groups.[20] On the other hand, the pH 7.4 solution shows an additional absorption band at ~325 nm immediately after preparation (t = 0 h, Figure 7B), which has been previously observed in the literature and attributed to deprotonated hydroxyl groups.[20-22] Over time, the intensity of the peak at 275 nm increases in intensity whereas

the peak at 325 nm decreases. Similarly, in an oxidation study of TA at pH 7.8, Weber et al. observed an increase in the intensity of a peak at 280 nm and a decrease at 320 nm.[11] Although the peak wavelengths do not match perfectly (possibly due to the slight difference in pH and different buffers used), the similar shifts observed in Figure 7B suggest that the changes observed over time are also due to TA oxidation. Furthermore, Figure 7B shows the emergence of new peaks at 253 nm and ~375 nm over time, much like the emergent peaks at 255 and 370 observed by Liu et al. under similar conditions.[20] In another study, Erel-Unal et al. suggested that peaks emerging at 263 nm and 360 nm in the spectra of pH >7 TA solutions were associated with oxidation products of TA.[22]

Overall, the observed overnight changes in the absorbance spectra of the TA solution at pH 7.4 indicate instability and possible oxidation of TA, which could contribute to some degree of aggregation even at short times after solution preparation. This stands in contrast with the apparent stability of TA solutions at pH 4.5 and highlights the effect of pH and buffer on the properties of TA.

Fourier Transform Infrared Spectroscopy

To support the UV-Vis results, TA powders were also analyzed by FTIR to determine the effects of the buffer and pH on the functional groups of TA. The FTIR spectra in Figure 8 compare the TA precursor powder and TA powder dried from a 1 mM solution prepared in PBS, pH 7.4.

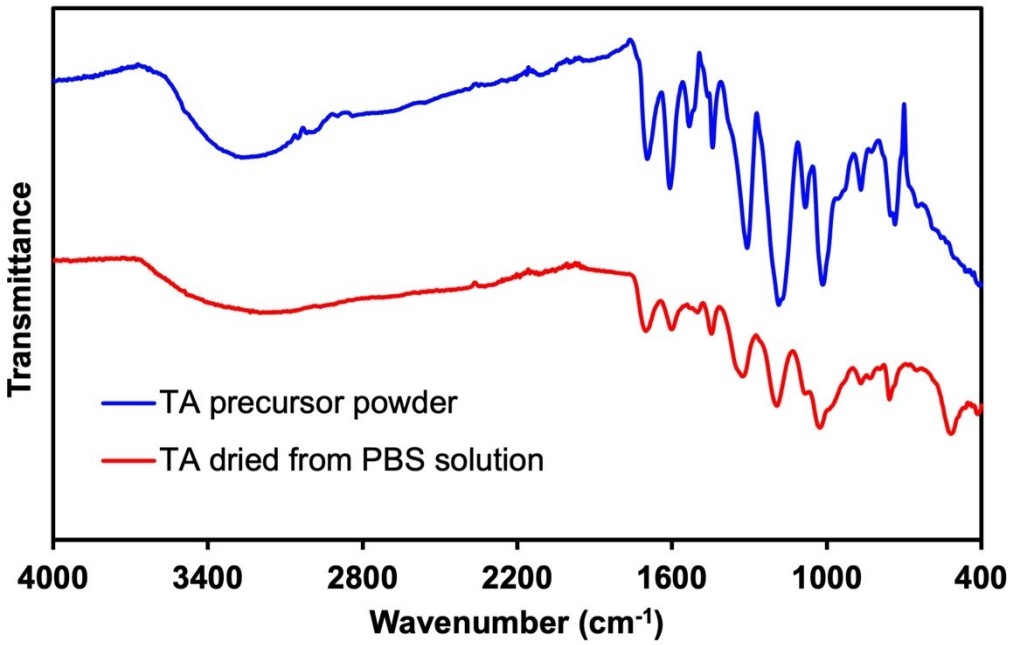

Figure 8: FTIR spectra of TA precursor powder, the material used to prepare TA solutions for all other experiments, and TA dried from PBS solution, prepared by evaporating a 1 mM TA solution that had been prepared in PBS buffer at pH 7.4.

In both samples, the spectra in Figure 8 show the characteristic peaks of TA, namely, at 1612 cm^{-1} for C=C stretching vibrations of aromatic rings, 1317 cm^{-1} for aromatic C–OC stretching and aromatic C–O–H bending, 1190 cm^{-1} for O–CO stretching, and 1020 cm^{-1} for C–O–C asymmetric stretching.[24, 25] The peak at about 1705 cm^{-1} corresponds to C=O stretching of carboxylic acid groups and/or ester links (–C(O)O–)[24-26] and commonly appears in the FTIR spectrum of TA,[10, 25, 27] suggesting some possible degree of oxidation in both samples.

In the sample dried from PBS solution, the intensity of the intermolecular hydrogen bonded O–H stretching vibration at about 3250 cm^{-1} is lower and the band is broader,[24] while the relative intensity of the C=O peak at 1705 cm^{-1} is increased compared to its neighbouring peak. These shifts in intensity suggest increased TA oxidation in the sample dried from PBS solution at alkaline pH.[25, 28] This difference is not attributed to different moisture content, as both samples were equivalently dried in a desiccator before measurement, therefore their moisture content should be similarly low.

Mechanism of TA-Gold Interaction

Using both QCMD and SPR, we observe that the first layer of TA adsorbs readily to the gold surface in the experimental conditions used. Several types of TA-gold interactions are possible depending on the functional groups of TA. As described previously, it is likely that TA is oxidized to some extent due to the mildly alkaline buffer and the presence of dissolved oxygen. UV-Vis spectrophotometry and FTIR data support the suggested structural changes to TA in these conditions, e.g., the conversion of phenolic hydroxyl groups to carbonyl groups, and/or the presence of hydrolysis products.

Interactions between oxidized TA and gold surfaces have been characterized in the literature in the context of gold nanoparticle (NP) synthesis, as TA is sometimes used as a reducing and stabilizing agent in the synthesis of metal NPs.[27, 29, 30] In TA-mediated metal NP synthesis, TA participates in both reduction and subsequent stabilization of metal ions (such as Au^{3+})—phenolic groups are oxidized during metal ion reduction, and carboxyl groups or oxidized catechol moieties on TA are proposed to attach to the metal surface.[27, 29, 30] Although Au ions are not being reduced in this study, since some oxidized or partially-oxidized forms of TA are likely to exist in solution under our experimental conditions, adsorption of TA to the gold surface can be expected to occur through a similar process. As for unoxidized TA, adsorption to the gold surface is also possible through dispersion forces.

Conclusions

Natural, plant-based molecules are an interesting avenue for functional coating research with green chemistry. In this work, we studied the adsorption behaviour of TA, an inexpensive, naturally available polyphenol, following in the wake of recent advances in functional wet coatings of pDA and similar polyphenols. We demonstrated the ability of TA to form coatings on gold surfaces in physiological-like conditions from a wide range of TA concentrations.

We confirmed that TA is capable of building up multilayers upon an initial monolayer in mildly alkaline pH conditions. The monolayer density was found to increase with TA concentration; a plausible explanation is that at low concentrations TA adsorbs in a flat configuration, whereas at high concentrations TA adsorbs edge-on. This increases the apparent monolayer coverage (including adsorbed water) from 0.8 to about 2.5 mg/m^2. After monolayer coverage TA continues to adsorb, forming bi- and multilayers. The initial kinetics did not follow

the theory which predicts adsorption rates proportional to concentration. This is ascribed to self-association of TA—increasing TA concentration leads to an increase in the number of TA aggregates, alongside only a slight increase in the number of freely dissolved TA molecules. This explains the small increase in initial adsorption rate, provided the aggregates do not adsorb under our experimental conditions. Also, after 30 min of coating in our experimental conditions, the apparent adsorbed mass of TA was nearly the same at concentrations above 100 μM; therefore, high coating solution concentrations, which may be more harsh or pose other limitations depending on the application, are not needed to achieve TA coatings at this timescale.

This work is limited to the study of gold surfaces, which are common in electronics, electrochemistry, nanotechnology, and some medical implants. We focused only on physiological-like coating conditions, namely, pH 7.4 in buffered saline, which points our findings toward biological applications and similar uses with mild conditions. Moreover, the use of polyphenols for functional coatings is promising, and the adsorption behaviour of similar species on a wide variety of surfaces opens the door to a myriad of applications. Thus, future work should continue to elucidate the adsorption and film-forming behaviour of tannic acid and other polyphenols under various conditions for different applications of green chemistry.

Supporting Information: Modeled structures of TA, results of 2 hour adsorption experiments, and conductivity study of TA solutions.

Acknowledgements: We thank Professor Nathalie Tufenkji (McGill University) and her group members for access to the QCMD. This work is supported, in part, by an Alliance grant from the Natural Sciences and Engineering Research Council of Canada (NSERC).

References

1. Barrett, D. G.; Sileika, T. S.; Messersmith, P. B., Molecular diversity in phenolic and polyphenolic precursors of tannin-inspired nanocoatings. *Chem. Commun.* **2014,** *50* (55), 7265-7268.

2. Sileika, T.; Barrett, D.; Zhang, R.; Lau, K. H. A.; Messersmith, P. B., Colorless Multifunctional Coatings Inspired by Polyphenols Found in Tea, Chocolate, and Wine. *Angew. Chem., Int. Ed. Engl.* **2013,** *52*.

3. Ball, V.; Meyer, F., Deposition kinetics and electrochemical properties of tannic acid on gold and silica. *Colloids Surf., A* **2016,** *491*, 12-17.

4. Ali, E. E.; Elmakki, M. O.; Gavette, M. L.; Doyle, B. J.; Timpe, S. J., Protein Binding Characteristics of the Principal Green Tea Catechins: A QCM Study Comparing Crude Extract to Pure EGCG. *Biochem. Res. Int.* **2019,** *2019*, 6154170.

5. Ramassamy, C., Emerging role of polyphenolic compounds in the treatment of neurodegenerative diseases: a review of their intracellular targets. *Eur. J. Pharmacol.* **2006,** *545* (1), 51-64.

6. Gaudreault, R.; Hervé, V.; van de Ven, T. G. M.; Mousseau, N.; Ramassamy, C., Polyphenol-Peptide Interactions in Mitigation of Alzheimer's Disease: Role of Biosurface-Induced Aggregation. *J. Alzheimer's Dis.* **2021,** *81* (1), 33-55.

7. Gaudreault, R.; Dargahi, M.; Weckman, N.; Olsson, A.; Omanovic, S.; Schwartz, G.; Tufenkji, N., Green Chemistry – with a Special Emphasis on Tannin Molecules for the Protection of Aluminum Boilers. In *AWT 2013 Annual Convention and Exposition*, Uncasville, CT, USA, 2013.

8. Haddad, M.; Gaudreault, R.; Sasseville, G.; Nguyen, P. T.; Wiebe, H.; van de Ven, T. G. M.; Bourgault, S.; Mousseau, N.; Ramassamy, C., Molecular Interactions of Tannic Acid with Proteins Associated with SARS-CoV-2 Infectivity. *Int. J. Mol. Sci.* **2022,** *23* (5), 2643.

9. Wang, S.-C.; Chen, Y.; Wang, Y.-C.; Wang, W.-J.; Yang, C.-S.; Tsai, C.-L.; Hou, M.-H.; Chen, H.-F.; Shen, Y.-C.; Hung, M.-C., Tannic acid suppresses SARS-CoV-2 as a dual inhibitor of the viral main protease and the cellular TMPRSS2 protease. *Am. J. Cancer Res.* **2020,** *10* (12), 4538-4546.

10. Geißler, S.; Barrantes, A.; Tengvall, P.; Messersmith, P. B.; Tiainen, H., Deposition Kinetics of Bioinspired Phenolic Coatings on Titanium Surfaces. *Langmuir* **2016,** *32* (32), 8050-8060.

11. Weber, F.; Barrantes, A.; Tiainen, H., Silicic Acid-Mediated Formation of Tannic Acid Nanocoatings. *Langmuir* **2019,** *35* (9), 3327-3336.

12. Sauerbrey, G., Verwendung von Schwingquarzen zur Wägung dünner Schichten und zur Mikrowägung. *Z. Phys.* **1959,** *155* (2), 206-222.

13. Lapointe, M.; Farner, J. M.; Hernandez, L. M.; Tufenkji, N., Understanding and Improving Microplastic Removal during Water Treatment: Impact of Coagulation and Flocculation. *Environ. Sci. Technol.* **2020,** *54* (14), 8719-8727.

14. Al-Soufi, W.; Piñeiro, L.; Novo, M., A model for monomer and micellar concentrations in surfactant solutions: Application to conductivity, NMR, diffusion, and surface tension data. *J. Colloid Interface Sci.* **2012,** *370* (1), 102-110.

15. Dabros, T.; van de Ven, T. G. M., Collision-Induced Dispersion of Droplets Attached to Solid Particles. *J. Colloid Interface Sci.* **1994,** *163* (1), 28-36.

16. Solin, K.; Beaumont, M.; Rosenfeldt, S.; Orelma, H.; Borghei, M.; Bacher, M.; Opietnik, M.; Rojas, O., Self-Assembly of Soft Cellulose Nanospheres into Colloidal Gel Layers with Enhanced Protein Adsorption Capability for Next-Generation Immunoassays. *Small* **2020,** *16*, 202004702.

17. Dultz, S.; Mikutta, R.; Kara, S. N. M.; Woche, S. K.; Guggenberger, G., Effects of solution chemistry on conformation of self-aggregated tannic acid revealed by laser light scattering. *Sci. Total Environ.* **2021,** *754*, 142119.

18. Abouelmagd, S. A.; Abd Ellah, N. H.; Amen, O.; Abdelmoez, A.; Mohamed, N. G., Self-assembled tannic acid complexes for pH-responsive delivery of antibiotics: Role of drug-carrier interactions. *Int. J. Pharm.* **2019,** *562*, 76-85.

19. An, J.-H.; Dultz, S., Adsorption of tannic acid on chitosan-montmorillonite as a function of pH and surface charge properties. *Appl. Clay Sci.* **2007,** *36* (4), 256-264.

20. Liu, F.; Kozlovskaya, V.; Zavgorodnya, O.; Martinez-Lopez, C.; Catledge, S.; Kharlampieva, E., Encapsulation of anticancer drug by hydrogen-bonded multilayers of tannic acid. *Soft Matter* **2014,** *10* (46), 9237-9247.

21. Chariyarangsitham, W.; Krungchanuchat, S.; Khuemjun, P.; Pilapong, C., Effect of advanced oxidation and amino acid addition on antioxidant capability, iron chelating property and anti-cancer activity of tannic acid. *Arabian Journal of Chemistry* **2021,** *14* (9), 103312.

22. Erel-Unal, I.; Sukhishvili, S. A., Hydrogen-Bonded Multilayers of a Neutral Polymer and a Polyphenol. *Macromolecules* **2008,** *41* (11), 3962-3970.

23. Al-Soufi, W.; Novo, M., A Surfactant Concentration Model for the Systematic Determination of the Critical Micellar Concentration and the Transition Width. *Molecules* **2021,** *26* (17).

24. Silverstein, R. M.; Webster, F. X.; Kiemle, D. J., *Spectrometric identification of organic compounds*. 7th ed. / ed.; John Wiley & Sons: Hoboken, NJ, 2005.

25. Ranoszek-Soliwoda, K.; Tomaszewska, E.; Socha, E.; Krzyczmonik, P.; Ignaczak, A.; Orlowski, P.; Krzyzowska, M.; Celichowski, G.; Grobelny, J., The role of tannic acid and sodium citrate in the synthesis of silver nanoparticles. *J. Nanopart. Res.* **2017,** *19* (8), 273.

26. Cowen, S.; Al-Abadleh, H. A., DRIFTS studies on the photodegradation of tannic acid as a model for HULIS in atmospheric aerosols. *Physical Chemistry Chemical Physics* **2009,** *11* (36), 7838-7847.

27. Aswathy Aromal, S.; Philip, D., Facile one-pot synthesis of gold nanoparticles using tannic acid and its application in catalysis. *Physica E: Low-dimensional Systems and Nanostructures* **2012,** *44* (7), 1692-1696.

28. Yang, J.; Li, M.; Wang, Y.; Wu, H.; Zhen, T.; Xiong, L.; Sun, Q., Double Cross-Linked Chitosan Composite Films Developed with Oxidized Tannic Acid and Ferric Ions Exhibit High Strength and Excellent Water Resistance. *Biomacromolecules* **2019,** *20* (2), 801-812.

29. Ahmad, T., Reviewing the Tannic Acid Mediated Synthesis of Metal Nanoparticles. *Journal of Nanotechnology* **2014,** *2014*, 954206.

30. Savin, R.; Benzaamia, N.-O.; Njel, C.; Pronkin, S.; Blanck, C.; Schmutz, M.; Boulmedais, F., Nanohybrid biosensor based on mussel-inspired electro-cross-linking of tannic acid capped gold nanoparticles and enzymes. *Materials Advances* **2022,** *3* (4), 2222-2233.

Bridging text between Chapter 2 and Chapter 3

In the previous chapter, QCMD was used as the primary experimental technique to study the adsorption of TA to a gold surface. QCMD is a technique well-suited to small scale processes, as it allows for remarkably precise measurement of mass deposition. This precision allowed for a mechanism of mono- and bilayer formation to be proposed. This was complimented with an estimate of adsorbed monolayer mass based on surface area calculations.

Gold, as a chemically inert metal, is used extensively in scientific research. However, the practical applications of gold in very commonplace materials are limited. Thus, to focus on materials where the unique properties of TA would be a useful asset, we turn from inorganic to organic substrates and focus on the adsorption of TA to KP in Chapter 3.

In the following chapter, different characterization techniques are used, focusing more on the practical aspects of developing new biorenewable materials. The TA adsorption capacity of KP is determined with mass balance techniques by measuring solution concentrations using UV-Vis spectrophotometry and dry mass quantification. The bench-scale experimental setup translates well to prototyping and scale-up for practical applications, demonstrated through the incorporation of TA into paper handsheets. These results can directly be used in the future development and characterization of KP-based paper modified with TA.

Chapter 3: Adsorption of tannic acid onto kraft pulp fibers

Hannah Wiebe [1], Mohammadhadi Moradian [1], Theo G.M. van de Ven [1] *

[1] Department of Chemistry, Quebec Centre for Advanced Materials, Pulp & Paper Research Centre, McGill University, 3420 University Street, Montreal, QC H3A 2A7, Canada
* Correspondence: theo.vandeven@mcgill.ca

Abstract

In the healthcare field, many strategies are employed to prevent against infections and the transmission of pathogens. The introduction of antimicrobial properties to materials such as wound dressings, hospital surfaces, and personal protective equipment is one strategy used to improve healthcare outcomes and is the subject of a breadth of recent research. Tannic acid (TA), a naturally-occurring polyphenolic compound, has been the focus of several works as an additive in bio-based materials such as films, hydrogels, textiles, and papers to enhance their antimicrobial and antioxidant properties. Considering some of the interesting biological abilities of TA, TA-treated cellulose products may have useful applications in medical or consumer products. In this work, the physical adsorption of TA to cellulosic kraft pulp fibers is studied. Using both UV-Vis spectrophotometry and mass balance methods, the TA adsorption capacity of the fibers is quantified. Monolayer coverage of the surface of the fibers is calculated theoretically to be about 70 mg TA/g of pulp, whereas experimentally a plateau in TA uptake is observed near 120 mg TA/g pulp with a post-adsorption rinsing step. Without washing, TA adsorbs to the pulp above monolayer coverage. The kinetics data are fit to the modified Langmuir adsorption model, which fits the adsorption kinetics well at higher TA concentrations. Additionally, paper handsheets are fabricated from the TA-treated fibers and are characterized by FTIR and diffuse reflectance to confirm incorporation of TA into the paper. TA-treated papers have potential applications such as inserts or layers in antimicrobial face masks.

Introduction

A core issue of healthcare is protection against pathogens such as viruses and bacteria, and many recent studies have sought to identify new antimicrobial materials to assist in the prevention of infection by pathogens. Several such studies have focused on the use of polyphenols, naturally-derived compounds often possessing interesting bioactive and/or antimicrobial properties, as

additives in bio-based materials such as films hydrogels, textiles, and papers.[1-4] Tannic acid (TA) is a polyphenolic molecule consisting of a central glucose unit with five di-galloyl (or ten galloyl) moieties (Figure 1), and is usually extracted from several species of trees.[1, 3] An inexpensive and widely available compound, TA is recognized for its low toxicity (LD_{50} (oral, rat) of 2260 mg/kg),[5] and as a food additive TA is categorized as "generally recognized as safe" (GRAS).[6] Historically, tannins have been used in the tanning of animal skins owing to their ability to bind and precipitate proteins.[7] Tannins are also proposed to play a role in plant defence systems, e.g., by protecting plant tissues against decay and/or by increasing resistance to pathogens,[7] which has inspired recent work focused on the antimicrobial properties of tannins for applications such as food packaging and healthcare.

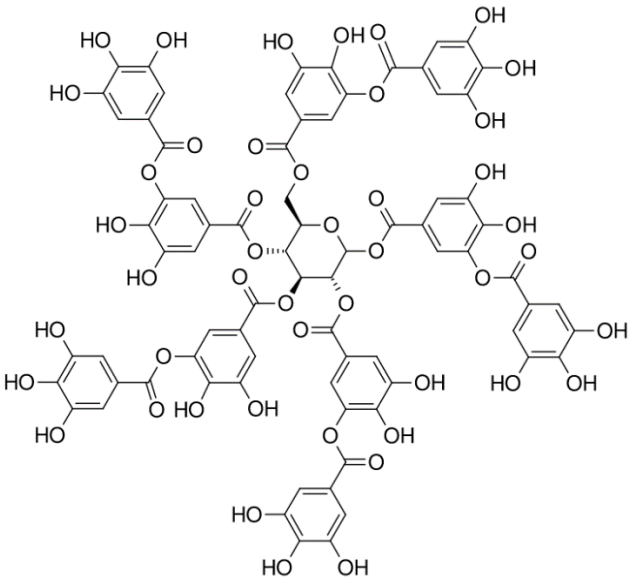

Figure 1: Structure of tannic acid (TA) with a central glucose unit and five di-galloyl moieties.

A recent review summarized the antiviral activity of tannic acid; TA or TA-rich natural extracts have been shown to be effective antivirals against Influenza A virus, HPV, noroviruses, and HSV-1 by inhibiting virus-receptor binding.[1] Furthermore, TA has been shown to possess antibacterial activity against a variety of common bacterial pathogens including *Staphylococcus aureus*, *Escherichia coli*, *Listeria monocytogenes*, and other microorganisms.[1, 6-8] The potential of TA to prevent SARS-CoV-2 infectivity has also been studied in the context of the recent pandemic—TA has been shown to inhibit the activity of the human cellular TMPRSS2 and viral $3CL^{pro}$ proteases which are involved in viral infection.[9, 10]

Building on the demonstrated antimicrobial and antiviral properties of TA, several works have employed TA as an additive to biopolymeric substrates in the fabrication of antimicrobial materials. A review by Kaczmarek summarizes recent developments in TA-based biomaterials including antioxidant TA-collagen composite hydrogels, antibacterial TA-chitosan films and TA-silk hydrogels, and TA-agarose hydrogels which prevented biofilm formation.[1] In another study, the treatment of silk fabrics by adsorbing with TA was shown to improve the antioxidant and antibacterial properties of the textiles.[11] In addition to biopolymers such as collagen, chitosan, and silk, TA has also been incorporated into materials based on cellulose, the most abundant biopolymer. Composites of bacterial cellulose, TA, and magnesium chloride have been developed for the prevention of biofilm formation in wound sites. These composite films displayed antibacterial activity and were able to inhibit biofilm formation.[4] Also, jute fabrics have been treated with TA and metal salts to form TA-metal-cellulose complexes within the fibers, and the treated textile was shown to have enhanced antimicrobial properties.[2] Bleached kraft pulp (KP) is a material derived from wood which has had almost all of its lignin and some of its hemicellulose removed and thus consists mainly of fibers of cellulose and hemicellulose. This biorenewable material is primarily used to make paper, but can also be used as a precursor to cellulosic textiles and nanomaterials. Some studies have treated KP with TA with the aim of inducing covalent bonds, i.e., chemisorption. For instance, Widsten et al. added TA to KP using the enzyme laccase to induce covalent bonding between the tannin and the pulp; paper handsheets produced from this pulp had improved antibacterial resistance compared to untreated paper.[3] In addition, Ji et al. developed TA-treated paper through the covalent bonding of TA to aldehyde groups on oxidized cellulose fibers. The paper, intended for food packaging, possessed antioxidative properties as well as reduced water vapour transmission.[12] However, to our knowledge, the non-covalent adsorption of TA to KP, i.e., physisorption, has not been studied in detail. With this work we hope to investigate the adsorption mechanism of TA to KP for the use of TA in functionalized paper materials.

Studying the adsorption of potentially antimicrobial additives such as TA to useful substrates is key to the fabrication of functional materials aiming to reduce infectivity. When it comes to respiratory viruses, the spread of virus particles can occur through direct contact, respiratory droplets, and aerosols, as is the case with severe acute respiratory syndrome coronavirus 2 (SARS-CoV-2).[13, 14] The use of face masks has been shown to reduce transmission

of respiratory viral infections including SARS-CoV-2 by trapping these droplets and aerosolized particles.[13] During the COVID-19 pandemic, many local and national authorities recommended face masks or implemented mandates in certain contexts to reduce virus transmission. The ability of face masks to filter particles depends on the size of the particles as well as the mask material, number of layers, and the presence of moisture.[14] High-porosity masks made from nanofibers can improve efficiency of capture of small particles (nanoparticles with diameter <0.3 μm such as viruses).[14] Furthermore, the use of additives in mask materials also has the potential to improve capture efficiency; e.g., the antimicrobial activity of cotton fabric was shown to improve when the fabric was coated with copper iodide particles capped with Hibiscus flower extract.[15] Given the demonstrated antimicrobial abilities of TA in biopolymeric materials, and the potential for TA to inhibit SARS-CoV-2 infectivity, the use of TA as an additive in face mask filter materials may improve the ability of masks to prevent virus transmission. TA may also improve the material properties of paper through resistance to degradation by microbes; Widsten et al. note that "antimicrobial phenols can be potentially applied on lignocellulosic materials to prevent biodeterioration."[3] In this work, we study the adsorption of TA to cellulose KP fibers to determine the TA adsorption capacity of KP and the mechanisms of adsorption. The kinetics of adsorption and the effects of different washing methods are investigated in detail to determine the optimal conditions for the production of functionalized paper. Handsheets made from TA-coated fibers are fabricated and characterized for potential applications such as inserts or layers in antiviral face masks.

Experimental

Materials and Preparation

Bleached softwood kraft pulp sheets (Domtar, Canada) were torn by hand into small pieces, soaked in water overnight, and disintegrated into well-dispersed fibers using a laboratory pulp disintegrator. The dispersed pulp, stored in wet form, contained approximately 7% dry mass. Tannic acid was acquired from Sigma Aldrich and dissolved in water to prepare a 10% (w/w) stock solution. Deionized (DI) water was used in all experiments.

KP-TA Adsorption

To study the adsorption of TA to KP, a portion of wet pulp containing approximately 1 g dry mass was added to a 150 mL beaker. A known amount of TA stock solution and additional

water were added to bring the total mass in the beaker to 50 g, such that the pulp concentration in the beaker was 2% (w/w) and the TA concentration ranged from 0.05 to 40 g/L. The contents were stirred with an overhead shear mixer for 10 min to allow TA to adsorb to the pulp. After the adsorption time, three methods were used to determine the mass of TA adsorbed by the pulp at equilibrium (Γ_e). These methods represent three post-adsorption treatments of the pulp: (1) without washing, (2) with washing by rinsing, and (3) with washing by immersion. A schematic is included below (Figure 2) to summarize the three methods.

1) Without washing

The contents of the beaker (pulp and TA solution) were filtered through a 75 μM mesh screen. A sample of the filtrate was taken to determine the equilibrium concentration of non-adsorbed TA by UV-Vis spectrophotometry. The absorbance of the sample at 275 nm in a quartz cuvette was measured, applying a UV-Vis calibration curve and the appropriate dilution factor to determine the equilibrium TA concentration, C_e (g TA/L). The mass of non-adsorbed TA in the filtrate was found by multiplying C_e by the liquid volume in the experiment (49 mL). Then, the mass of TA taken up by the pulp, Γ_e (mg TA/g pulp), was determined from a mass balance on the amount of TA initially added and the amount of TA remaining in the filtrate.

2) Washing by rinsing

The effect of washing the pulp by rinsing with fresh water was studied. After the 10 min adsorption time, the contents of the beaker were filtered through the 75 μm mesh screen, as above. With the pulp still on the screen, water from a squeeze bottle was used to thoroughly rinse the pulp and remove excess TA solution from within the fibers. The pulp was gently pressed with a spatula to expel and collect the rinsing water. The filtrate, combined with the rinsing water (approximately 20 mL total), was dried in a 105 ºC oven for 24 h to determine its solid content—the mass of non-adsorbed TA including any TA removed by rinsing. The mass of TA taken up by the pulp after rinsing (Γ_e) was again calculated by a mass balance.

3) Washing by immersion

To study the effect of washing by immersing the pulp in water, first, KP-TA adsorption experiments were set up in the beaker as above. However, all quantities were scaled down by 50% (i.e., the dry mass of pulp used was approximately 0.5 g and the total mass in the beaker was 25 g). After the 10 min adsorption time, the entire contents of the beaker (pulp and TA solution) were added to a large beaker containing 2.975 L of water and stirred for an additional 10 min. The

contents were then filtered through the 75 µM mesh screen, and the filtrate was sampled and analyzed by UV-Vis spectrophotometry as above to determine the concentration of non-adsorbed TA in the washing solution. Once again, the mass of non-adsorbed TA was calculated, and the mass of TA taken up by the pulp after washing (Γ_e) was calculated by a mass balance.

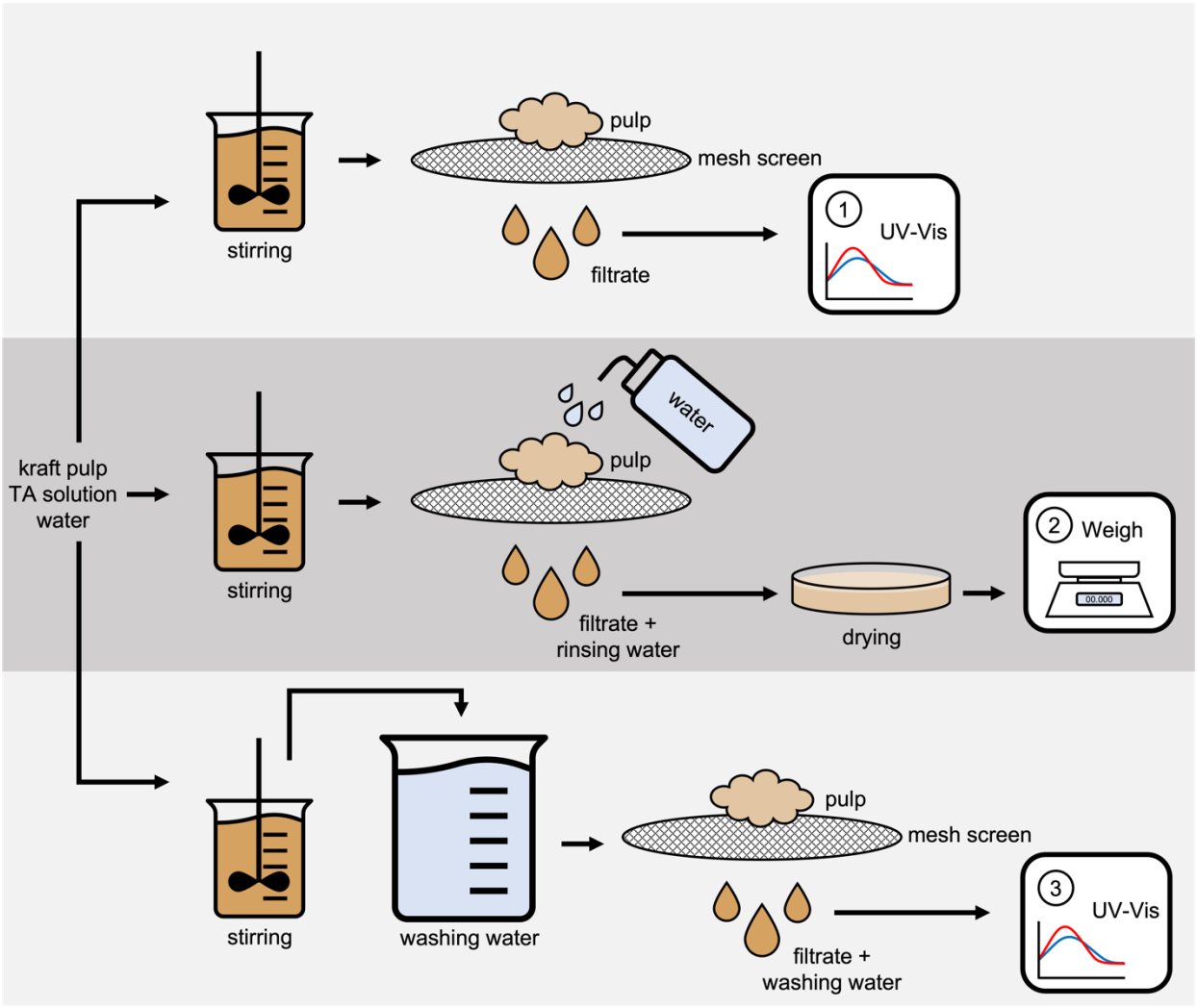

Figure 2: Schematic of kraft pulp (KP)-TA adsorption experiments and sample collection. Three methods are used to study the effect of different washing methods: (1) without washing, the non-adsorbed TA concentration was measured by UV-Vis absorbance at 275 nm; (2) washing by rinsing, the mass of non-adsorbed TA was determined by dry weight measurement; and (3) washing by immersion, the non-adsorbed TA concentration was measured by UV-Vis absorbance at 275 nm.

KP-TA Adsorption Kinetics

To study the kinetics of KP-TA adsorption, experiments were set up in the beaker according to the scheme above. After starting the experiment by adding the stock TA solution, samples were taken at increasing time intervals (15 s, 30 s, 60 s, 90 s, and so on), filtered through a 20 μM nylon filter, and measured by UV-Vis as described above to determine the concentration of TA in the solution. The uptake of TA by the pulp (Γ) was determined by a mass balance on the mass of TA initially added and the mass of non-adsorbed TA in the solution at each point in time.

Fabrication of TA-Coated Paper

Paper samples known as handsheets were made using laboratory-scale papermaking equipment according to the procedure described in TAPPI standard T-205 sp-02. A portion of wet pulp containing approximately 1.25 g dry mass was used to target a paper basis weight of 62 ± 2 g/m^2. To make TA-coated paper, quantities of TA at 100%–400% of the dry pulp mass were dissolved in water and combined with the pulp for a total mass of 142 g (initial TA concentrations of approximately 8–33 g/L). The pulp and TA were stirred for 10 min with the overhead shear mixer to allow TA to adsorb to the pulp. Then, the pulp or pulp-TA mixture was added to water in the cylinder of a handsheet machine to a total volume of 7 L, and evenly dispersed with a perforated plate stirrer for 6 s. The water was drained from the pulp leaving a wet handsheet on a 16 cm diameter screen. Water was removed from the handsheet with blotting paper by applying even pressure from a couch roll and plate. No pressing stage was used in this procedure in order to yield a more porous paper. The wet handsheet was dried overnight between drying rings.

The 0% TA (control) and 400% TA handsheets as well as TA powder were characterized by Fourier transform infrared (FTIR) spectroscopy using a Perkin-Elmer spectrometer (single diamond ATR) from 4000 to 400 cm^{-1}. The spectra were obtained by combining 50 scans with a resolution of 4 cm^{-1}.

The control and TA-coated handsheets as well as TA powder were also characterized by UV-Vis reflectance measurement. The reflectance of solid samples in the 280–800 nm range was measured using a Cary 5000 UV-Vis spectrophotometer with a praying mantis diffuse reflectance sample holder. At least three pieces of each handsheet sample were measured to generate averaged spectra. The average reflectance over the 280–800 nm range was also calculated from at least three measurements.

Results and Discussion

Estimates of Monolayer Coverage

The uptake of TA by KP corresponding to monolayer coverage can be estimated through surface area calculations. First, we estimate the area occupied by one TA molecule to be about 7 nm^2 based on its diameter of approximately 3 nm as determined by molecular modeling.[16]

A wide range for the specific surface area of KP is reported in the literature. Values for the external pulp surface area have been reported between 1 and 10 m^2/g.[17-19] On the other hand, the internal surface area, which accounts for the surface area of the lumen and pores within the pulp, can range between 100 and 1000 m^2/g depending on the technique used to measure it.[17-20] Due to the collapse of internal volume upon drying from water, surface area measurement of dry fibers typically only measures the former external surface area, whereas with wet fibers the internal lumen and pores can be accessed by sufficiently small molecules.[17] For the purposes of these calculations we will take the internal surface area of the pulp accessible by TA molecules to be about 300 m^2/g, based on the reported specific surface area of pulp fibers excluding nanopores less than 3.2 nm in diameter.[20]

Monolayer coverage of the pulp surface area can be estimated by dividing the KP specific surface area by the area of a TA molecule. However, "monolayer coverage" does not always correspond to 100% coverage of the available surface area, since the arrangement of molecules packed on the surface can prevent additional molecules from adsorbing on bare areas. For the random deposition of spherical particles adsorbing on a surface, monolayer coverage corresponds to approximately 55% coverage of the available area.[21] Thus, monolayer coverage of pulp by TA can be calculated from Equation 1:

$$\Gamma_{monolayer} = 0.55 \frac{A_{pulp}}{A_{TA}} \quad (1)$$

Taking the specific surface area of wet KP to be 300 m^2/g and assuming 55% coverage is reached,

$$\Gamma_{monolayer} = \frac{0.55\left(300 \frac{m^2}{g\ pulp}\right)}{7(6.022 \times 10^{23}) \frac{nm^2}{mol\ TA}} \left(\frac{1701.2\ g\ TA}{mol\ TA}\right) = 70 \frac{mg\ TA}{g\ pulp}$$

For reference, we can also consider a monolayer only on the external surface of the pulp, i.e., the hydrodynamic surface area. Taking an external surface area of just 1 m^2/g:

$$\Gamma_{monolayer,ext} = \frac{0.55\left(1\frac{m^2}{g\ pulp}\right)}{7(6.022\times10^{23})\frac{nm^2}{mol\ TA}}\left(\frac{1701.2\ g\ TA}{mol\ TA}\right) = 0.22\ \frac{mg\ TA}{g\ pulp}$$

In summary, theoretical estimates put a monolayer coverage of TA on the external and accessible internal surface area of KP at approximately 70 mg TA/g KP, whereas a monolayer on only the external pulp area is approximately 0.22 mg TA/g KP.

KP-TA Adsorption

The uptake of TA by KP (Γ_e) for the three post-adsorption treatments (without washing, with washing by rinsing, and with washing by immersion) is plotted as a function of initial TA concentration (C_0) in Figure 3. Without a washing step, the uptake of TA increases consistently as the initial TA concentration increases, i.e., the maximum uptake of TA by pulp is not reached in the range of TA concentrations studied. However, the two washing methods yield distinctly different results due to the differences in the post-adsorption treatments.

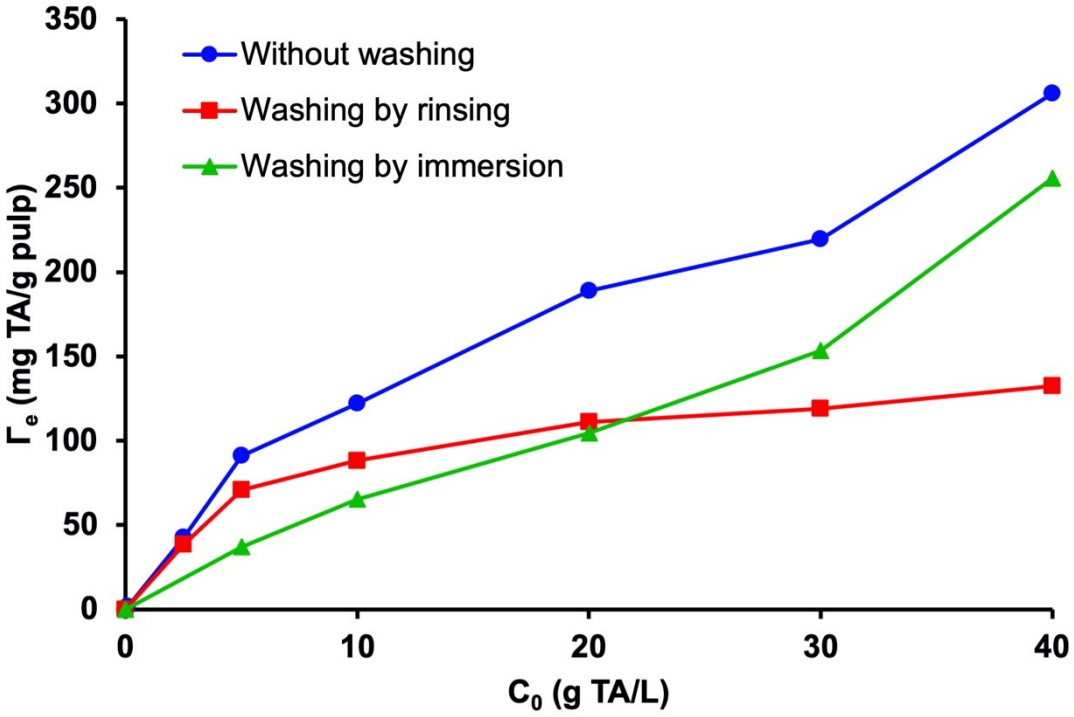

Figure 3: Uptake of TA by KP fibers as a function of initial TA concentration, for three post-adsorption treatments: without washing, washing by rinsing with water, and washing by immersion in a large amount of water.

Washing by rinsing

With the second post-adsorption treatment method, the "washing by rinsing" method, it can be seen that TA is removed from the pulp by rinsing, as the uptake curve is lower than the "without washing" curve. As C_0 increases, the uptake of TA initially increases significantly, then transitions to a small linear increase at high C_0. This transition in slope occurs near an initial TA concentration of 5 g/L, where the uptake is approximately 70 mg TA/g pulp, corresponding well with our estimate of monolayer coverage of the pulp surface area. Since the uptake curves of the "without washing" and "washing by rinsing" methods are similar below Γ_e = 70 mg TA/g pulp, this could imply that the TA monolayer is strongly adsorbed and cannot be removed by washing. However, at higher C_0, more adsorbed TA appears to be removed by rinsing. The small linear increase could correspond to TA that persists after rinsing—perhaps a TA bilayer or a buildup of TA in certain internal areas of the pulp such as the pores that are less accessible by the rinsing water.

Washing by immersion

The third post-adsorption treatment method studied, on the other hand, does not result in a large reduction in TA uptake at high C_0. In the "washing by immersion" method, the pulp and TA solution are added to ~3 L of water, rather than rinsing with clean water to wash the pulp. The immersion method results in a consistently lower uptake of TA in comparison to the "without washing" results, indicating that the immersion method does cause some adsorbed TA to be removed from the pulp. In comparison to the "washing by rinsing" method, the final TA uptake is lower at low C_0 but higher at high C_0. At low concentrations, the pulp is in contact with a large volume of washing water for a longer period of time, possibly causing partial desorption of the adsorbed monolayer. At higher concentrations, washing by immersion is less effective at removing TA multilayers from the pulp due to a lower driving force for desorption—the washing liquid also contains the non-adsorbed TA from the original beaker, which makes it less effective at removing TA than the continuous replacement of clean water with the rinsing method.

We chose to study the "washing by immersion" method because it is most similar to the conditions of laboratory-scale papermaking. This washing step uses a similar water to pulp ratio as the dispersion of pulp in the sheet former (about 7 L of water per 1.25 g of pulp). Thus, these results have useful implications for the fabrication of handsheets. We note that the point at which washing by immersion becomes less effective than washing by rinsing at removing excess TA

occurs at approximately 20 mg/mL initial TA concentration. Also, at this point monolayer coverage of the pulp has already been achieved; in other words, concentrations above 20 mg/mL are not needed to coat the pulp effectively with a monolayer of TA as the excess would be washed away.

In a practical application of TA as an additive in paper, only the TA adsorbed to the external surface of the fibers, the hydrodynamic surface area, is relevant since any TA adsorbed within the fibers will not interact with other fibers or particles. Given that a monolayer on the external surface area of the pulp may be only about 1/300 of the monolayer coverage of the internal surface area, it is clear that this coverage is quickly exceeded in these experimental conditions. Even at the lowest C_0 tested in this study (0.05 g/L), the uptake after 10 min is 0.41 mg TA/g pulp, almost double our estimate of monolayer coverage on the external pulp surface area. The use of a large excess of TA ensures a rapid coating formation, but may pose drawbacks such as wastage or excess TA draining and being released in the waste water.

Modified Langmuir Adsorption Model

The adsorption data can be fit to the modified Langmuir model, which was originally developed to analyze the deposition of filler particles such as calcium carbonate onto pulp fibers in an aqueous system.[22] The modified Langmuir theory was developed from the original Langmuir model for the adsorption of gas molecules onto solid surfaces; it describes adsorption kinetics as a dynamic equilibrium between deposition and desorption of particles.[23] This theory was chosen as a suitable model because it originally was used to describe a similar system to the one in this study, the adsorption of particles onto fiber surfaces. One benefit of the modified Langmuir model is that it accounts for situations where there are not enough particles in the system for full surface coverage.[23]

The modified Langmuir equation[22] is as follows:

$$\frac{d\theta}{dt} = k_{ads}(n_0 - \theta)(1 - \theta) - k_{des}\theta \qquad (2)$$

where θ is the fractional coverage of the pulp by TA, and k_{ads} and k_{des} are the adsorption and desorption rate constants, respectively. The parameter n_0 is the initial concentration of TA normalized to the maximum amount that can adsorb, Γ_{max}:

$$n_0 = \frac{C_0}{\Gamma_{max}} \qquad (3)$$

where both C_0 and Γ_{max} are expressed in units of grams of TA per gram of KP, thus n_0 is dimensionless. Similarly, the fractional coverage θ is the uptake of TA by the pulp normalized to Γ_{max}.

At steady state, $\frac{d\theta}{dt} = 0$ and Equation 2 can be linearized as:

$$\frac{1}{\Gamma_\infty} = \frac{K}{C_\infty} + \frac{1}{\Gamma_{max}} \tag{4}$$

where Γ_∞ and C_∞ are the amounts of TA adsorbed to the pulp and remaining in solution, respectively, at steady state. K is the ratio of rate constants:

$$K = \frac{k_{ads}}{k_{des}} \tag{5}$$

Using the experimental data in Figure 3 ("Without washing"), a Langmuir plot of $1/\Gamma_\infty$ versus $1/C_\infty$ is shown in Figure 4. The "Without washing" data set was used because allows for a comparison of the model with the adsorption kinetics data in the following section. According to Equation 4, the slope and intercept are used to obtain K and $1/\Gamma_{max}$, respectively. The linear fit corresponds to K = 1.89 and Γ_{max} = 0.79 g TA/g pulp, or 790 mg/g.

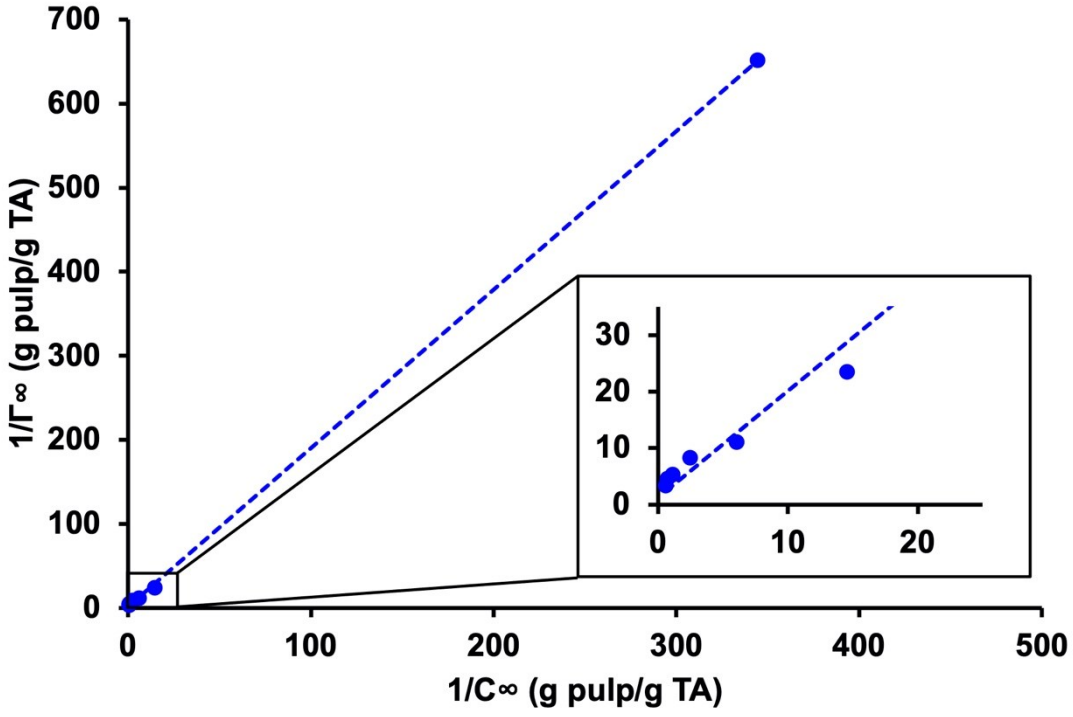

Figure 4: Langmuir plot of TA adsorption onto KP fibers without post-adsorption washing. Inset: a section of the graph is enlarged for visibility.

KP-TA Adsorption Kinetics

The fit of the modified Langmuir model can be compared with experimental adsorption kinetics data. The analytical solution of Equation 2 is as follows:[22]

$$\theta = \frac{2n_0(\lambda - 1) + \theta_0[A(1-\lambda) + B(\lambda + 1)]}{A(\lambda - 1) + B(\lambda + 1) + \theta_0(1 - \lambda)} \quad (6)$$

where the initial condition at time t = 0 is $\theta = \theta_0$, and

$$\lambda = e^{Bk_{ads}t} \quad (7)$$

$$A = K + n_0 + 1 \quad (8)$$

$$B = \sqrt{(n_0 - 1)^2 + 2K(n_0 + 1) + K^2} \quad (9)$$

We take the initial condition $\theta_0 = 0$ since no TA is adsorbed to the pulp at the start of the experiment. Taking the parameters K and Γ_{max} from above, the only remaining unknown is k_{ads}. At short times, Equation 2 can be approximated as:

$$\theta = k_{ads} n_0 t \quad (10)$$

thus, k_{ads} can be estimated from the initial slope of experimental kinetics data (θ versus time).

The experimentally measured uptake of TA by KP over time is shown as points in Figure 5 for three initial concentrations of TA (20 g/L, 5 g/L, and 0.1 g/L). Here, the uptake is expressed as θ, or fractional coverage (relative to Γ_{max}). Fast initial adsorption kinetics are observed even for very low TA concentrations; about 70% of the maximum TA uptake adsorbs within the first few seconds. With 0.1 g/L, although the solution concentration is not sufficient for internal and external monolayer coverage, full coverage of the external area is quickly attained. At the first data point recorded where t = 10 s, the TA uptake is already 0.56 mg TA/g pulp, whereas our estimation of a TA monolayer covering only the external pulp surface area was only 0.22 mg TA/g pulp. Adsorption equilibrium is reached within approximately 5 min for initial concentrations of 5 g/L and 20 g/L TA. For the lower concentration of 0.1 g/L TA, the kinetics are slower as expected, but a maximum uptake of TA by the pulp is still reached within 10 min. Over time, however, the uptake seems to decrease, indicating possible desorption at this concentration.

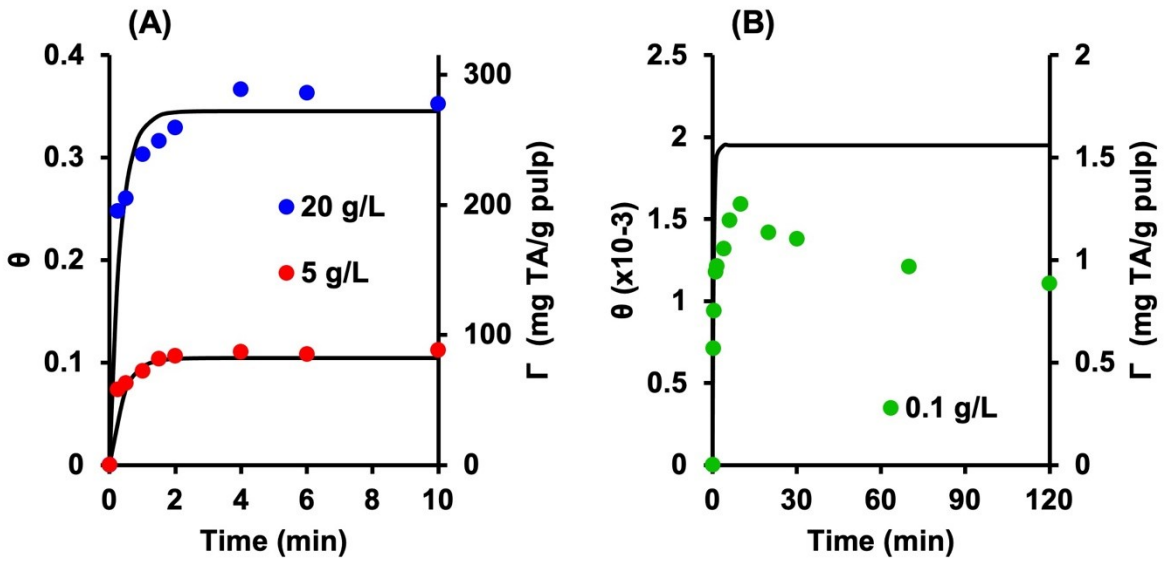

Figure 5: Kinetics of TA-KP adsorption for initial TA concentrations of (A) 20 g/L, 5 g/L, and (B) 0.1 g/L. The left y-axes are the fractional coverage of the pulp by TA relative to the maximum uptake given by the modified Langmuir model (Γ_{max}); the right y-axes are the TA uptake in mg/g. Experimental data (points) are compared with the fit of the modified Langmuir model (solid lines) with K = 1.89, k_{ads} = 0.8 s^{-1}, and Γ_{max} = 790 mg TA/g pulp.

To calculate the model kinetics values, first, k_{ads} was calculated from the initial slope using the three data sets (Equation 10). For 20 g/L, 5 g/L and 0.1 g/L, the initial slope yielded k_{ads} values of 0.74, 0.91, and 180 s^{-1}, respectively. Since k_{ads} should be a constant, an approximate average value of k_{ads} = 0.8 s^{-1} was taken to apply the model (therefore $k_{des} \cong 1.5$ s^{-1}). The initial slope for 0.1 g/L was not considered in the estimation of k_{ads} because it is not consistent with the other two data sets; the initial adsorption rate is much faster than expected in comparison to the other two concentrations. The values of θ given by the modified Langmuir model using Equation 6 (with K = 1.89, k_{ads} = 0.8 s^{-1}, and Γ_{max} = 790 mg TA/g pulp) are overlaid as solid lines in Figure 5.

Comparing the modified Langmuir model (solid lines) with the experimental data (points), the model fits the adsorption kinetics well for 20 and 5 g/L, but not for the much lower concentration of 0.1 g/L (Figure 5). At 20 and 5 g/L the TA concentration is quite high, and molecules are likely to be present, to some extent, in an aggregated form.[16] With the model fit to k_{ads} from these two higher concentrations, it shows the steady state equilibrium between adsorption and desorption of molecules and aggregates that causes the observed plateau in θ. At 0.1 g/L, on the other hand, there are likely far fewer aggregates present, so the model does not agree with the

experimental data. The TA uptake at 0.1 g/L is mostly the adsorption of single TA molecules with an apparent high affinity—much higher than that of aggregates, so k_{ads} is high by comparison.

As for the equilibrium TA uptake at 0.1 g/L, the desorption at long times is not accounted for; it is possible that the rate constant k_{des} is time-dependent. This could be the result of TA rearrangement, wherein the roughly two-dimensional molecules of TA initially adsorbed in a denser, edge-on configuration would desorb to allow for other molecules to adsorb in a less-dense, flat configuration. The flat or face-on configuration is favourable due to a larger contact area with the fiber surface. At long times, this would lead to the observed net overall desorption with a characteristic time on the order of one hour, eventually reaching a steady state with TA molecules adsorbed face-on.

Fabrication of TA-Coated Paper

TA-coated handsheets fabricated through a laboratory-scale papermaking setup are shown in Figure 6A for different added quantities of TA. Addition of TA to the pulp causes a visible change in the colour of the paper. As mentioned, papers were made without a pressing stage to have a more porous structure (Figure 6B). We observed that higher quantities of added TA started to interfere with handsheet fabrication. With TA added at 300% and 400% of the pulp weight, the treated pulp tended to clump together, having a negative impact on handsheet formation (Figure 6C). This led to a more fragile wet handsheet with small areas of higher and lower pulp density in the sheet.

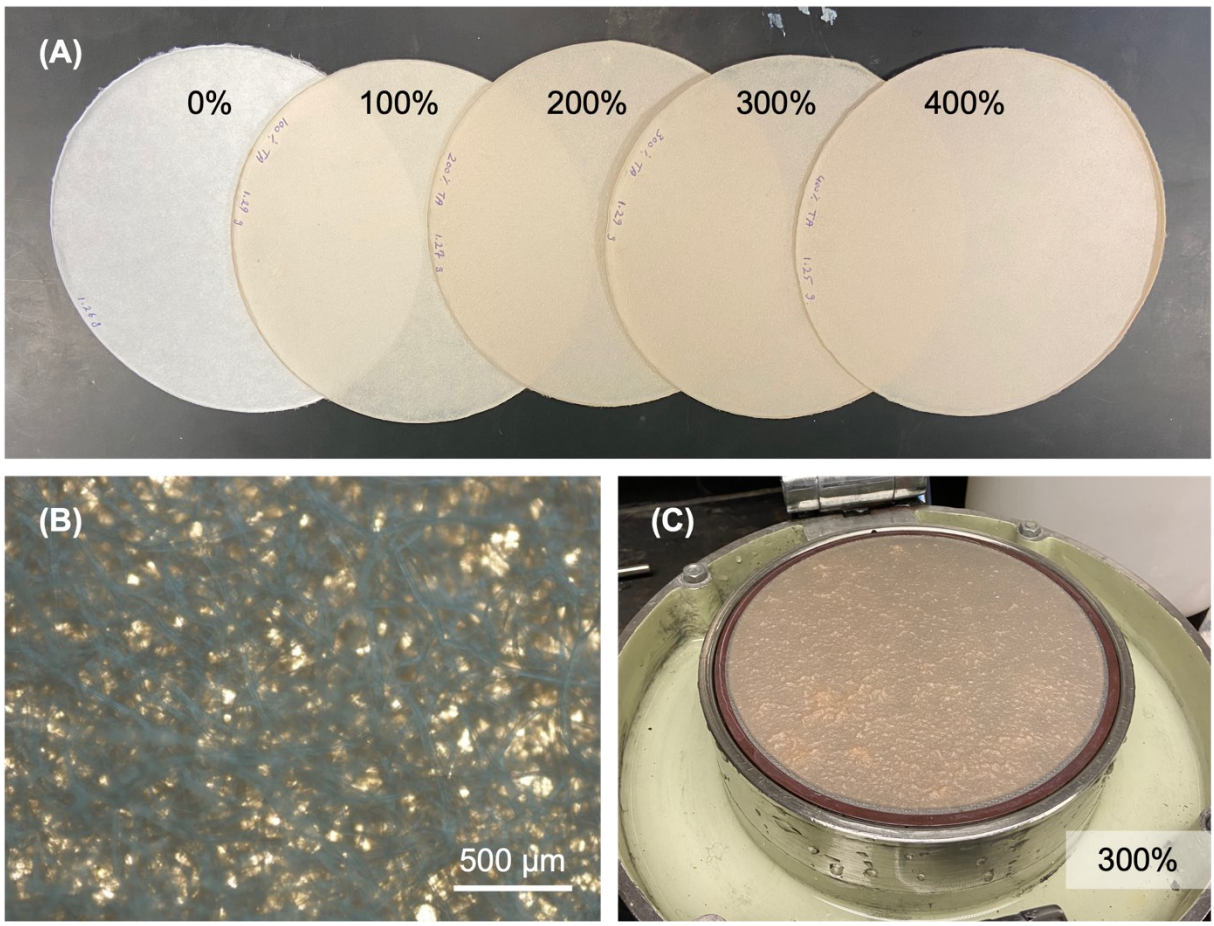

Figure 6: (A) From left to right, handsheets made from kraft pulp (KP) with TA added at 0% (control) to 400% of the pulp weight (dry basis); (B) Optical microscopy picture of the porous paper made without any pressing stage; (C) Wet handsheet made with TA at 300% of the pulp weight, showing fiber flocculation and uneven paper formation on the screen of the handsheet former.

FTIR characterization of the 0% TA paper (KP only), 400% TA paper, and TA powder is shown in Figure 7. The KP spectrum displays the characteristic peaks of cellulose, namely the broad peak around 3320 cm^{-1} due to stretching of –OH groups, and the peaks at 2900 cm^{-1} (C–H stretching), 1160 cm^{-1} (C–O asymmetric bridge stretching), and 895 cm^{-1} (β-glycosidic linkages between glucose units).[4, 24, 25] In the TA spectrum, we observe key peaks also identified by Zhang et al. in their characterization of TA, namely the broad band at 3600–3000 cm^{-1} characteristic of –OH stretching in tannins, as well as peaks at 1700 cm^{-1} (C=O stretching), 1610 cm^{-1} and 1533 cm^{-1} (C=C stretching) and 1020 cm^{-1} (vibration of substituted benzene).[4, 26] In the KP-TA paper sample, key peaks from KP (3320 cm^{-1}, 2900 cm^{-1}, and 1160 cm^{-1}) and TA (1700 cm^{-1}, 1610 cm^{-1}, and 1533 cm^{-1}) are present, indicating that TA was incorporated into the KP paper. No shifts

or emergence of new peaks are observed, suggesting that TA adsorbs physically, i.e., with no formation of new covalent bonds.

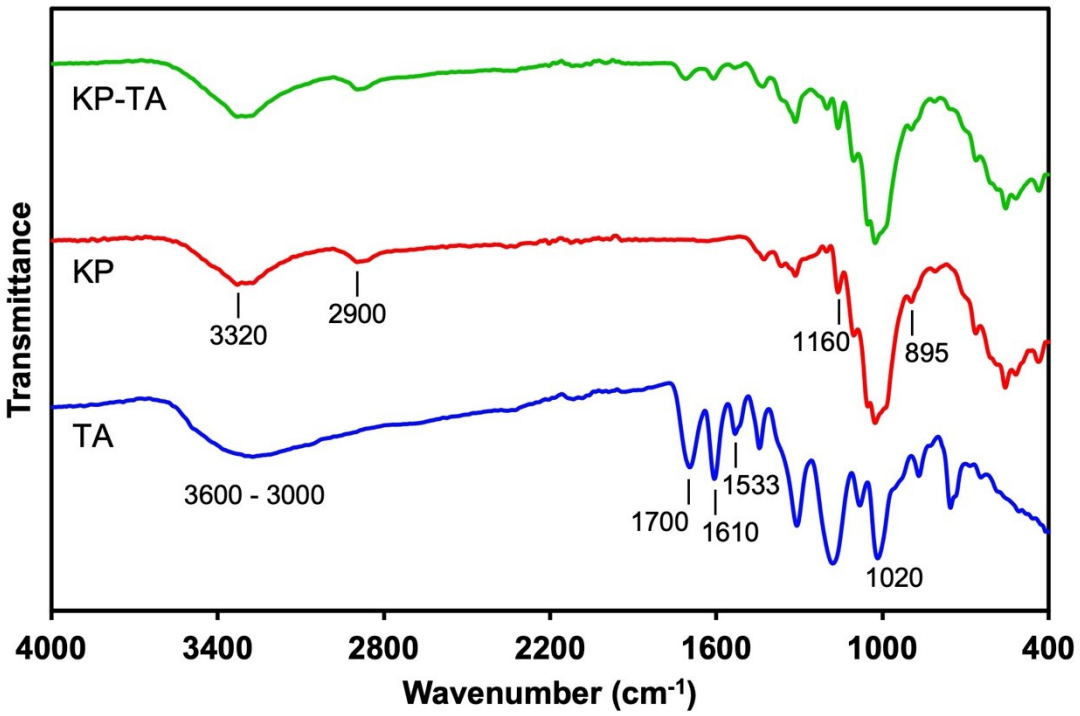

Figure 7: FTIR spectra for tannic acid ("TA"), paper made from kraft pulp ("KP"), and KP paper with TA added at 400% of the pulp weight ("KP-TA").

In this study, the mechanism of TA-KP interaction is likely hydrogen bonding between phenolic –OH groups on TA and –OH groups on cellulose. In other studies involving TA and cellulose, Ji et al. observed covalent bonds between TA and aldehyde groups on oxidized cellulose,[12] and Higazy et al. and Zhang et al. observed chelating bonds between TA, cellulose hydroxyl groups, and metal ions (Zn^{2+} and Mg^{2+}).[2, 4] In this system, with no agents used on either TA or cellulose to induce covalent bonds, hydrogen bonding and weak van der Waals forces are the possible interactions between TA and unmodified cellulose. In addition, owing to the many phenolic –OH groups on TA and –OH groups on separate cellulose fibers, a bridging effect could be possible. Indeed, we observed during adsorption experiments that upon addition of TA to the pulp suspension, the pulp fibers flocculated slightly, as if TA molecules were bridging the fibers, or covering some surface charge groups on the fibers. As noted above, this flocculation affected handsheet formation, especially at high quantities of added TA (Figure 6C). At lower quantities,

e.g., 100% and 200% TA, the fibers were still well dispersible in the sheet former and a uniform handsheet could be fabricated.

We have shown that a monolayer of adsorbed TA is resistant to washing during the papermaking process, so TA coated papers can be achieved without covalent bonding induced by using additives. Also, low solution concentrations are required to achieve monolayer coverage on the useful surface area, the external surface of the pulp fibers. However, since it was shown above that the rate of desorption may exceed the rate of adsorption in certain cases at long time scales, further research should experimentally confirm whether TA has the potential to leach from papers coated with TA by physisorption.

The optical properties of the handsheets were studied by UV-Vis diffuse reflectance measurement, a method commonly used for comparison of the brightness of manufactured paper. Figure 8 compares the reflectance spectra of the fabricated handsheets as well as the TA powder. The average reflectance of each of the TA-coated papers is lower than that of the KP-only paper (0% TA), as TA absorbs visible light particularly in the 400–500 nm range used for brightness characterization. Increasing the amount of TA added to the handsheets decreases the average reflectance of the paper. This technique confirms what can be observed visually in Figure 6A, that incorporating TA into paper causes a change in colour and a reduction in brightness of the paper.

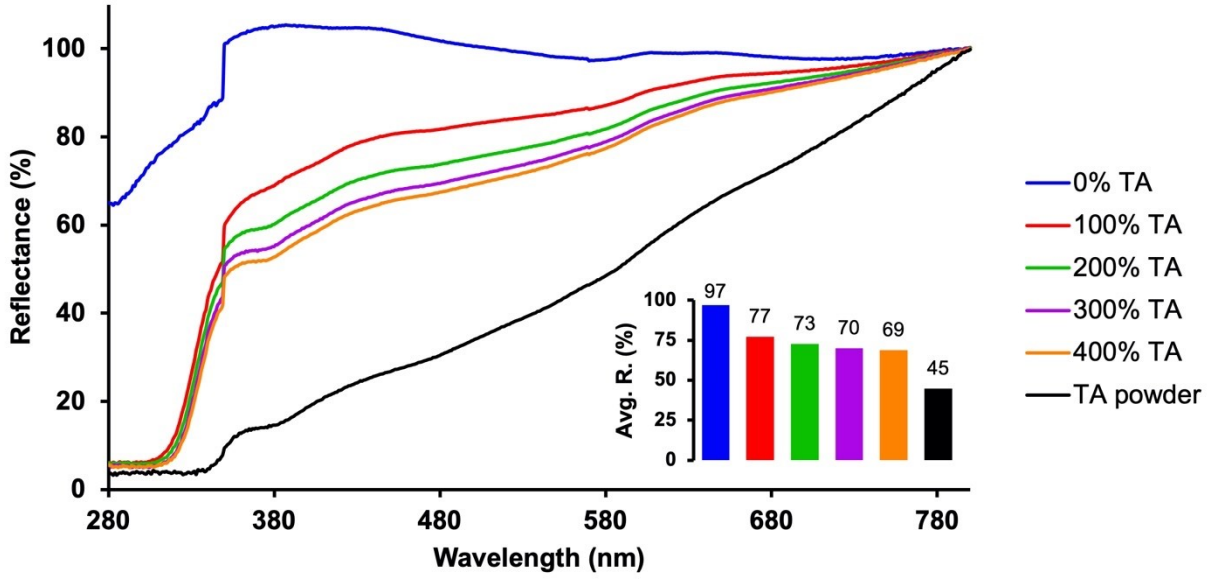

Figure 8: Reflectance spectra of the TA powder and KP papers made with 0%–400% added TA. The inset shows the average reflectance from at least three measurements of the TA powder and papers.

Conclusions

In this work, the adsorption of TA to cellulosic KP was studied for the use of TA as a potential additive to paper. TA was found to adsorb readily to pulp fibers, with fast initial adsorption kinetics. TA monolayer coverage of the external hydrodynamic surface area, i.e., the area of the pulp fibers most relevant to paper functionality, was estimated by surface area calculation to be about 0.22 mg TA/g pulp. Experimentally, TA was found to adsorb rapidly to this external area, indicating that functionalizing KP fibers with TA by physisorption is a rapid and straightforward process that can be done using TA solution concentrations as low as 0.1 g/L. As for the entire accessible surface area of the fibers, which includes the external and internal surfaces of the fibers, monolayer coverage was estimated to be approximately 70 mg TA/g KP. This TA uptake was achieved experimentally when the solution concentration of TA was sufficient (5 g/L and higher). Study of the adsorption kinetics at high and low TA concentrations suggested that the affinity of single TA molecules adsorbed face-on to KP fibers is higher than that of TA molecules adsorbed edge-on, whereas the affinity of TA aggregates is the lowest.

Three post-adsorption treatments of the pulp were compared: no pulp washing, washing by rinsing with fresh water, and washing by immersion as in handsheet fabrication. Washing by rinsing was found to remove excess TA, leaving behind the adsorbed TA monolayer plus a slight excess, showing that TA has a high affinity for KP fibers. However, omitting the washing step or washing the pulp by immersion in water left more than a monolayer of TA on and/or within the pulp fibers at high TA concentrations. The effect of washing conditions on TA uptake may be useful for application scenarios such as papermaking in which pulp fibers are washed with large quantities of water.

In the context of the COVID-19 pandemic, antiviral and antibacterial functional materials are of great importance as we develop new strategies and lines of defence against pathogens. The development of antiviral materials has the potential to greatly assist healthcare protection efforts. With previous works having demonstrated the antimicrobial capabilities of biopolymer-TA composites, our TA-coated handsheets may be a promising material for applications such as antimicrobial packaging or paper-based filters in face masks. The prototype handsheets demonstrated that TA could be incorporated into a KP-based paper handsheet, and adsorption studies suggest that even low coating solution concentrations (0.1 g/L) can rapidly lead to coverage

of the active surface of the fibers. Future work should further characterize these handsheets for specific applications, e.g., by studying their antimicrobial, mechanical, and barrier properties.

Acknowledgements: We would like to thank Dr. Hatem Titi for performing the UV-Vis diffuse reflectance measurements.

References

1. Kaczmarek, B., Tannic Acid with Antiviral and Antibacterial Activity as A Promising Component of Biomaterials—A Minireview. *Materials* **2020,** *13* (14).

2. Higazy, A.; Hashem, M.; ElShafei, A.; Shaker, N.; Hady, M. A., Development of anti-microbial jute fabrics via in situ formation of cellulose–tannic acid–metal ion complex. *Carbohydr. Polym.* **2010,** *79* (4), 890-897.

3. Widsten, P.; Heathcote, C.; Kandelbauer, A.; Guebitz, G.; Nyanhongo, G. S.; Prasetyo, E. N.; Kudanga, T., Enzymatic surface functionalisation of lignocellulosic materials with tannins for enhancing antibacterial properties. *Process Biochem.* **2010,** *45* (7), 1072-1081.

4. Zhang, Z.-Y.; Sun, Y.; Zheng, Y.-D.; He, W.; Yang, Y.-Y.; Xie, Y.-J.; Feng, Z.-X.; Qiao, K., A biocompatible bacterial cellulose/tannic acid composite with antibacterial and anti-biofilm activities for biomedical applications. *Materials Science and Engineering: C* **2020,** *106*, 110249.

5. Gaudreault, R.; Hervé, V.; van de Ven, T. G. M.; Mousseau, N.; Ramassamy, C., Polyphenol-Peptide Interactions in Mitigation of Alzheimer's Disease: Role of Biosurface-Induced Aggregation. *J. Alzheimer's Dis.* **2021,** *81* (1), 33-55.

6. Chung, K. T.; Jr, S. S.; Lin, W. F.; Wei, C., Growth inhibition of selected food-borne bacteria by tannic acid, propyl gallate and related compounds. *Lett. Appl. Microbiol.* **1993,** *17* (1), 29-32.

7. Scalbert, A., Antimicrobial properties of tannins. *Phytochemistry* **1991,** *30* (12), 3875-3883.

8. Akiyama, H.; Fujii, K.; Yamasaki, O.; Oono, T.; Iwatsuki, K., Antibacterial action of several tannins against Staphylococcus aureus. *J. Antimicrob. Chemother.* **2001,** *48* (4), 487-491.

9. Haddad, M.; Gaudreault, R.; Sasseville, G.; Nguyen, P. T.; Wiebe, H.; van de Ven, T. G. M.; Bourgault, S.; Mousseau, N.; Ramassamy, C., Molecular Interactions of Tannic Acid with Proteins Associated with SARS-CoV-2 Infectivity. *Int. J. Mol. Sci.* **2022,** *23* (5), 2643.

10. Wang, S.-C.; Chen, Y.; Wang, Y.-C.; Wang, W.-J.; Yang, C.-S.; Tsai, C.-L.; Hou, M.-H.; Chen, H.-F.; Shen, Y.-C.; Hung, M.-C., Tannic acid suppresses SARS-CoV-2 as a dual inhibitor of the viral main protease and the cellular TMPRSS2 protease. *Am. J. Cancer Res.* **2020,** *10* (12), 4538-4546.

11. Zhang, W.; Yang, Z.-Y.; Cheng, X.-W.; Tang, R.-C.; Qiao, Y.-F., Adsorption, Antibacterial and Antioxidant Properties of Tannic Acid on Silk Fiber. *Polymers* **2019,** *11* (6), 970.

12. Ji, Y.; Xu, Q.; Jin, L.; Fu, Y., Cellulosic paper with high antioxidative and barrier properties obtained through incorporation of tannin into kraft pulp fibers. *Int. J. Biol. Macromol.* **2020,** *162*, 678-684.

13. Liang, M.; Gao, L.; Cheng, C.; Zhou, Q.; Uy, J. P.; Heiner, K.; Sun, C., Efficacy of face mask in preventing respiratory virus transmission: A systematic review and meta-analysis. *Travel Medicine and Infectious Disease* **2020,** *36*, 101751.

14. Liao, M.; Liu, H.; Wang, X.; Hu, X.; Huang, Y.; Liu, X.; Brenan, K.; Mecha, J.; Nirmalan, M.; Lu, J. R., A technical review of face mask wearing in preventing respiratory COVID-19 transmission. *Current Opinion in Colloid & Interface Science* **2021,** *52*, 101417.

15. Archana, K. M.; Rajagopal, R.; Krishnaswamy, V. G.; Aishwarya, S., Application of green synthesised copper iodide particles on cotton fabric-protective face mask material against COVID-19 pandemic. *Journal of Materials Research and Technology* **2021,** *15*, 2102-2116.

16. Wiebe, H.; van de Ven, T. G. M.; Gaudreault, R., Adsorption of Tannic Acid onto Gold Surfaces. Manuscript submitted for publication, 2022.

17. Herrington, T. M.; Petzold, J. C., Surface area of papermaking woodpulps used by the British paper industry. *Cellulose* **1995,** *2* (2), 83-94.

18. Köhnke, T.; Lund, K.; Brelid, H.; Westman, G., Kraft pulp hornification: A closer look at the preventive effect gained by glucuronoxylan adsorption. *Carbohydr. Polym.* **2010,** *81* (2), 226-233.

19. Petlicki, J.; van de Ven, T. G. M., Adsorption of polyethylenimine onto cellulose fibers. *Colloids and Surfaces A: Physicochemical and Engineering Aspects* **1994,** *83* (1), 9-23.

20. Lovikka, V. A.; Khanjani, P.; Väisänen, S.; Vuorinen, T.; Maloney, T. C., Porosity of wood pulp fibers in the wet and highly open dry state. *Microporous Mesoporous Mater.* **2016,** *234*, 326-335.

21. Dabros, T.; van de Ven, T. G. M., Collision-Induced Dispersion of Droplets Attached to Solid Particles. *J. Colloid Interface Sci.* **1994,** *163* (1), 28-36.

22. Kamiti, M., *The Kinetics of Deposition of Calcium Carbonate onto Surfaces*. McGill University (Canada): 1994.

23. Alince, B.; Petlicki, J.; van de Ven, T. G. M., Kinetics of colloidal particle deposition on pulp fibers 1. Deposition of clay on fibers of opposite charge. *Colloids and Surfaces* **1991,** *59*, 265-277.

24. Keshk, S. M. A. S., Homogenous reactions of cellulose from different natural sources. *Carbohydr. Polym.* **2008,** *74* (4), 942-945.

25. Yang, H.; Chen, D.; van de Ven, T. G. M., Preparation and characterization of sterically stabilized nanocrystalline cellulose obtained by periodate oxidation of cellulose fibers. *Cellulose* **2015,** *22* (3), 1743-1752.

26. Ricci, A.; Olejar, K. J.; Parpinello, G. P.; Kilmartin, P. A.; Versari, A., Application of Fourier Transform Infrared (FTIR) Spectroscopy in the Characterization of Tannins. *Applied Spectroscopy Reviews* **2015,** *50* (5), 407-442.

Chapter 4: Discussion

In the two manuscripts presented (Chapters 2 and 3), the adsorption of TA to two different surfaces was studied using several experimental techniques, allowing for analysis of the underlying adsorption processes in different experimental conditions.

In Chapter 2 we studied the layer formation mechanism of TA on gold in physiological-like conditions. To our knowledge, although other studies have used QCMD to investigate TA-gold adsorption in acidic conditions and TA adsorption on other substrates in buffered alkaline conditions, TA layer formation on gold in PBS (pH 7.4) has not been studied for a wide range of concentrations. Many other works also focused on layer buildup with longer timescales to achieve thicker coatings whereas in this work we focused on the first 30 minutes; this allowed us to develop a molecular orientation-based model of monolayer formation.

In buffered, slightly alkaline solutions, we confirmed that TA readily adsorbs to the gold surface. The mechanism of interaction between gold and TA was discussed briefly in the manuscript; both unoxidized and oxidized forms of TA were suggested to adsorb to the gold surface by different mechanisms: unoxidized TA by dispersion forces, and oxidized TA by a similar mechanism to that which occurs in the context of gold nanoparticle (AuNP) synthesis. This interaction is similar to the molecular interactions between citrate and gold. Although TA is often used as a stabilizing agent in the synthesis of gold nanoparticles, citrate is a more commonly used molecule for this purpose. As a result, the intermolecular interactions between citrate and gold are more extensively characterized in this context. Citrate molecules adsorb to the AuNP surface through the coordination of one or more carboxyl moieties.[44] The chelating ability of citrate enforces the stability of AuNPs by preventing gold atoms from migrating from the surface; in addition, the adsorbed citrate molecules confer a change in the surface charge of the AuNPs.[44] Thus, it is possible that oxidized forms of TA may interact with the gold surface in a similar fashion. As discussed in Chapter 2, the adsorption interaction between TA and gold may involve the coordination of C=O groups (originating from oxidized phenolic –OH groups) on galloyl moieties to the gold surface. Molecular modeling of TA and gold could help to confirm this hypothesis. For example, Monti et al. used molecular dynamics simulations to investigate the modes of citrate adsorption to gold and were able to determine which functional groups on citrate are most likely to coordinate with the surface.[44]

The role of TA oxidation on adsorption and multilayer deposition should also be discussed in the context of the body of work on oxidized catechol adsorption and film formation. For example, the mechanism of dopamine film deposition in alkaline conditions has been hypothesized to involve oxidation of the catechol to quinone and subsequent self-polymerization.[21] Several comparable studies of TA coating formation referenced in Chapter 2 also involve oxidizing conditions, i.e., alkaline pH and/or the presence of dissolved oxygen. Geißler et al. found TA coatings continuously deposited for several hours on titanium surfaces in such conditions (pH 7.8 with stirring of the TA solution).[45] On the other hand, Ball and Meyer found that TA adsorbed only as a thin monolayer film on gold, with QCM frequency changes levelling off after 10 minutes. In their study, TA solutions were prepared in sodium acetate buffer at a pH of 5.0 intended to prevent TA oxidation.[46] This may suggest that some degree of oxidation of TA is a requisite for the buildup of thicker multilayer films. In other words, only TA monolayers form at pH 5.0 because the molecules can adsorb to the initial surface but TA-TA multilayer aggregation is not favourable, whereas in oxidizing conditions TA readily adsorbs onto itself and can build up thicker bi- and multilayers. The mechanism of oxidized TA-TA interaction and self-polymerization may involve coordination with metal ions such as sodium, magnesium, or silica, as suggested by Geißler et al. and Weber et al,[45, 47] and should be further investigated. Considering the affinity of TA particles to themselves in oxidizing conditions, coating discontinuation would occur when TA forms aggregates in solution to the extent that the aggregates are too large to deposit on the surface. This was indeed observed in the study of Geißler et al., where TA deposition stopped after about 5 hours, coinciding with precipitation in the coating solution.[45] The influence of coating solution conditions is very important for controlled film formation of a specific thickness. By controlling the influence of oxidation and coating times, monolayer and multilayer TA coating thicknesses can be achieved. Furthermore, these phenomena are relevant to biomedical applications, as physiological conditions may lead to some degree of TA oxidation.

One limitation of this study is that adsorption was studied using only two experimental techniques, QCMD and SPR. The SPR results confirm the findings by QCMD, i.e., that in the experimental conditions used TA adsorbs in two phases, initial fast adsorption onto gold followed by slower adsorption of bi-and multilayers of TA. However, the SPR instrument used did not allow for the determination of adsorbed mass. One advantage of methods such as SPR and ellipsometry is that in some cases they can allow for the measurement of adsorbed mass without water. This

type of measurement would be advantageous considering the assumptions made in Chapter 2 regarding the water content of the adsorbed TA. In that manuscript, surface area calculations are used to estimate the mass of a TA monolayer detected by QCMD, including co-adsorbed water that would be detected by the instrument. A theoretical estimate of 65% water was used based on findings of our previous study involving adsorbed proteins. For a more accurate estimate, Weber et al. compared nanoplasmic spectroscopy and QCMD results to determine that the water content of their TA coatings was about 32%.[47] Measurement of TA adsorbed on gold by ellipsometry could allow for further comparison of the experimental methods and a more accurate determination of the true water content of adsorbed TA.

TA layers deposited on gold could be additionally characterized by an optical method such as atomic force microscopy (AFM) to support the proposed model of mono- and bilayer formation. The AFM technique makes use of a sharp probe tip which scans the surface of a sample; as the tip moves in response to the surface topography, a laser beam deflected on the back of the probe allows for this motion to be measured. AFM can be used to image a surface and to determine the thickness of a film by measuring the height differential between a coated area and the bare substrate during a scan. AFM has been previously used to characterize TA coatings with thicknesses measured in the tens of nanometers.[45, 47] In our case, the thickness of TA monolayers adsorbed on gold can be expected to be on the order of a few nanometers given the molecular dimensions of TA. Since we expect monolayers adsorbed from low and high solution concentrations (e.g., 1 μM and 500 μM) to form in the flat and edge-on configurations, respectively, their different heights should, in theory, be discernible by AFM. However, it is unknown whether the height differences would remain distinguishable upon drying, as the molecular orientations may change when the coating is no longer hydrated. Thus, AFM measurement in fluid conditions may be necessary to support the hypothesis of concentration-dependent TA monolayer thickness.

This work contributes to the many investigations into the formation of polyphenolic coatings found in the literature. One practical application of these findings is in the biomedical field, as the TA coatings in this work were studied in physiological-like conditions. Both TA and gold are well suited to biomedical applications. TA has low toxicity and has already been incorporated into several biocompatible materials.[24] For instance, in a study by Sileika et al., TA coatings were found to exhibit antioxidant and antibacterial effects with very low cytotoxicity, which the authors suggest “may have important implications for modulating the acute

inflammatory response to implanted medical devices."[22] TA films studied in physiological conditions are a good candidate for biomedical applications such as bioactive films that are stable at physiological pH.[16] Gold already has several uses in medicine, e.g., as a corrosion-resistant biocompatible plating material for implants and stents. The biomedical applications of gold nanoparticles, such as in imaging, sensing, and drug delivery, have also been widely studied.[48] Therefore, future work could characterize TA films formed on gold for biocompatibility, bioactivity, and antimicrobial and antioxidant activity.

In Chapter 3, we turned to the study of adsorption on a larger scale with the adsorption of TA on cellulosic KP fibers. The experiments confirmed that TA adsorbs rapidly to cellulose, and hydrogen bonding interactions are suggested as the mechanism of interaction. At high concentrations, TA was found to adsorb well beyond our calculated estimates of monolayer coverage on the internal and external surface areas of the KP fibers. The adsorption data were fit to the modified Langmuir model, which was originally developed to describe the deposition of mineral fillers on pulp fibers. Future work on the TA-KP system could investigate the kinetics of adsorption more thoroughly at low TA concentrations, where desorption was observed at long times and consequently the fit of the modified Langmuir model was poor, likely because of a time-dependence of the desorption rate coefficient. Molecular rearrangement of the TA monolayer was proposed as an explanation of the observed desorption, which is similar to the rearrangement hypothesis proposed in Chapter 2. In both scenarios, whether adsorbing on gold or KP, we suggested that a competition in kinetics between adsorption and rearrangement results in TA monolayers of different densities. This hypothesis explains the concentration dependence of TA monolayer mass density with gold, and it also could explain why TA desorption from KP is observed at long times with low bulk concentrations.

As for the applied aspects of this work, in the manuscript we suggested using TA-coated papers as inserts or layers in face masks. During the COVID-19 pandemic, the use of face masks was widespread in many areas to prevent viral transmission. The antimicrobial properties of TA and its ability to bind to proteins make it a promising additive to enhance the ability of filters and masks to trap virus particles and prevent them from spreading through the air. In particular, we have demonstrated that TA may be a useful polyphenol against SARS-CoV-2 infectivity. In Haddad & Gaudreault et al., "Molecular Interactions of Tannic Acid with Proteins Associated with SARS-CoV-2 Infectivity," we found that TA binds with high affinity to several viral and human

cellular proteins involved in SARS-CoV-2 infection, including the receptor binding domain of the spike protein found on the surface of the virus.[26] In this work, proteins were adsorbed on the gold surface of a QCMD sensor, then the adsorption of TA was monitored as solutions of the polyphenol were flowed over the protein-coated surface. The molecular ratio of adsorbed TA to adsorbed protein was used to compare the ability of TA to bind to each of the studied proteins. QCMD allowed for demonstration of the high affinity between TA and the proteins and supported other experimental methods in demonstrating the potential of TA as a drug or antiviral material. Excerpts from this work are included in Appendix 2.

To develop TA-coated papers for use in an application such as filters or face masks, characterization of the papers would need to demonstrate their ability to trap virus (or model virus) particles and establish whether TA enhances this ability. Given the demonstrated affinity of TA to SARS-CoV-2 proteins including those found on the surface of the virus, we hope that TA would reduce the transmission of virus particles through such functionalized papers. Characterization tests could apply techniques such as those used by Gustafsson and Mihranyan to characterize nanocellulose-based virus retention filter papers; the authors quantified the pore size distribution of the filters, tested their pressure-dependent hydraulic permeability, and assessed their ability to filter virus-sized nanoparticles from water.[49] The ability of TA to capture virus particles could also be studied by comparing the capacity of TA-functionalized and control paper samples to adsorb viral proteins (such as RBD) from solution. To effectively capture nanoscale virus particles, the pore size distribution of papers may need to be modulated using pressing and/or fine additives such as cellulose microfibrils or nanocellulose.

In Chapter 3, characterization of the TA-coated paper handsheets was limited to techniques that confirmed the successful incorporation of TA into the paper. Fourier transform infrared spectroscopy (FTIR) confirmed that TA was introduced into the handsheets and showed the absence of new covalent bonds, i.e., TA was incorporated into paper via physisorption, in contrast to previous studies that used various methods of chemisorption. Diffuse reflectance measurements also confirmed the addition of TA and showed the correlation of optical brightness properties with the quantity of added TA. However, future work should continue to characterize the physical and chemical properties of these papers, fine-tune the parameters of the fabrication process, and test the papers in the context of filtration for applications such as in face masks.

Conclusion

In summary, the two manuscripts included in this work investigated the adsorption process of the plant polyphenol tannic acid in two systems, adsorption to gold in physiological-like conditions, and adsorption to kraft pulp in the context of papermaking. The objectives of this research were to determine the ways in which the properties of TA affect the coating formation mechanism on different surfaces.

In Chapter 2, an estimate of the mass density of a TA monolayer was made starting from the area occupied by adsorbed TA molecules. This estimate was verified experimentally; TA monolayers were detected by QCMD near this mass density when accounting for bound water. Later we hypothesized that the two-dimensional structure of TA leads to the formation of monolayers of different mass because of different possible orientations on the surface and packing densities. This hypothesis also explained why, at intermediate TA concentrations that lead to a mix of flat and edge-on packing, bilayer adsorption was observed to be very slow; the "uneven" surface resulting from mixed molecular orientations makes it difficult for additional TA to adsorb on top. The effects of the buffered mild alkaline experimental conditions on the stability of TA in solution were discussed, supported by UV-Vis spectrophotometry and FTIR. Aggregation resulting from this instability explained several observations in the adsorption trends, e.g., an initial adsorption rate that does not scale linearly with adsorbate concentration.

In Chapter 3, TA was found to adsorb to KP with rapid initial kinetics, quickly forming a monolayer on the external surface of the fibers (based again on surface area estimations). Monolayers also form on the internal surfaces, i.e., the fiber pores and lumen, which may be resistant to rinsing with fresh water. The many polyphenolic –OH groups present on TA at its unadjusted, slightly acidic pH were suggested to form hydrogen bonds with the –OH groups on cellulose. Through application of a modified Langmuir model, TA adsorption was shown to find a balance between adsorption and desorption at steady state, explaining why KP does not eventually adsorb 100% of the available TA in solution. However, future work should continue to study the desorption phenomenon observed at long times with a low solution concentration, as this did not fit the model used.

With much recent work in the literature being focused on the formation mechanisms and applications of functional polyphenolic coatings, the findings in these works serve to further our understanding of TA coating formation. TA coatings are promising for their antimicrobial and

antioxidant properties and have potential applications in the biomedical field. TA-functionalized paper materials were proposed as filters for use in face masks, which may have an enhanced ability to capture virus particles. As research and industry shift more to focus on the use of biorenewable materials, green chemistry is a pathway to solutions that are beneficial to both human health and to ecosystems. Thus, it is important to continue fundamental research on functional renewable materials such as TA that originate from natural sources.

Master Reference List

1. Anastas, P. T.; Warner, J. C., Green chemistry. *Frontiers* **1998,** *640*, 1998.

2. Scalbert, A., Antimicrobial properties of tannins. *Phytochemistry* **1991,** *30* (12), 3875-3883.

3. Baldwin, A.; Booth, B. W., Biomedical applications of tannic acid. *J. Biomater. Appl.* **2022,** *36* (8), 1503-1523.

4. Hagerman, A. E.; Butler, L. G., Chapter 10 - Tannins and Lignins. In *Herbivores: their Interactions with Secondary Plant Metabolites (Second Edition)*, Rosenthal, G. A.; Berenbaum, M. R., Eds. Academic Press: San Diego, 1991; pp 355-388.

5. Gaudreault, R.; Hervé, V.; van de Ven, T. G. M.; Mousseau, N.; Ramassamy, C., Polyphenol-Peptide Interactions in Mitigation of Alzheimer's Disease: Role of Biosurface-Induced Aggregation. *J. Alzheimer's Dis.* **2021,** *81* (1), 33-55.

6. Li, X.; Deng, Y.; Zheng, Z.; Huang, W.; Chen, L.; Tong, Q.; Ming, Y., Corilagin, a promising medicinal herbal agent. *Biomedicine & Pharmacotherapy* **2018,** *99*, 43-50.

7. Isbrucker, R. A.; Edwards, J. A.; Wolz, E.; Davidovich, A.; Bausch, J., Safety studies on epigallocatechin gallate (EGCG) preparations. Part 2: Dermal, acute and short-term toxicity studies. *Food Chem. Toxicol.* **2006,** *44* (5), 636-650.

8. Hagerman, A. E., Chemistry of Tannin-Protein Complexation. In *Chemistry and Significance of Condensed Tannins*, Hemingway, R. W.; Karchesy, J. J.; Branham, S. J., Eds. Springer US: Boston, MA, 1989; pp 323-333.

9. Díaz Hidalgo, R. J.; Córdoba, R.; Nabais, P.; Silva, V.; Melo, M. J.; Pina, F.; Teixeira, N.; Freitas, V., New insights into iron-gall inks through the use of historically accurate reconstructions. *Heritage Science* **2018,** *6* (1), 63.

10. White, T., Tannins—their occurrence and significance. *J. Sci. Food Agric.* **1957,** *8* (7), 377-385.

11. García-Villalba, R.; González-Sarrías, A.; Giménez-Bastida, J. A.; Selma, M. V.; Espín, J. C.; Tomás-Barberán, F. A., 3.11 - Metabolism of Dietary (Poly)phenols by the Gut Microbiota. In *Comprehensive Gut Microbiota*, Glibetic, M., Ed. Elsevier: Oxford, 2022; pp 149-175.

12. Nazzaro, F.; Fratianni, F.; De Feo, V.; Battistelli, A.; Da Cruz, A. G.; Coppola, R., Chapter Two - Polyphenols, the new frontiers of prebiotics. In *Advances in Food and Nutrition*

Research, da Cruz, A. G.; Prudencio, E. S.; Esmerino, E. A.; da Silva, M. C., Eds. Academic Press: 2020; Vol. 94, pp 35-89.

13. Ahmad, T., Reviewing the Tannic Acid Mediated Synthesis of Metal Nanoparticles. *Journal of Nanotechnology* **2014,** *2014*, 954206.

14. An, J.-H.; Dultz, S., Adsorption of tannic acid on chitosan-montmorillonite as a function of pH and surface charge properties. *Appl. Clay Sci.* **2007,** *36* (4), 256-264.

15. Chariyarangsitham, W.; Krungchanuchat, S.; Khuemjun, P.; Pilapong, C., Effect of advanced oxidation and amino acid addition on antioxidant capability, iron chelating property and anti-cancer activity of tannic acid. *Arabian Journal of Chemistry* **2021,** *14* (9), 103312.

16. Erel-Unal, I.; Sukhishvili, S. A., Hydrogen-Bonded Multilayers of a Neutral Polymer and a Polyphenol. *Macromolecules* **2008,** *41* (11), 3962-3970.

17. Lee, Y.; Chung, H. J.; Yeo, S.; Ahn, C.-H.; Lee, H.; Messersmith, P. B.; Park, T. G., Thermo-sensitive, injectable, and tissue adhesive sol–gel transition hyaluronic acid/pluronic composite hydrogels prepared from bio-inspired catechol-thiol reaction. *Soft Matter* **2010,** *6* (5), 977-983.

18. Lee, H.; Scherer, N. F.; Messersmith, P. B., Single-molecule mechanics of mussel adhesion. *Proceedings of the National Academy of Sciences* **2006,** *103* (35), 12999-13003.

19. Waite, J. H.; Tanzer, M. L., Polyphenolic Substance of *Mytilus edulis*: Novel Adhesive Containing L-Dopa and Hydroxyproline. *Science* **1981,** *212* (4498), 1038-1040.

20. Lee, H.; Lee, B. P.; Messersmith, P. B., A reversible wet/dry adhesive inspired by mussels and geckos. *Nature* **2007,** *448* (7151), 338-341.

21. Lee, H.; Dellatore, S. M.; Miller, W. M.; Messersmith, P. B., Mussel-Inspired Surface Chemistry for Multifunctional Coatings. *Science* **2007,** *318* (5849), 426-430.

22. Sileika, T.; Barrett, D.; Zhang, R.; Lau, K. H. A.; Messersmith, P. B., Colorless Multifunctional Coatings Inspired by Polyphenols Found in Tea, Chocolate, and Wine. *Angew. Chem., Int. Ed. Engl.* **2013,** *52*.

23. Dargahi, M.; Olsson, A.; Tufenkji, N.; Gaudreault, R., Green Technology: Tannin-Based Corrosion Inhibitor for Protection of Mild Steel. *CORROSION* **2015,** *71*, 1321-1329.

24. Kaczmarek, B., Tannic Acid with Antiviral and Antibacterial Activity as A Promising Component of Biomaterials—A Minireview. *Materials* **2020,** *13* (14).

25. WHO Director-General's opening remarks at the media briefing on COVID-19 - 11 March 2020. *World Health Organization.* **March 11, 2020**.

26. Haddad, M.; Gaudreault, R.; Sasseville, G.; Nguyen, P. T.; Wiebe, H.; van de Ven, T. G. M.; Bourgault, S.; Mousseau, N.; Ramassamy, C., Molecular Interactions of Tannic Acid with Proteins Associated with SARS-CoV-2 Infectivity. *Int. J. Mol. Sci.* **2022,** *23* (5), 2643.

27. Higazy, A.; Hashem, M.; ElShafei, A.; Shaker, N.; Hady, M. A., Development of anti-microbial jute fabrics via in situ formation of cellulose–tannic acid–metal ion complex. *Carbohydr. Polym.* **2010,** *79* (4), 890-897.

28. Zhang, Z.-Y.; Sun, Y.; Zheng, Y.-D.; He, W.; Yang, Y.-Y.; Xie, Y.-J.; Feng, Z.-X.; Qiao, K., A biocompatible bacterial cellulose/tannic acid composite with antibacterial and anti-biofilm activities for biomedical applications. *Materials Science and Engineering: C* **2020,** *106*, 110249.

29. Sauerbrey, G., Verwendung von Schwingquarzen zur Wägung dünner Schichten und zur Mikrowägung. *Z. Phys.* **1959,** *155* (2), 206-222.

30. Quevedo, I. R.; Olsson, A. L.; Clark, R. J.; Veinot, J. G.; Tufenkji, N., Interpreting deposition behavior of polydisperse surface-modified nanoparticles using QCM-D and sand-packed columns. *Environmental Engineering Science* **2014,** *31* (7), 326-337.

31. Gaudreault, R.; Dargahi, M.; Weckman, N.; Olsson, A.; Omanovic, S.; Schwartz, G.; Tufenkji, N., Green Chemistry – with a Special Emphasis on Tannin Molecules for the Protection of Aluminum Boilers. In *AWT 2013 Annual Convention and Exposition*, Uncasville, CT, USA, 2013.

32. Chen, H., Chemical Composition and Structure of Natural Lignocellulose. 2014; pp 25-71.

33. O'Sullivan, A. C., Cellulose: the structure slowly unravels. *Cellulose* **1997,** *4* (3), 173-207.

34. Sjostrom, E., The origin of charge on cellulosic fibers. *Nordic Pulp & Paper Research Journal* **1989,** *4* (2), 90-93.

35. Harrington, J. J., Hierarchical modelling of softwood hygro-elastic properties. **2002**.

36. Rowell, R. M., *Handbook of Wood Chemistry and Wood Composites*. 2 ed.; Taylor & Francis: 2012.

37. Young, R. A.; Kundrot, R.; Tillman, D. A., Pulp and Paper. In *Encyclopedia of Physical Science and Technology (Third Edition)*, Meyers, R. A., Ed. Academic Press: New York, 2003; pp 249-265.

38. Sjöström, E., Chapter 7 - Wood Pulping. In *Wood Chemistry (Second Edition)*, Sjöström, E., Ed. Academic Press: San Diego, 1993; pp 114-164.

39. Whiting, P.; Pulp, D. A. I. G., The Topochemistry of Delignification Shown by Pulping Middle Lamella and Secondary Wall Tissue from Black Spruce Wood. *J. Wood Chem. Technol.* **1981,** *1* (2), 111-122.

40. Ali, A.; Ali, S.; Saleem, H.; Hussain, T., Effect of tannic acid and metallic mordants on the dyeing properties of natural dye extracted from Acacia nilotica bark. *Asian J. Chem.* **2010,** *22* (9), 7065.

41. Burkinshaw, S. M.; Kumar, N., The mordant dyeing of wool using tannic acid and FeSO4, Part 1: Initial findings. *Dyes and Pigments* **2009,** *80* (1), 53-60.

42. Espinosa-Jiménez, M.; González-Caballero, F.; González-Fernández, C.; Pardo, G., The adsorption of tannic acid on hydrophilic cotton and its effect on the electrokinetic properties of this cellulose fibre in a cationic dye solution. *Acta Polym.* **1987,** *38* (1), 96-100.

43. Rosmarin, R. Sustainability sells: Why consumers and clothing brands alike are turning to sustainability as a guiding light. 2020. https://www.businessinsider.com/sustainability-as-a-value-is-changing-how-consumers-shop.

44. Monti, S.; Barcaro, G.; Sementa, L.; Carravetta, V.; Ågren, H., Characterization of the adsorption dynamics of trisodium citrate on gold in water solution. *RSC Advances* **2017,** *7* (78), 49655-49663.

45. Geißler, S.; Barrantes, A.; Tengvall, P.; Messersmith, P. B.; Tiainen, H., Deposition Kinetics of Bioinspired Phenolic Coatings on Titanium Surfaces. *Langmuir* **2016,** *32* (32), 8050-8060.

46. Ball, V.; Meyer, F., Deposition kinetics and electrochemical properties of tannic acid on gold and silica. *Colloids Surf., A* **2016,** *491*, 12-17.

47. Weber, F.; Barrantes, A.; Tiainen, H., Silicic Acid-Mediated Formation of Tannic Acid Nanocoatings. *Langmuir* **2019,** *35* (9), 3327-3336.

48. Elahi, N.; Kamali, M.; Baghersad, M. H., Recent biomedical applications of gold nanoparticles: A review. *Talanta* **2018,** *184*, 537-556.

49. Gustafsson, S.; Mihranyan, A., Strategies for Tailoring the Pore-Size Distribution of Virus Retention Filter Papers. *ACS Applied Materials & Interfaces* **2016,** *8* (22), 13759-13767.

Appendix 1: Supporting Information for "Adsorption of tannic acid onto gold surfaces"

This appendix contains the supporting information for the manuscript in Chapter 2, submitted for publication.

Structure of Tannic Acid

The structure of tannic acid (TA) generated by molecular modeling is shown in Figure S1. The largest dimensions are measured at 27.9 and 26.1 Å; thus, the projected area of a single TA molecule is estimated at 7.3 nm^2. These dimensions are in agreement with the theoretical diameter of 28 Å reported by Weber et al.[1]

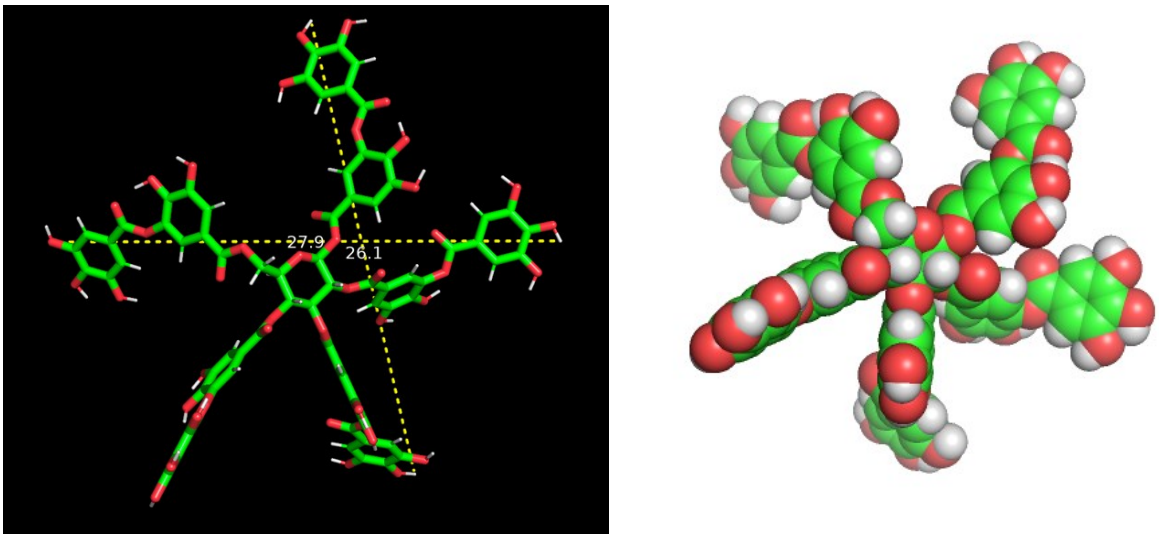

Figure S1: One possible structure of tannic acid (TA) top view. Figure generated with GROMACS v2021.2 and PyMol v2.5.0.

TA Adsorption at Long Times

The apparent mass of TA, measured by quartz crystal microbalance with dissipation monitoring (QCMD), adsorbed to the gold sensor for experiments extended to 2 h is shown in Figure S2. Data shown here are from single experiments, which differ slightly from the data averaged from multiple experiments shown in Figure 2. Nevertheless, the general trend in mass adsorbed after 30 min (Figure 2) shows that the curve for 1 mM TA stands in between 10 µM and 500 µM, which is consistently observed even after 120 minutes.

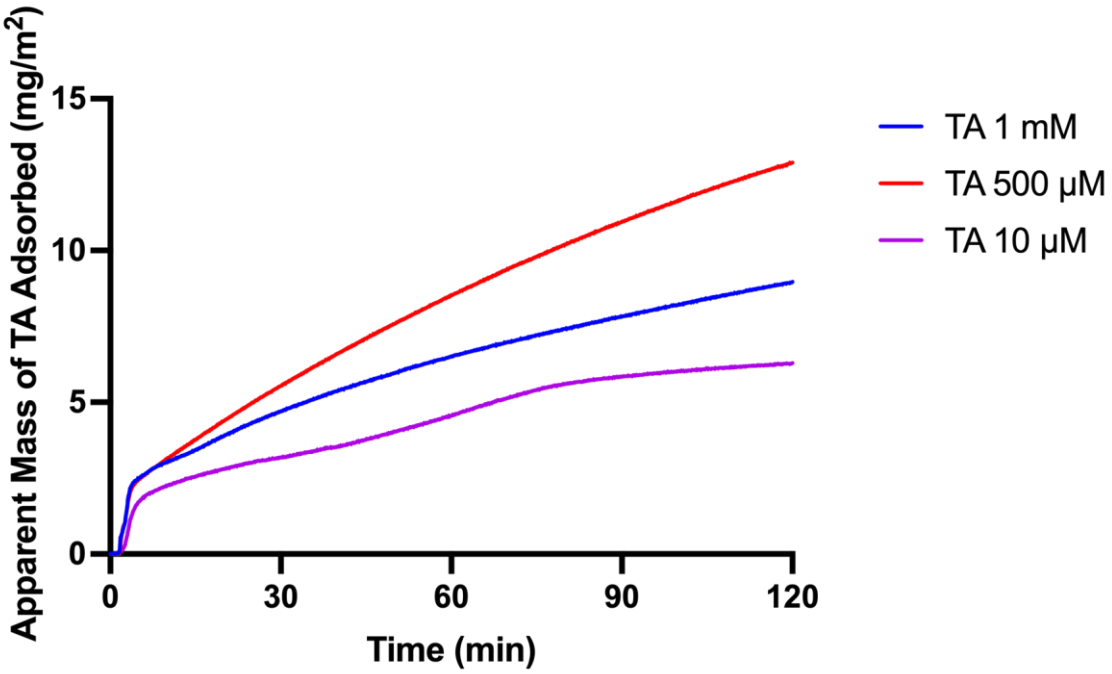

Figure S2: Apparent mass of TA adsorbed on gold quartz crystal microbalance with dissipation monitoring (QCMD) sensor surface for three sample experiments which were extended to 2 hours in duration, demonstrating the continuous buildup of adsorbed TA at long times.

Conductivity of TA Solutions

The conductivity of TA solutions of different concentrations is shown in Figure S3. From the intersection of the slopes of the conductivity curve at low and high concentrations, the critical aggregation concentration of TA was found to be 0.70 mM.

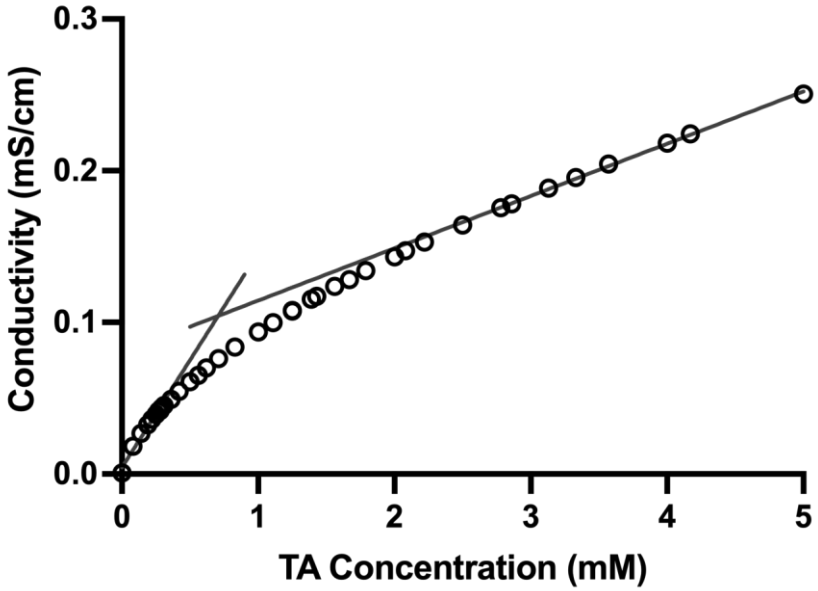

Figure S3: Conductivity of TA solutions in deionized water at 22ºC as a function of concentration. Solid lines: the conductivity is linear at low and high TA concentrations; the intersection of these lines is the critical aggregation concentration, calculated to be 0.70 mM TA.

References

1. Weber, F.; Barrantes, A.; Tiainen, H., Silicic Acid-Mediated Formation of Tannic Acid Nanocoatings. *Langmuir* **2019,** *35* (9), 3327-3336.

Table of Contents Graphic/Graphical Abstract

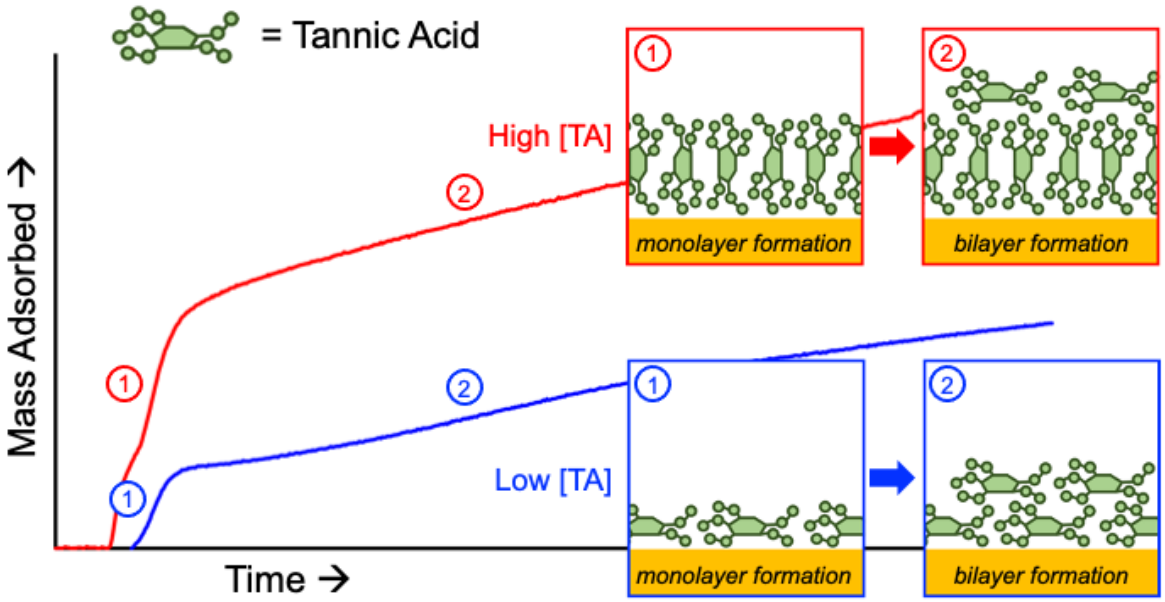

Appendix 2: Adsorption of tannic acid to proteins

Introduction

This appendix contains excerpts from "Molecular Interactions of Tannic Acid with Proteins Associated with SARS-CoV-2 Infectivity" by Mohamed Haddad & Roger Gaudreault et al.[26] Hannah Wiebe was the primary author of the quoted text sections below.

This work sought to investigate the interactions between TA and proteins involved in various steps of SARS-CoV-2 cellular entry and replication. In ELISA binding assays on seven natural compounds, TA was shown to reduce the binding between the spike protein RBD receptor binding domain (RBD) (N501Y variant) and its cellular receptor angiotensin-converting enzyme 2 (ACE2) by up to 95%. Considering this result, the interactions between TA and RBD, transmembrane protease serine 2 (TMPRSS2), and 3-chymotrypsin like protease (3CLpro) were characterized by experimental methods (enzyme inhibition assays, SPR, and QCMD) and computational methods (protein-ligand molecular docking and molecular dynamics simulations).

Results

QCMD characterization of TA/RBD Interactions

"We… perform QCMD experiments to observe the adsorption of TA onto RBD (Figure 2B). First, RBD is adsorbed to the gold surface of the QCMD sensor, with an average total mass of 5.0 ± 2.4 mg/m2 of RBD (N501Y), and then TA solutions (10 to 500 μM) are flowed over the protein-coated sensor for 30 min, with results showing that the amount of TA adsorbed increases with TA concentration. At this time, equilibrium adsorption is not reached, thus the adsorption isotherm is only approximate. Moreover, the kinetics of TA adsorption on RBD are shown in Figure S3A. Consequently, both SPR and QCMD methods show similar trends—TA binds to RBD with a high affinity.

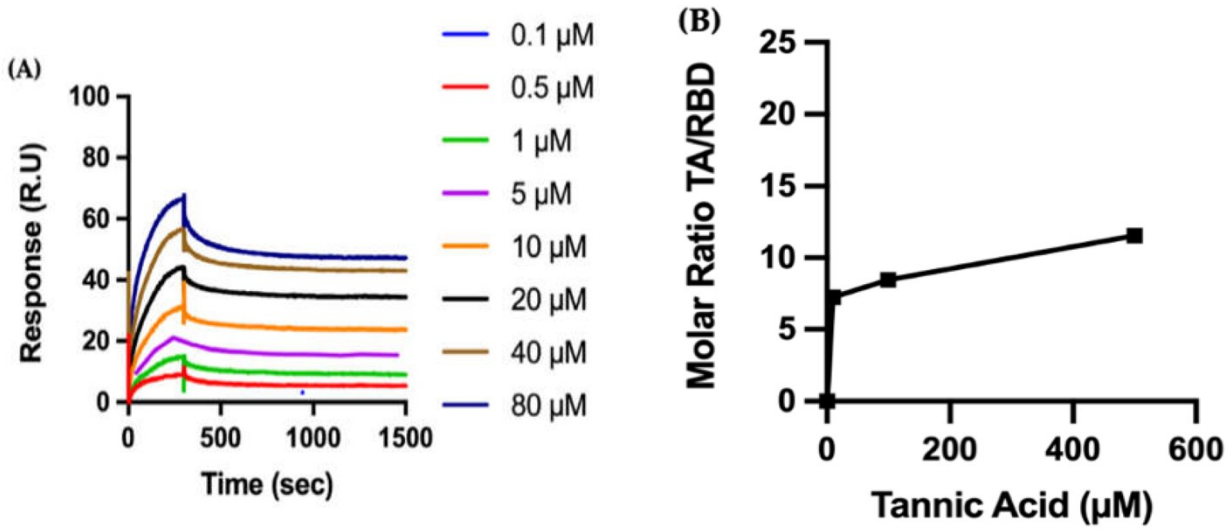

Figure 2. Biophysical characterization of the molecular interaction between TA and RBD: (A) Binding of polyphenol TA to immobilized RBD by surface plasmon resonance (SPR). The recombinant protein RBD (N501Y) is immobilized on a carboxymethylated dextran (CM5) sensor chip, and increasing concentrations of TA are injected to evaluate binding kinetics. (B) RBD is adsorbed to a gold quartz crystal microbalance with dissipation monitoring (QCMD) sensor, and various concentrations of TA are flowed over the surface for 30 min. TA adsorption is shown by the dimensionless molar ratio of adsorbed TA from solution to adsorbed RBD. The initial slope is a measure of the affinity of TA to RBD."

QCMD characterization of TA/TMPRSS2 Interactions

"QCMD is used to measure the adsorption of TA onto TMPRSS2 (Figure 4B). TMPRSS2 is adsorbed to the gold QCMD sensor, with an average total mass of 6.3 ± 2.6 mg/m^2 of TMPRSS2. TA solutions (10 to 500 μM) are then flowed over the TMPRSS2 protein-coated surface for 30 min, and TA adsorption is observed to increase at higher concentrations of TA. The kinetics of TA adsorption on TMPRSS2 as a function of time are also shown in Figure S3B.

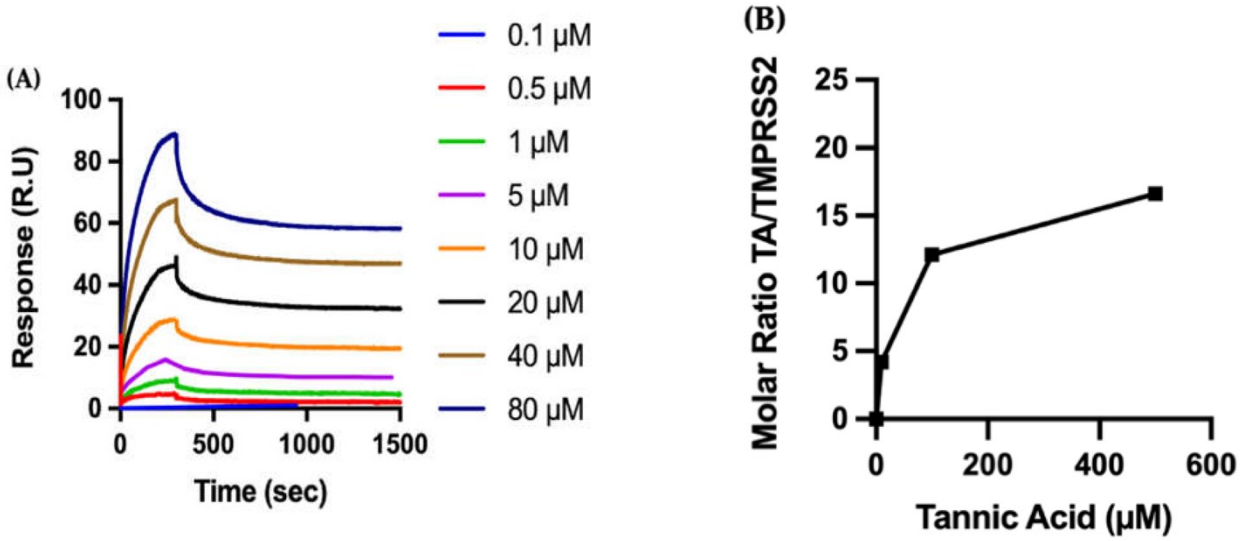

Figure 4. Biophysical characterization of the molecular interactions between TA and TMPRSS2. (A) The recombinant protein TMPRSS2 is immobilized on a CM5 sensor chip, and increasing concentrations of TA are injected to evaluate binding kinetics by SPR. (B) TMPRSS2 is adsorbed to a gold QCMD sensor, and various concentrations of TA are flowed over the surface for 30 min. TA adsorption is expressed by the dimensionless molar ratio of adsorbed TA to adsorbed TMPRSS2."

QCMD characterization of TA/3CLpro Interactions

"We also perform QCMD experiments to observe the adsorption of TA onto 3CLpro (Figure 6B). First, 3CLpro is adsorbed to the gold surface of the QCMD sensor, with an average total mass of 4.2 ± 2.9 mg/m^2 of 3CLpro, and then TA solutions (10 to 500 μM) are flowed over the protein-coated sensor for 30 min, wherein TA adsorption is observed to increase with higher TA concentrations. In addition, Figure S3C shows the kinetics of TA adsorption on 3CLpro as a function of time. Overall, both SPR and QCMD methods show similar trends, i.e., TA binds to 3CLpro with a high affinity.

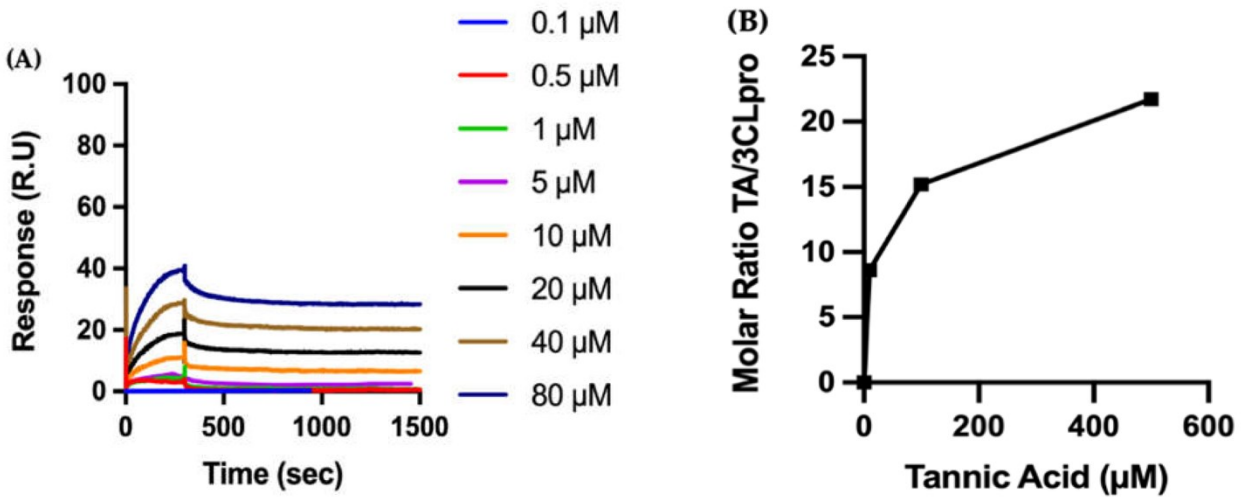

Figure 6. Biophysical characterization of the molecular interactions between the polyphenol TA on immobilized 3CLpro: (A) The recombinant protein 3CLpro is immobilized on a CM5 sensor chip, and increasing concentrations of TA are injected to evaluate binding kinetics by SPR. (B) 3CLpro is adsorbed to a gold QCMD sensor, and various concentrations of TA are flowed over the surface for 30 min. TA adsorption is expressed by the dimensionless molar ratio of adsorbed TA to adsorbed 3CLpro."

Discussion

QCMD experiments suggested a high affinity adsorption between TA and the three proteins studied. When interpreted alongside the other techniques used in this paper, the results suggest that TA has strong interactions with RBD, TMPRSS2, and 3CLpro.

"Although both SPR and QCMD methods provide the kinetics of adsorption and interaction, SPR allows for the measurement of the association and dissociation rate constants, whereas QCMD gives the adsorbed weight of protein and ligand as a function of time… In this work, both SPR and QCMD methods show high affinity between TA and RBD, TMPRSS2, and 3CLpro."

The QCMD method does have some limitations including the fact that co-adsorbed water is detected by the frequency shift of the crystal sensor. Also, although experiments were performed in PBS at pH 7.4 (similar to physiological conditions), other aspects of a physiological viral infection microenvironment are not accounted for.

"In principle, rate constants can be found from both [SPR and QCMD] methods (from mathematical models), but this is more difficult for QCMD because the exact adsorbed mass is unknown (the co-adsorbed water overestimates the dry mass of ligand and protein [62])."

"The SPR and QCMD methods apply certain assumptions to treat the experimental data… when treating the QCMD data, the Sauerbrey equation assumes a thin, rigid film, which may not hold true for large proteins, and QCMD also detects co-adsorbed water molecules, which was accounted for by an assumption that proteins and TA adsorbed with the same weight fraction of bound water (Section 4.4.2 and 4.4.3)."

Overall, QCMD combined with the other methods used in this study showed that TA is an excellent therapeutic candidate against SARS-CoV-2. TA was shown to inhibit the interactions between RBD/ACE2 and inhibit the enzymatic activities of TMPRSS2, involved in cellular entry by the virus, and 3CLpro, involved in virus replication. Thus, TA as a safe and naturally occurring compound should be studied further to assess its effects on clinical SARS-CoV-2 infectivity.

Experimental

Below are excerpts from the "Materials and Methods" section for the QCMD experiments, detailing the experimental setup, theory, and data processing.

"4.4. Quartz Crystal Microbalance with Dissipation Monitoring (QCMD)

4.4.1. QCMD Procedure

QCMD adsorption experiments were performed using a QSense Explorer (Biolin Scientific, Gothenburg, Sweden) with gold-coated quartz crystal sensors (QSX 301, Biolin Scientific). Prior to each experiment, sensors were cleaned by rinsing five times with DI water, then soaking in 2% Hellmanex® III solution (Sigma-Aldrich) while in a sonication bath for 20 min. Sensors were then rinsed 10 times with DI water, once with ethanol, 10 times with DI water, then dried under a flow of air. Finally, sensors were placed in a UV/ozone chamber for 20 min.

To coat the sensor with protein, a 100 µL drop of 1 µg/mL protein solution (RBD (N501Y), TMPRSS2, or 3CLpro in PBS, pH 7.4) was pipetted carefully onto the working surface of the sensor. The protein was allowed to adsorb from the drop for 30 min, after which the remaining solution was removed by pipette and the sensor was dried under a gentle flow of air. The sensor was inserted into the QCMD flow module, and PBS was flowed over the surface using a peristaltic pump at a flowrate of ~100 µL/min until the resonance frequency of the crystal stabilized ($|\Delta f| <$ 0.1 Hz/min).

TA adsorption to the protein-functionalized sensor was studied by flowing TA solutions (10 to 500 µM in PBS, pH 7.4) continuously over the sensor. All test solutions were prefiltered

through a 0.45-µm syringe filter. The resonance frequency and dissipation shift of the crystal were measured for 30 min.

Desorption of mass from the sensor was evaluated by flowing PBS for 15 min following TA adsorption, but no appreciable desorption of TA was observed in all experiments. All experiments were performed at room temperature (22 °C) and at least in duplicate.

The relationship between the shift in resonance frequency of an oscillating quartz crystal and the mass deposited on its surface is given by the Sauerbrey equation [79]:

$$\Delta m = -(C/n)\,\Delta f \quad (1)$$

where C is the sensitivity constant (17.7 ng cm^{-2} Hz^{-1} for a 5 MHz quartz crystal), n is the overtone number (1, 3, 5, 7, or 9), and Δf is the shift in resonance frequency at the specified overtone n [80,81]. The third overtone (n = 3) was used in all experiments. To account for variability in the mass of protein adsorbed to the sensor, the quantity of TA adsorbed was normalized to the amount of protein adsorbed on the sensor. The Δm was converted to a molar quantity of TA and divided by the amount of protein (in moles) adsorbed after drop coating, resulting in a dimensionless molar ratio.

4.4.2. Water Content in the Protein Layer Adsorbed on the QCMD Sensor

When particles adsorb to a QCMD sensor, water molecules within (intrinsic) and between particles in the adsorbed layer are also sensed in the frequency shift [62,82]. Thus, the reported mass of protein adsorbed to the sensor, e.g., 5.0 ± 2.4 mg/m^2 for RBD (N501Y), is an overestimate of the actual amount of protein (dry basis) adsorbed.

Nevertheless, monolayer coverage of the sensor surface by protein can be estimated geometrically by approximating the RBD (N501Y) protein as a sphere with a diameter of 3.65 nm (radius of gyration of approximately 1.825 nm calculated with GROMACS v2021.2, 23 February 2022, https://www.gromacs.org (Figure S18). Since a random deposition of spheres forming a monolayer corresponds to 55% coverage of the available surface area [83], a monolayer of RBD (N501Y) is estimated to be 1.78 mg/m^2 according to the following calculations. Consequently, this suggests a weight fraction of approximately 35% for the protein and 65% water, although this fraction will be altered when TA adsorbs onto the protein layer, e.g., from protein conformational changes.

Mass of one RBD (N501Y) protein:

$$20340\frac{g}{mol}\left(\frac{1\ mol}{6.022\times10^{23}\ molec}\right)=3.377\times10^{-20}\frac{g}{molec} \quad (2)$$

Area occupied by one RBD (N501Y) protein:

$$\frac{\pi\left(\frac{3.65\ nm}{2}\right)^{2}}{molec}=10.5\frac{nm^{2}}{molec} \quad (3)$$

Monolayer of RBD (N501Y) surface coverage:

$$0.55\left(\frac{3.377\times10^{-20}\frac{g}{molec}}{10.5\frac{nm^{2}}{molec}}\right)\left(\frac{10^{9}\ nm}{m}\right)^{2}\left(\frac{10^{3}\ mg}{g}\right)=1.78\frac{mg}{m^{2}} \quad (4)$$

4.4.3. Molar Ratio of TA/Protein on the Sensor Surface

The amount of TA adsorbed onto the protein layer after 30 min is reported as a dimensionless molar ratio of TA to RBD, TMPRSS2, or 3CLpro (Figure 2B, Figure 4B and Figure 6B, respectively). The mass of the adsorbed protein layer varies between experiments (e.g., 5.0 ± 2.4 mg/m^2 for RBD (N501Y)), as does the amount of TA adsorbed to the protein layer; this normalization accounts for the variance in adsorbed protein.

Moreover, it is likely that the amount of H_2O molecules associated with TA (H_2O:TA) differs from the amount of H_2O molecules with the protein (H_2O:protein) on a weight basis. For example, although it has been estimated that about 43 H_2O molecules form a monolayer around gallic acid [84], a building block of TA (D-glucose after 10 galloylation reactions), only about five H_2O molecules form stronger directional bonds with the hydrophilic part of GA, similar to what was reported experimentally by Martinez et al. [85]. However, here we hypothesize a similar water weight fraction between TA and protein to normalize and estimate the dimensionless molar (TA/protein) ratio. Under this assumption, a water weight fraction of 65% corresponds to approximately 175 H_2O molecules per TA molecule, or ~17 H_2O per galloyl group of TA. This number is higher than the reported five H_2O molecules in close contact, but lower than the 43 associated H_2O molecules in bulk water, thus it may be a reasonable approximation for the water fraction upon TA adsorption to the protein layer. Alternatively, there could be five H_2O per galloyl group with the remaining water located between TA molecules."

Supporting Information

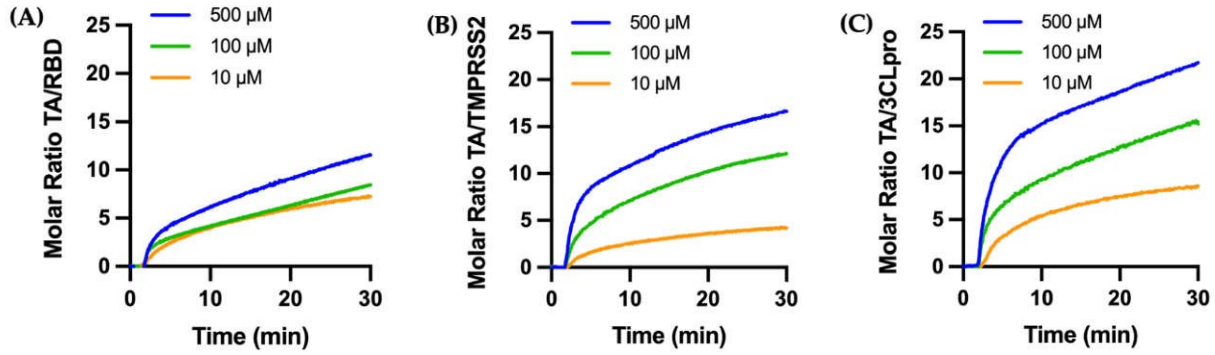

"Figure S3. Kinetics of TA adsorption to protein-coated surfaces as measured by quartz crystal microbalance with dissipation monitoring (QCMD), expressed as the dimensionless molar ratio of adsorbed TA from solution to adsorbed protein, for: (A) TA/RBD, (B), TA/TMPRSS2, and (C) TA/3CLpro systems. When particles adsorb to the QCMD sensor, water molecules within (intrinsic) and between particles in the adsorbed layer are also sensed in the frequency shift [62,82]. Here we hypothesize a similar water weight fraction for TA and protein to normalize and estimate the dimensionless molar (TA:protein) ratio. The linear increase in adsorbed mass towards 30 minutes is due to bi- and multilayer adsorption of TA.

A monolayer of adsorbed TA occurs at the intersection between the steepest initial slope of the molar ratio-time curve (due to the adsorption of TA on protein) and the second slope (due to multilayer adsorption of TA on TA). It can be seen from Figure S3 that the amount of adsorbed TA at monolayer coverage increases with TA concentration. A likely explanation is that at low TA concentrations TA adsorbs in a flat configuration, whereas at high concentrations TA adsorbs mainly edge-on and/or as aggregates."

References

62. Solin, K.; Beaumont, M.; Rosenfeldt, S.; Orelma, H.; Borghei, M.; Bacher, M.; Opietnik, M.; Rojas, O.J. Self-Assembly of Soft Cellulose Nanospheres into Colloidal Gel Layers with Enhanced Protein Adsorption Capability for Next-Generation Immunoassays. *Small* **2020**, *16*, 2004702.

79. Sauerbrey, G. Verwendung von Schwingquarzen zur Wägung dünner Schichten und zur Mikrowägung. *Z. Für Phys.* **1959**, *155*, 206–222.

80. Quevedo, I.R.; Olsson, A.L.; Clark, R.J.; Veinot, J.G.; Tufenkji, N. Interpreting deposition behavior of polydisperse surface-modified nanoparticles using QCM-D and sand-packed columns. *Environ. Eng. Sci.* **2014**, *31*, 326–337.

81. Lapointe, M.; Farner, J.M.; Hernandez, L.M.; Tufenkji, N. Understanding and improving microplastic removal during water treatment: Impact of coagulation and flocculation. *Environ. Sci. Technol.* **2020**, *54*, 8719–8727.

82. Olsson, A.L.; Wargenau, A.; Tufenkji, N. Optimizing bacteriophage surface densities for bacterial capture and sensing in quartz crystal microbalance with dissipation monitoring. *ACS Appl. Mater. Interfaces* **2016**, *8*, 13698–13706.

83. Dabros, T.; Van De Ven, T. Collision-induced dispersion of droplets attached to solid particles. *J. Colloid Interface Sci.* **1994**, *163*, 28–36.

84. Gaudreault, R.; Van de Ven, T.; Whitehead, M. A theoretical study of the interactions of water with gallic acid and a PEO/TGG complex. *Mol. Simul.* **2006**, *32*, 17–27.

85. Martinez, N.; Junquera, E.; Aicart, E. Ultrasonic, density, and potentiometric characterization of the interaction of gentisic and gallic acids with an apolar cavity in aqueous solution. *Phys. Chem. Chem. Phys.* **1999**, *1*, 4811–4817.